

# United States Naval Postgraduate School



A NUMERICAL INVESTIGATION OF THE NON-LINEAR  
MECHANICS OF WAVE DISTURBANCES IN PLANE  
POISEUILLE FLOWS

by

T. H. Gawain and W. H. Clark

2 September 1971

This document has been approved for public release  
and sale; its distribution is unlimited.

QA911  
.G16

20091105006

**LIBRARY**  
**NAVAL POSTGRADUATE SCHOOL**  
**MONTEREY, CALIF. 93940**

**NAVAL POSTGRADUATE SCHOOL**  
Monterey, California

Rear Admiral A. S. Goodfellow, Jr.  
Superintendent

M. U. Clauser  
Academic Dean

**ABSTRACT:**

The response of a plane Poiseuille flow to disturbances of various initial wavenumbers and amplitudes is investigated by numerically integrating the equation of motion. It is shown that for very low amplitude disturbances the numerical integration scheme yields results that are consistent with those predictable from linear theory. It is also shown that because of non-linear interactions a growing unstable disturbance excites higher wavenumber modes which have the same frequency, or phase velocity, as the primary mode. For very low amplitude disturbances these spontaneously generated higher wavenumber modes have a strong resemblance to certain modes computed from the linear Orr-Sommerfeld equation.

In general it is found that the disturbance is dominated for a long time by the primary mode and that there is little alteration of the original parabolic mean velocity profile. There is evidence of the existence of an energy equilibrium state which is common to all finite-amplitude disturbances despite their initial wavenumbers. This equilibrium energy level is roughly 3-5% of the energy in the mean flow which is an order of magnitude higher than the equilibrium value predicted by existing non-linear theories.

T. H. Gawain  
T. H. Gawain  
Professor of Aeronautics

W. H. Clark  
W. H. Clark  
Visiting Assistant Professor

Approved by:

  
R. W. Bell  
Chairman  
Department of Aeronautics

Released by:

  
C. E. Menneken  
Dean of Research Administration

NPS-57Gn71091A

2 September 1971

## TABLE OF CONTENTS

	Page
1. Introduction . . . . .	1
2. Background . . . . .	2
3. Basic Equations . . . . .	6
4. Numerical Model . . . . .	11
5. Linear Calculations . . . . .	16
6. Numerical Integration of the Vorticity Equation . . . . .	21
a) Small Amplitude Disturbances . . . . .	21
b) Finite Amplitude Disturbances . . . . .	25
7. Conclusions. . . . .	36
References . . . . .	39
Figures . . . . .	41
Appendix (Program Listing) . . . . .	78
Distribution List . . . . .	118
Form DD 1473 . . . . .	120

## 1. Introduction

In this paper we present some results from a numerical investigation of the phenomena of stability, transition and turbulence in incompressible channel flows. Ideally, the goal of such an investigation would be to numerically integrate the Navier-Stokes equations and thereby be able to follow the growth of some unstable disturbance which perturbs an initial laminar Poiseuille flow. It would then be possible to observe in detail how this growing disturbance eventually produces a fully developed, stationary turbulent flow. Presumably, if one were to repeat such a calculation for a large number of initial disturbances then the final turbulent flow could be described by an ensemble average over all the initial conditions.

The results of such a computation would represent an exact (to within the limits of the numerical model) solution to the turbulence problem. Since turbulence is an inherently three-dimensional phenomenon, these computations would have to be carried out on a three-dimensional grid; unfortunately, the computational grid would have to be large enough to contain the large "eddies" representing the initial disturbance and still be able to resolve the smallest energy dissipation length scales of the final turbulence. Even at low Reynolds numbers the ratio of the larger length scale to the smallest scale is several orders of magnitude. The number of grid points is proportional to the cube of this ratio; hence, a complete three-dimensional solution is impractical, if not impossible, despite the large storage capacity of modern computers. (Emmons 1970) To overcome this impractically large storage requirement we have drastically simplified the problem by treating the flow on a

two-dimensional basis. It is recognized that a two-dimensional treatment can not adequately represent true physical turbulence. Never-the-less the two-dimensional problem can be handled without further approximation and, as will be pointed out in the next section, two-dimensional solutions are of interest in their own right.

## 2. Background

During the past decade considerable effort was devoted to developing theories for the response of plane Poiseuille flows to finite-amplitude disturbances. The most significant contribution of these theories (in particular, those of Stuart and Watson (1960) and Reynolds and Potter (1967)) was in showing that the square of the amplitude ( $|A_1|^2$ ) of an initially infinitesimal unstable disturbance is governed by an equation of the form

$$\frac{d |A_1|^2}{dt} = k_1 |A_1|^2 + k_2 |A_1|^4 \quad (1)$$

Equation 1, which can be derived from the Navier-Stokes equations, is an approximation valid in a region in the  $(\alpha-R_e)$ -plane which is close to the "neutral curve". Here  $R_e$  denotes the Reynolds number and  $\alpha$  the wave number of the disturbance. For disturbances with very small amplitudes the second term on the right of equation 1 must be negligible; hence, the square of the disturbance amplitude has an exponential growth and the constant,  $k_1$ , is related to the exponential amplification factor of the linear theory (i.e.,  $k_1 = -2 \sqrt{\beta_{11}}$ ). Of particular interest is the case of  $k_1 > 0$  for which the flow is unstable to small disturbances.

If  $k_2 < 0$  then it is possible that the higher order terms will eventually balance the leading term and the amplitude growth is limited such that

$$\frac{d |A_1|^2}{dt} \rightarrow 0 \quad (1b)$$

$$|A_1|^2 \rightarrow -k_1/k_2$$

as

$$t \rightarrow +\infty$$

Under such conditions a "supercritical equilibrium state" is said to exist. On the other hand, if  $k_1 > 0$  and  $k_2 > 0$  then no positive limiting value for  $|A_1|^2$  is possible according to equation 1. It is possible to evaluate  $k_2$  based on Stuart's (1960) theory and the necessary calculations have been carried out by Pekeris and Shkoller (1967) and Reynolds and Potter (1967). These authors have found that under certain conditions  $k_2 < 0$  for some unstable disturbances. Both Pekeris and Shkoller and Reynolds and Potter have found that for regions near the lower branch of the "neutral curve"  $k_2 < 0$  while  $k_2 > 0$  near the upper branch. Hence, one can conclude that disturbances whose wavelength corresponds to a point near the lower branch can grow according to the non-linear theory and reach a supercritical equilibrium state. On the other hand, for unstable disturbances whose wavelength corresponds to a point in the  $(\alpha, R_e)$  plane near the upper branch the non-linear theory does not seem to be applicable. At least the existing theories give us no information about the growth of such a disturbance beyond the linear range of amplitudes.

Such "supercritical equilibrium states" are not observed experimentally in channel flows; instead the initial instabilities lead immediately to three dimensional turbulent flows. It seems, that no experimental verification of this aspect of finite-amplitude theory is possible. A computer simulation of a two dimensional channel flow is, perhaps, the best way of investigating the two dimensional response of a plane Poiseuille flow to an initial unstable disturbance. A computer simulation offers, in addition to its two dimensionality, the advantage of providing an "exact" solution to the equations of motion ("exact" to within the limits of a finite difference representation) without introducing any approximations concerning the relative magnitudes of the various modes of which the disturbance is composed.

The present paper presents the results of a numerical investigation of the response of a plane Poiseuille flow to various initial disturbances. An attempt has been made to present the results in a manner that will facilitate comparison with the existing non-linear theory. The difficulty in making such comparisons is due to the fact that the theories mentioned concern the growth of an unstable disturbance with zero initial amplitude (at time  $t = -\infty$ ) which grows at first according to linear theory and finally reaches an amplitude of such magnitude that the non-linear equations are appropriate. In a numerical simulation, with limited computation time available, the initial disturbance must have some finite amplitude. The growth rates predicted by the finite-amplitude theories are very small and the time required to follow the growth of a very small disturbance to the non-linear range consumes enormous amounts of computer time. For this reason the numerical

investigator is tempted to start his calculations by using a disturbance whose amplitude is of such magnitude that the entire linear range can be bypassed. It will be pointed out in Section 6 that there seem to be significant qualitative differences in the flow when large initial amplitudes are used as compared with those for which very small initial amplitudes are used in the calculations.

Another aspect of the present investigation was to determine under what circumstances, if any, a two dimensional representation of the flow could be made to resemble in some respects three dimensional turbulent flows.

It is clear that the "supercritical equilibrium states" in which the unstable disturbance mode remains dominant do not resemble turbulence in which the disturbance energy is distributed over a wide spectral range. Also in a "supercritical equilibrium state" the resultant mean velocity profile differs only slightly from the parabolic laminar profile while for turbulent flows the mean velocity profiles bear little resemblance to the original laminar one. It is recognized that there are significant differences between two dimensional and true three dimensional turbulence. This is particularly evident in the energy spectrum and mechanism for the transfer of energy and vorticity between the various spectral components (Lilly (1968) and Kraichnan (1967)).

However, could it be possible that for some choice of initial disturbance mode shapes and amplitudes the structure of the resultant two dimensional flow could lie somewhere between the (relative)

simplicity of a supercritical equilibrium state and the "complete chaos" characterizing a true turbulent flow? This aspect of the present paper will be discussed in Section 6.

### 3. Basic Equations

Consider the two dimensional flow of an incompressible fluid between two parallel planes. The governing equations of motion are

$$\frac{\partial \zeta}{\partial t} - \frac{\partial \Psi}{\partial y} \frac{\partial \zeta}{\partial x} + \frac{\partial \Psi}{\partial x} \frac{\partial \zeta}{\partial y} = \frac{1}{R_e} \nabla^2 \zeta \quad (2a)$$

and

$$\zeta = \nabla^2 \Psi \quad (2b)$$

where  $\zeta$  and  $\Psi$  are the vorticity and stream function respectively with  $\zeta$  and  $\Psi$  defined by

$$u = - \frac{\partial \Psi}{\partial y}; \quad v = \frac{\partial \Psi}{\partial x} \quad (3a)$$

$$\zeta = \frac{\partial v}{\partial x} - \frac{\partial u}{\partial y}. \quad (3b)$$

The variables are assumed to be normalized on suitable characteristic lengths and velocities which are shown in Figure 1 along with other parameters of interest. The velocity components can be expressed as

$$u = U(y) + u'; \quad v = v'; \quad \zeta = - \frac{dU}{dy} + \zeta' \quad (4)$$

$$\Psi = \frac{1}{3} \left( \frac{1}{3} y^3 - y \right) + \Psi'$$

where the primed quantities which depend on  $x$ ,  $y$ ,  $t$  represent the instantaneous departure of the flow from the original laminar flow.

Substituting equations 4 into equations 2 results in

$$\frac{\partial \zeta'}{\partial t} + U \frac{\partial \zeta'}{\partial x} - 3 \frac{\partial \psi'}{\partial x} - \frac{\partial \psi'}{\partial y} \frac{\partial \zeta'}{\partial x} + \frac{\partial \psi'}{\partial x} \frac{\partial \zeta'}{\partial y} = \frac{1}{R_e} \nabla^2 \zeta' \quad (5a)$$

$$\zeta' = \nabla^2 \psi' \quad (5b)$$

The conditions of zero slip at the wall and constant mass flow rate imply that the stream function,  $\psi'$ , satisfy the boundary conditions

$$\psi' = \frac{\partial \psi'}{\partial y} = 0 \quad \text{at} \quad y = \pm 1. \quad (6)$$

By considering periodic solutions to equation 2 the boundary conditions in the streamwise direction are fixed by

$$\psi'(x, y, t) = \psi'(x \pm 2nL, y, t) \quad (7a)$$

$$\zeta'(x, y, t) = \zeta'(x \pm 2nL, y, t) \quad (7b)$$

where the basic period is  $2L$ . Equations 5a and 5b with the boundary conditions (6) and (7) are to be solved for  $\psi'(x, y, t)$  for a given initial value of  $\psi'(x, y, 0)$ .

At this point it is convenient to define some parameters that are useful in describing the flow structure. The assumed periodicity implies homogeneity in the streamwise direction; hence, all averaging is done with respect to the streamwise coordinate,  $x$ . The average value of any quantity,  $q(x, y, t)$ , is denoted by an overbar and obtained by integrating over one period of the basic wavelength.

$$\bar{q}(y, t) = \frac{1}{2L} \int_{-L}^{L} q(x, y, t) dx \quad (8)$$

It should again be emphasized that in our representation the flow is arbitrarily divided into a laminar and a disturbance part. Hence, the total streamwise velocity component is given by

$$u(x,y,t) = U(y) + u'(x,y,t) \quad (9)$$

and the mean velocity is

$$\bar{u}(y,t) = U(y) + \bar{u}'(y,t) \quad (10)$$

The difference between the mean and local values of any quantity is referred to as the turbulent part of that quantity and is denoted by a circumflex. Thus we have

$$\hat{u}(x,y,t) = u(x,y,t) - \bar{u}(y,t) = u' - \bar{u}' \quad (11a)$$

$$\hat{v}(x,y,t) = v'(x,y,t) \quad (11b)$$

$$\hat{\psi}(x,y,t) = \psi'(x,y,t) - \bar{\psi}'(y,t) \quad (11c)$$

$$\hat{\zeta}(x,y,t) = \zeta'(x,y,t) - \bar{\zeta}'(y,t) \quad (11d)$$

and

$$\hat{u} = - \frac{\partial \hat{\psi}}{\partial y} \quad (11e)$$

$$\bar{u}' = - \frac{\partial \bar{\psi}'}{\partial y} \quad (11f)$$

$$\hat{v} = \frac{\partial \hat{\psi}}{\partial x} \quad (11g)$$

$$\bar{v}' = \frac{\partial \bar{\psi}'}{\partial x} = 0 \quad (11h)$$

The turbulent kinetic energy is

$$\hat{E}(x,y,t) = \frac{1}{2} \left[ \left( - \frac{\partial \hat{\psi}}{\partial y} \right)^2 + \left( \frac{\partial \hat{\psi}}{\partial x} \right)^2 \right] \quad (12a)$$

The mean value is

$$\bar{E} (y, t) = \frac{1}{2L} \int_{-L}^L \hat{E} (x, y, t) dx \quad (12b)$$

and the normalized sum of turbulent kinetic energy over a domain extending from the upper to the lower wall and for one period of the basic disturbance is

$$\hat{E}(t) = \frac{1}{2} \int_{-1}^1 dy \left\{ \frac{1}{2L} \int_{-L}^L \hat{E} (x, y, t) dx \right\} \quad (12c)$$

Similarly, the kinetic energy in the mean flow is

$$E (y, t) = \frac{1}{2} \left[ U(y) - \frac{\partial \bar{\Psi}}{\partial y} \right]^2 \quad (13a)$$

and the normalized sum over the domain is

$$E (t) = \frac{1}{2} \int_{-1}^1 E (y, t) dy \quad (13b)$$

The normalized energy in the initial laminar flow is

$$E_l = \frac{1}{2} \int_{-1}^1 \frac{1}{2} U^2 dy = .600 . \quad (13c)$$

We can represent the periodic disturbance by means of a Fourier series as follows:

$$\psi' (x, y, t) = \sum_{n=-\infty}^{\infty} f_n (y, t) e^{-i n \alpha x} \quad (14a)$$

$$\zeta' (x, y, t) = \sum_{n=-\infty}^{\infty} g_n (y, t) e^{-i n \alpha x} \quad (14b)$$

with

$$f_n(y, t) = \frac{1}{2L} \int_{-L}^L \psi'(x, y, t) e^{inx} dx \quad (15a)$$

$$f_{-n} = f_n^*$$

$$g_n(y, t) = \frac{1}{2L} \int_{-L}^L \zeta'(x, y, t) e^{inx} dx \quad (15b)$$

$$g_{-n} = g_n^*$$

where  $\alpha = \pi/L$ , and superscript \* denotes a complex conjugate. From 5b

$$g_n = f_n'' - (n\alpha)^2 f_n \quad (15c)$$

Notice that the mean value of the disturbance streamfunction and vorticity is simply

$$\bar{\psi}'(y, t) = f_0(y, t) \quad (16)$$

$$\bar{\zeta}'(y, t) = g_0(y, t) \quad (17)$$

The mean value of the turbulent kinetic energy is given by

$$\bar{E}(y, t) = \sum_{n=-\infty}^{\infty} E_n(y, t) - E_0(y, t) \quad (18)$$

where each of the components of the energy spectrum function,  $E_n(y, t)$ , is given by

$$E_n(y, t) = \frac{1}{2} \left( |f_n'|^2 + \left(\frac{n\pi}{L}\right)^2 |f_n|^2 \right) \quad (19)$$

The normalized total turbulent kinetic energy over the domain is

$$\hat{E}(t) = \sum_{n=-\infty}^{\infty} E_n(t) - E_o(t) \quad (19a)$$

where

$$E_n(t) = \frac{1}{2} \int_{-1}^1 E_n(y, t) dy \quad (19b)$$

#### 4. The Numerical Model

A rectangular grid of dimensions  $2 \times 2L$  is used with  $M \times N$  grid points located as shown in Figure 2. For the calculations presented herein  $64 \times 201$  grid points were used. The indices  $k$ ,  $j$ , and  $\ell$  denote stations along  $x$ ,  $y$ , and  $t$  respectively and  $\delta x$ ,  $\delta y$ ,  $\delta t$  are the corresponding intervals. The value of the disturbance streamfunction  $\psi'(x, y, t)$  is then denoted by  $\psi_{K,J}^\ell$ . The use of the primes will be discarded from this point unless necessary for clarity. Equations 5a and 5b are expressed in finite difference form as follows

$$\begin{aligned} \frac{\zeta_{K,J}^{\ell+1} - \zeta_{K,J}^{\ell-1}}{2\delta t} &= 3 \frac{\psi_{K+1,J}^\ell - \psi_{K-1,J}^\ell}{2\delta x} - U_J \frac{\zeta_{K+1,J}^\ell - \zeta_{K-1,J}^\ell}{2\delta x} \\ &\quad + J_{K,J}^\ell + \frac{1}{R_e} \overline{\Delta^2} \zeta_{KJ}^\ell \end{aligned} \quad (20a)$$

$$\begin{aligned} \zeta_{K,J}^\ell &= \Delta^2 \psi_{K,J}^\ell = \frac{1}{\delta x^2} (\psi_{K+1,J}^\ell - 2\psi_{K,J}^\ell + \psi_{K-1,J}^\ell) \\ &\quad + \frac{1}{\delta y^2} (\psi_{K,J+1}^\ell - 2\psi_{K,J}^\ell + \psi_{K,J-1}^\ell) \end{aligned} \quad (20b)$$

where  $\overline{\Delta^2}$  represents the modified form of the Laplacian differential operator of DuFort and Frankel (1958) defined as

$$\begin{aligned}\overline{\Delta^2} \zeta_{K,J}^\ell &= \frac{1}{\delta x^2} [\zeta_{K+1,J}^\ell - (\zeta_{K,J}^{\ell+1} + \zeta_{K,J}^{\ell-1}) + \zeta_{K-1,J}^\ell] \\ &\quad + \frac{1}{\delta y^2} [\zeta_{K,J+1}^\ell - (\zeta_{K,J}^{\ell+1} + \zeta_{K,J}^{\ell-1}) + \zeta_{K,J-1}^\ell]\end{aligned}\tag{21}$$

and  $J_{K,J}^\ell$  is the total energy and mean square vorticity conservation form of the non-linear advection terms introduced by Arakawa (1966).

i.e.,

$$\begin{aligned}J_{K,J}^\ell &= \frac{1}{3} \left\{ \Delta_y \Psi_{K,J}^\ell \Delta_x \zeta_{K,J}^\ell - \Delta_x \Psi_{K,J}^\ell \Delta_y \zeta_{K,J}^\ell \right\} \\ &\quad + \frac{1}{3} \left\{ \Delta_y (\Psi \Delta_x \zeta)_{K,J}^\ell - \Delta_x (\Psi \Delta_y \zeta)_{K,J}^\ell \right\} \\ &\quad + \frac{1}{3} \left\{ \Delta_x (\zeta \Delta_y \Psi)_{K,J}^\ell - \Delta_y (\zeta \Delta_x \Psi)_{K,J}^\ell \right\}\end{aligned}\tag{23}$$

where  $\Delta_x$  and  $\Delta_y$  denote ordinary first central differences.

Equation 20a is solved explicitly for  $\zeta_{K,J}^{\ell+1}$  at each time step from the known values of  $\Psi_{K,J}^\ell$ ,  $\zeta_{K,J}^\ell$ , and  $\zeta_{K,J}^{\ell-1}$ . The corresponding values of the  $\Psi_{K,J}^{\ell+1}$  are obtained from equation 20b. Equation 20b represents a set of simultaneous algebraic equations to be solved for the  $\Psi_{K,J}^\ell$ ,  $K = 1, 2, \dots, M$ ;  $J = 1, 2, \dots, N$  at each time step. Because of the large number of mesh points used in this investigation, conventional techniques are not suitable and an alternative method is used. We express the variables  $\zeta_{K,J}^\ell$  and  $\Psi_{K,J}^\ell$  in terms of their discrete Fourier transforms as follows:

$$\psi_{K,J}^{\ell} = \sum_{n=1}^{M} f_{n,J}^{\ell} e^{-i \theta_{n,K}} \quad (24a)$$

$$\zeta_{K,J}^{\ell} = \sum_{n=1}^{M} g_{n,J}^{\ell} e^{-i \theta_{n,K}} \quad (24b)$$

with

$$f_{n,J}^{\ell} = \frac{1}{M} \sum_{k=1}^{M} \psi_{K,J}^{\ell} e^{i \theta_{n,k}} \quad (24c)$$

$$g_{n,J}^{\ell} = \frac{1}{M} \sum_{k=1}^{M} \zeta_{K,J}^{\ell} e^{i \theta_{n,k}} \quad (24d)$$

where

$$\theta_{n,k} = \frac{2 \pi (n-1)(k-1)}{M} \quad k,n = 1,2,\dots,M$$

Substituting equations 24 into equation 20b yields the following equation for the Fourier components of  $\psi_{K,J}^{\ell}$  :

$$f_{n,J+1} - \alpha_n^* f_{n,J} + f_{n,J-1} = \delta_y^2 g_{n,J} \quad (25)$$

$$n = 1,2,\dots,M$$

$$J = 1,2,\dots,N$$

where

$$\alpha_n^* = 2 \left[ 1 - (\delta y / \delta x)^2 (\cos \theta_{n,2} - 1) \right].$$

The transforms and inverse transforms defined by equations 24 are computed by the fast Fourier algorithm of Cooley and Tukey (1965) while equations 25 are tri-diagonal and are easily solved for the  $f_{n,J}$ 's by Gauss elimination.

The assumed periodicity in  $x$  is automatically satisfied through equations 24. The boundary conditions at the walls (equation 6) are solved by setting  $\psi_{K,1}^{\ell} = \psi_{K,N}^{\ell} = 0$  for all times and the no slip condition is satisfied in the following way. We express  $\psi_{K,J}^{\ell}$  in terms of  $\psi_{K,1}^{\ell}$  through a Taylor series expansion about a point on the wall.

$$\begin{aligned}\psi_{K,2}^{\ell} &= \psi_{K,1}^{\ell} + A_1 \delta y + A_2 \delta y^2 + A_3 \delta y^3 + \dots \\ \psi_{K,3}^{\ell} &= \psi_{K,1}^{\ell} + 2A_1 \delta y + 4A_2 \delta y^2 + 8A_3 \delta y^3 + \dots \\ \psi_{K,4}^{\ell} &= \psi_{K,1}^{\ell} + 2A_1 \delta y + 9A_2 \delta y^2 + 27A_3 \delta y^3 + \dots \\ &\vdots \\ \text{etc.}\end{aligned}\tag{26}$$

The no slip condition ( $\partial\psi'/\partial y = 0$ ) is satisfied if we require that  $A_1 = 0$  which implies that (since  $\psi_{K,1}^{\ell} = 0$ )

$$\psi_{K,2}^{\ell} = \frac{1}{2} \psi_{K,3}^{\ell} - \frac{1}{9} \psi_{K,4}^{\ell}\tag{27a}$$

and

$$\psi_{K,N-1}^{\ell} = \frac{1}{2} \psi_{K,N-2}^{\ell} - \frac{1}{9} \psi_{K,N-3}^{\ell}\tag{27b}$$

for all  $k$  and  $\ell$ . The Poisson equation (5b) is satisfied (to second order) at the walls by

$$\zeta_{K,1}^{\ell} = 2A_2 = \frac{1}{\delta y^2} \left\{ \frac{3}{2} \psi_{K,3}^{\ell} - \frac{4}{9} \psi_{K,4}^{\ell} \right\}\tag{28a}$$

$$\zeta_{K,N}^{\ell} = \frac{1}{\delta y^2} \left\{ \frac{3}{2} \psi_{K,N-2}^{\ell} - \frac{4}{9} \psi_{K,N-3}^{\ell} \right\}\tag{28b}$$

The length of the time increment,  $\delta t$ , is fixed by the semi-empirical stability limit

$$\delta t = f \frac{\delta x}{\delta y} \left[ (U + u')_o \frac{\delta y + v'_o}{\delta x} \right] \quad (29)$$

where the velocity components  $(U + u')_o$  to  $v'_o$  are the maximum absolute magnitudes of velocity selected from a large sample of grid points.

Numerical experimentation has shown that for values of  $f \leq .6$  consistent results are obtained. Values of  $f$  near unity may lead to catastrophic instability in this explicit technique.

Since equation 20a is not "self starting" (it requires three time levels), the computation procedure starts with the forward difference representation

$$\begin{aligned} \frac{\zeta_{K,J}^{l+1} - \zeta_{K,J}^l}{\delta t} &= \frac{1}{2} \left\{ 3 \frac{\Psi_{K+1,J}^{l+1} - \Psi_{K-1,J}^{l+1}}{2\delta x} - U_J \frac{\zeta_{K+1,J}^{l+1} - \zeta_{K-1,J}^{l+1}}{2\delta x} \right. \\ &\quad \left. + J_{K,J}^{l+1} + \frac{1}{R_e} \Delta^2 \zeta_{K,J}^{l+1} \right\} \\ &+ \frac{1}{2} \left\{ 3 \frac{\Psi_{K+1,J}^l - \Psi_{K-1,J}^l}{2\delta x} - U_J \frac{\zeta_{K+1,J}^l - \zeta_{K-1,J}^l}{2\delta x} \right. \\ &\quad \left. + J_{K,J}^l + \frac{1}{R_e} \Delta^2 \zeta_{K,J}^l \right\}. \end{aligned} \quad (30)$$

Equation 30 is also used periodically during the calculations in order to suppress any instabilities associated with the central time differencing used in equation 20a.

The computation procedure can now be outlined step-by-step.

1. An initial distribution of  $\Psi_{K,J}^o$  is chosen and the corresponding  $\zeta_{K,J}^o$  are computed from equation 20b.

2. The time increment,  $\delta t$ , is computed from equation 29.
3. The values of  $\zeta_{K,J}^1$  are computed for all the interior points ( $J = 3, 4, \dots, N-2$ ) by iteratively solving equation 30.
4. The Fourier coefficients,  $g_{n,J}^1$  are computed from equation 24d, equation 25 is solved for the  $f_{n,J}^1$  and the corresponding values for the  $\Psi_{K,J}^1$  found from equation 24a for the interior points ( $J = 3, 4, \dots, N-2$ ).
5. The remaining grid points for  $\Psi_{K,J}^1$ ,  $\zeta_{K,J}^1$ ;  $J = 1, 2, N-1, N$  are computed from equations 27a, 27b, 28a,b and 20b.
6. For each time step the procedure in steps 3, 4, and 5 is repeated except the explicit central difference equation 20a is used in step 3 rather than equation 30.
7. Periodically, say every 50 time steps, a new time increment,  $\delta t$ , is computed (step 2) and a single time step using the implicit forward difference equation 30 is used.

For all of the computations presented in this paper a grid with dimensions  $M = 64$ ,  $N = 201$  was used which required a computation time of approximately 17 seconds per time step.

## 5. Linear Calculations

In an investigation such as this it is desirable to make some comparison between the results of our numerical computations and some known solution to the Navier Stokes equations. The imposed restraint of two dimensionality precludes any comparison with experimental data and, of course, there are no exact solutions to the non-linear equations of motion. The only alternative is to consider the limiting case of infinitesimal disturbances for which the results from linear theory

are available. For this reason, a rather thorough investigation of the linear solutions to equations 5a and 5b was undertaken. For small amplitude disturbances the non-linear terms in the vorticity transport equation are neglected and the equations of motion become

$$\frac{\partial \zeta'}{\partial t} + U \frac{\partial \zeta'}{\partial x} - 3 \frac{\partial \Psi'}{\partial x} = \frac{1}{R_e} \nabla^2 \zeta' \quad (31a)$$

$$\zeta' = \nabla^2 \Psi' \quad (31b)$$

The general solution to equations 31 can be expressed in the form

$$\Psi'(x, y, t) = \sum_{n=-\infty}^{\infty} \sum_{m=1}^{\infty} \Phi_{nm}(y) e^{-i(n\alpha x - \beta_{nm} t)} \quad (32a)$$

$$\zeta'(x, y, t) = \sum_{n=-\infty}^{\infty} \sum_{m=1}^{\infty} \theta_{nm}(y) e^{-i(n\alpha x - \beta_{nm} t)} \quad (32b)$$

with

$$\theta_{nm}'' = \Phi_{nm}'' - (n\alpha)^2 \Phi_{nm} \quad (32c)$$

$$\alpha = 2\pi/\lambda$$

where  $\lambda$  is the wavelength of the disturbance.

Substituting equation 32 into 31 results in the well known Orr-Sommerfeld equation for  $\Phi_{nm}(y)$ ; i.e.,

$$\begin{aligned} \Phi_{nm}^{IV} - 2(n\alpha)^2 \Phi_{nm}'' + (n\alpha)^4 \Phi_{nm} + i n\alpha R_e \left[ \left( U - \frac{\beta_{nm}}{n\alpha} \right) \left( \Phi_{nm}'' \right. \right. \\ \left. \left. - (n\alpha)^2 \Phi_{nm} \right) + U'' \Phi_{nm} \right] = 0 \end{aligned} \quad (33a)$$

with boundary conditions

$$\Phi_{nm} = \Phi'_{nm} = 0 \quad \text{at} \quad y = \pm 1. \quad (33b)$$

Solutions of 33a for  $\Phi_{nm}(y)$  for given  $\alpha$ ,  $n$ , and  $R_e$  can be made to satisfy the homogeneous boundary conditions (33b) only for the discrete eigenvalues,  $\beta_{nm}$ ,  $1 \leq m \leq \infty$ . For the given  $\alpha$ ,  $n$ , and  $R_e$  we are usually interested in determining if there exist corresponding  $\beta_{nm}$ 's which have negative imaginary parts. The corresponding disturbance,  $\Phi_{nm}(y)$ , then grows exponentially with time and the flow is unstable to disturbances at the specified  $\alpha$ ,  $n$ , and  $R_e$ .

For the present analysis we are interested in solutions to equation 20a; hence, we must consider the finite difference representation of the linearized equation. For small disturbances equation 20a becomes

$$\begin{aligned} \frac{\zeta_{K,J}^{l+1} - \zeta_{K,J}^{l-1}}{2\delta t} &= 3 \frac{\psi_{K+1,J}^l - \psi_{K-1,J}^l}{2\delta x} - U_J \frac{\zeta_{K+1,J}^l - \zeta_{K-1,J}^l}{2\delta x} \\ &\quad + 1/R_e \overline{\Delta^2} \zeta_{K,J}^l \end{aligned} \quad (34)$$

Again we will consider solutions of the form (32); hence, we have

$$\begin{aligned} \psi_{K,J}^l &= (\Phi_J)_{nm} e^{-i(n\alpha(k-1)\delta x - \beta_{nm} l \delta t)} \\ \zeta_{K,J}^l &= (\theta_J)_{nm} e^{-i(n\alpha(k-1)\delta x - \beta_{nm} l \delta t)} \end{aligned} \quad (35)$$

Substituting into 34 and 20b results in

$$\beta'_{nm} (\theta_J)_{nm} = i n \alpha' \left[ U_J (\theta_J)_{nm} + 3 (\Phi_J)_{nm} \right] + \frac{1}{R_e \delta y^2} \left[ (\theta_{J+1})_{nm} + \omega (\theta_J)_{nm} + (\theta_{J-1})_{nm} \right] \quad (36a)$$

$$(\theta_J)_{nm} = \frac{1}{\delta y^2} \left[ (\Phi_{J+1})_{nm} + \omega' (\Phi_J)_{nm} + (\Phi_{J-1})_{nm} \right] \quad (36b)$$

where

$$\omega = 2 \left( (\delta y / \delta x)^2 \cos n\alpha \delta x \right) \quad (37a)$$

$$\omega' = -2 \left[ 1 + \left( \frac{\delta y}{\delta x} \right)^2 (1 - \cos n\alpha \delta x) \right] \quad (37b)$$

$$\alpha' = \sin n\alpha \delta x / n \delta x \quad (37c)$$

and

$$\beta'_{nm} = 2 \left[ 1 + 1/R_e \delta x^2 \right] \cos \beta_{nm} \delta t + i \frac{\sin \beta_{nm} \delta t}{\delta t} \quad (37d)$$

$$i = \sqrt{-1}$$

When expression 36b for  $(\theta_J)_{nm}$  is substituted into equation 36a there results a homogeneous set of linear algebraic equations for the  $(\Phi_J)_{nm}$ . For given values of  $\alpha$ ,  $n$ ,  $R_e$ ,  $\delta x$ ,  $\delta y$ , and  $\delta t$  we wish to determine the eigenvalues and eigenvectors of the matrix of coefficients of the  $(\Phi_J)_{nm}$ . In particular, we are interested in those eigenvalues  $\beta_{nm}$  for which the imaginary part of  $\beta_{nm}$  is negative and in the associated eigenvectors  $(\Phi_J)_{nm}$ . The effects of  $\delta x$ ,  $\delta y$ , and  $\delta t$  on the linear solution are especially important for the present application.

The eigenvalues and eigenvectors have been computed for a number of Reynolds numbers and for a wide range of  $\alpha$ 's using the QR algorithm (Wilkinson 1965 or Fair 1971). For more details on these calculations the reader is referred to O'Brien (1970) or to the report by Gawain and Clark (1971). In the latter report some of the eigenvalues ( $\beta_{nm}$ ) and

eigenfunctions ( $\Phi_{nm}(y)$ ) are tabulated for the case  $\alpha = 1.0$ ,  $R_e = 6667$ . In the limit as  $\delta x$ ,  $\delta t \rightarrow 0$ , the problem is the same as that solved by Thomas (1953) although the methods used are quite different from those employed by Thomas. For the case  $\alpha = 1.0$ ,  $R_e = 6667$ , and  $\delta y = .01$  (in Thomas' notation this corresponds to  $\alpha = 1.0$ ,  $R_e = 10,000$ ,  $\delta y = .01$ ) we have solved equations 36 for  $n = 1, 2, 3$ , and 4. Our solutions show that there is only one unstable eigenvalue and this unstable solution occurs for  $n = 1$ . We shall order the eigenvalues,  $\beta_{nm}$ , so that for a given  $n$ , the  $m$ 's are arranged according to the stability of the computed eigenvalues. Hence, for the case  $\alpha = 1.0$ ,  $R_e = 6667$ ,  $\beta_{11}$  is the unstable eigenvalue with the corresponding eigenfunction  $\Phi_{11}(y)$ . Thomas gives a value of  $\beta_{11} = .3653 - i .0055$  and the corresponding mode shape,  $\Phi_{11}(y)$  is tabulated in his Table V. (Using our non-dimensionalization,  $\beta_{11}$  is exactly 1.5 times the value given by Thomas.) Our calculations yield the value  $\beta_{11} = .3593 - i .0041$  and the corresponding mode shape,  $\Phi_{11}(y)$ , is shown in Figure 3 for comparison with that of Thomas.

Now consider the influence of the finite difference parameters  $\delta x$ ,  $\delta y$ , and  $\delta t$  on the solutions to 36. The effect of  $\delta y$  on the growth rate ( $\beta_{11}$ ) is illustrated in Figure 4. As  $\delta y$  increases the flow becomes more and more stable and when  $\delta y = .05$ , the phenomenon of linear instability has been completely obscured by the crude finite difference representation of the equations of motion. Indeed, calculations with  $\delta y = .05$  for a wide range of Reynolds numbers and  $\alpha$ 's have shown no indication of linear instability.

The effect of varying  $\delta x$  was investigated at  $R_e = 6667$ ,  $\alpha = 1.0$ ,  $\delta y = .01$  and  $\delta t < .02$ . Figure 5 shows the variation with  $\delta x$  of the growth

rate ( $\Im \beta_{11}$ ) and phase velocity ( $\Re \beta_{11}$ ) for the unstable mode. For  $\delta x < .8$  the changes in the disturbance profile ( $\Phi_{11}(y)$ ) were insignificant.

Perhaps the most surprising discovery in this investigation of the linear behavior of the discrete representation of the equations of motion was the significance of the time interval,  $\delta t$ , on the disturbance growth rate ( $\Im \beta_{11}$ ). The effects of  $\delta t$  on this parameter are shown in Figure 6. There are significant departures from the "exact" value of  $\Im \beta_{11}$  for  $\delta t > .04$  while the phase velocity and mode shape are not significantly changed. Hence, in addition to the usual stability constraint (29) on the time interval,  $\delta t$ , it is necessary that  $\delta t < .04$  in the numerical integration scheme described in section 4.

We can now summarize the results presented in the preceding discussion. Increasing the  $y$  increment,  $\delta y$ , tends to make the flow more stable and for coarse grids ( $\delta y > .05$ ) the phenomenon of linear instability is completely obscured. The linear solution is comparatively insensitive to changes in  $\delta x$ , at least, until the  $x$ -increment is approximately the same length as the channel half-width. The growth rate of the disturbance is strongly influenced by the  $\delta t$  increment (due to the DuFort-Frankel representation of the diffusion term) and for large  $\delta t$  the growth rate is much higher than that predicted by the "exact" linear solution.

## 6. Numerical Integration of the Vorticity Equation

### (a) Small Amplitude Disturbances

We now return to the numerical integration of the vorticity equation using the techniques described in Section 4. As a check on the validity of the solution we first consider the limiting case of

small amplitude disturbances and compare the results obtained with the known results from the linear solution as described in the preceding section. To be more explicit, for a given Reynolds number and initial disturbance streamfunction,  $\psi'(x,y,0)$ , are the results from the numerical integration consistent with the values of  $\beta_{nm}$  and  $\Phi_{nm}(y)$  predicted by linear theory?

A series of calculations were made at  $R_e = 6667$  and the initial disturbance given by

$$\psi'(x,y,0) = \epsilon \left\{ f_1(y,0) e^{-i\alpha x} + f_1^*(y,0) e^{+i\alpha x} \right\} \quad (38)$$

where  $\epsilon$  is an amplitude factor. For  $\epsilon$  sufficiently small the non-linear terms in equation 5a should be negligible and the numerical integration should give results which are in agreement with the linear theory. As a first test we choose  $\alpha = 1.0$ ,  $R_e = 6667$ ,  $\epsilon = .005$  and the initial mode shape identical to the unstable mode computed from linear theory; i.e.,  $f_1(y,0) = \Phi_{11}(y)$ , where  $\Phi_{11}(y)$  was shown in Figure 3. The growth rate of the disturbance kinetic energy,  $\hat{E}(t)$ , as defined by equation 12c is shown in Figure 7. The computed growth rate gives a value of  $\beta_{11} = .0050$  which is in good agreement with the value given by Thomas. From equation 14 we can determine the phase,  $\varphi_n(y,t)$ , of any of the spectral components of  $\psi'(x,y,t)$  by

$$\varphi_n(y,t) \equiv \tan^{-1}(\Im f_n / \Re f_n) \quad (39)$$

The phase velocity,  $c_n$ , or rate of propagation, of any of the spectral components is then

$$c_n = \frac{1}{n\alpha} \frac{\partial \varphi_n}{\partial t} \quad (40)$$

For these computations the grid length,  $2L$ , was set equal to the wavelength,  $\lambda$ , of the disturbance; so for the disturbance (primary) mode,  $n = 1$ , and in the linear range we can identify  $c_1$  with  $\alpha \beta_{11}$  from the linear theory. Figure 10 shows that  $c_1$  is, indeed, a constant and the slope of this phase versus time plot shows that  $c_1 = .363$  which is in excellent agreement with Thomas' value of  $\alpha \beta_{11} = .3653$  and with our value of  $\alpha \beta_{11} = 3593$ .

Other short computations were carried out with, again,  $\alpha = 1.0$ ,  $R_e = 6667$ ,  $\epsilon = .005$ , but with the initial mode shape,  $f_1(y,0)$ , chosen to correspond to one of the stable modes computed from linear theory. These calculations were carried out by arbitrarily setting  $f_1(y,0)$  equal to the mode  $\Phi_{17}$ ,  $\Phi_{28}$ , and  $\Phi_{22}^*$  which are shown in Figure 9. The energy decay rates for these three cases are shown in Figure 10. From the energy decay rates and from the computed phase velocities (not shown here) the numerical integration technique yields the following values for the appropriate eigenvalues

$$\beta_{17} = 1.351 + i .138, \quad \beta_{28} = 1.425 + i .207$$

$$\beta_{22} = 1.456 + i .0764.$$

The linear matrix solution described in the preceding section gave the values

$$\beta_{17} = 1.363 + i .136; \quad \beta_{28} = 1.403 + i .192;$$

$$\beta_{22} = 1.462 + i .0742.$$

---

\* Since equation 33a is symmetrical in  $y$  it is possible to divide the solutions for  $\Phi_{nm}(y)$  into even and odd solutions. The boundary conditions are  $\Phi_{nm}(+1) = \Phi'_{nm}(+1) = 0$ , with  $\Phi''_{nm}(0) = \Phi'''(0) = 0$  for even solutions and  $\Phi_{nm}(0) = \Phi''_{nm}(0) = 0$  for odd solutions. For our numerical model with  $N$  lateral stations there are  $N-2$  unknown  $(\Phi_J)_{nm}$ 's; hence,  $N-2$  eigenvalues are computed for each  $n$ ,  $\alpha$ ,  $R_e$ . Of these  $N-2$  eigenvalues,  $\frac{N-1}{2}$  correspond to even solutions and  $\frac{N-3}{2}$  correspond to odd solutions.

A more critical test of the numerical integration is the ability to predict the correct mode shape,  $\Phi_{nm}(y)$ , for a disturbance of known wavelength and at a fixed  $R_e$ . Suppose in equation 38 we choose  $\alpha = 1.0$  but arbitrarily select the initial disturbance mode shape  $f_1(y,0)$ . The arbitrary function  $f_1(y,0)$  can be expressed in terms of the eigenfunctions,  $\Phi_{lm}(y)$ , of the Orr-Sommerfeld equation (33a) for the chosen  $\alpha$  and  $R_e$  (Schensted, 1961). i.e.,

$$f_1(y,0) = \sum_{m=1}^{\infty} A_m \Phi_{lm}(y) \quad (41a)$$

with

$$A_m = \int_{-1}^1 f_1(y,0) \chi_m(y) dy \quad (41b)$$

and

$$\chi_m(y) = \left( \frac{d^2}{dy^2} - \alpha^2 \right) \tilde{\Phi}_{lm}$$

where  $\tilde{\Phi}_{lm}(y)$  is the solution to the adjoint of equation 33a. However, the linear solution tells us that only one of the  $\Phi_{lm}$  in equation 41a is unstable; all other modes will decay with time. Hence, in the linear range only one mode,  $\Phi_{11}(y)$ , grows and will eventually dominate all the other terms in the expansion (41a). Therefore, the mode shape

$$f_1(y,t) \rightarrow \Phi_{11}(y) \text{ as } t \rightarrow \infty$$

where  $\Phi_{11}(y)$  is as shown in Figure 3 for the case  $\alpha = 1.0$ ,  $R_e = 6667$ . The initial shape chosen for  $f_1(y,0)$  is shown in Figure 11. The disturbance kinetic energy,  $\hat{E}(t)$ , is given in Figure 12 and the mode shapes,  $f_1(y,t)$ , are shown for various times during the calculations.

As expected, the disturbance energy at first rapidly decreases then grows according to linear theory while the computed mode shape is clearly tending towards the predicted shape of  $\Phi_{11}(y)$ .

From the results discussed in this section and from calculations at other wavenumbers,  $\alpha$ , we have found that the numerical integration scheme consistently gives results that are in excellent agreement with the linear theory. The agreement between the results of the numerical model and the predicted results for small amplitude disturbances is gratifying and gives some confidence in the non-linear calculations now to be discussed.

### b) Finite Amplitude Disturbances

Before discussing the results of the non-linear aspects of this investigation it is appropriate to give a very brief outline of the features of the existing non-linear theories which predict equations of the form of equation 1. The following discussion is from the paper by Pekeris and Shkoller (1967) which in turn outlines Stuart's (1960) theory for finite amplitude disturbances. If the Fourier representations for the disturbance streamfunction,  $\Psi'$ , and vorticity,  $\zeta'$ ; (equations 14 and 15) are substituted into the equation of motion (5a) the following equation for the modes results:

$$\frac{\partial g_n}{\partial t} = \frac{1}{R_e} (g_n'' - (n\alpha)^2 g_n) + i n \alpha [(U - f_o') g_n - (U'' - f_o'') f_n] \quad (42)$$

$$- i \alpha H_n \quad n = 0, 1, 2, \dots$$

where

$$g_n = f_n'' - (n\alpha)^2 f_n \quad (15c)$$

and

$$H_n = \sum_{s=1}^{\infty} \left\{ (n-s)(f_s' g_{n-s} - g_s' f_{n-s}) + (n+s)(f_s^{**} g_{n+s} - g_s^{**} f_{n+s}) \right\} \quad (42a)$$

If the parameter,  $\epsilon_0^2 \equiv |\beta_{11}|$ , is small (implying proximity to the neutral curve) then Stuart showed that in an approximation in which terms of order  $\epsilon_0^{3/2}$  are retained, only the  $f_0$ ,  $f_1$ , and  $f_2$  in (14a) are significant. Now expand  $f_1(y, t)$  in terms of the eigenfunctions,  $\Phi_{1m}$ , of the Orr-Sommerfeld equation as was done in equation (41a), so that

$$f_1(y, t) = \epsilon_0 \sum_{m=1}^{\infty} A_m(t) \Phi_{1m} \quad (43)$$

Stuart's asymptotic analysis for small  $\epsilon_0$  shows that only the first term in (43) is important, i.e.,

$$f_1(y, t) \approx \epsilon_0 A_1(t) \Phi_{11}(y) + O(\epsilon_0^3) \quad (44)$$

and that the terms  $f_0$  and  $f_2$  are of smaller order so that

$$f_0(y, t) = \epsilon_0^2 |A_1(t)|^2 G_0(y) + O(\epsilon_0^4) \quad (45)$$

$$f_2(y, t) = \epsilon_0^2 A_1^2(t) G_2(y) O(\epsilon_0)^4 \quad (46)$$

The functions  $G_0$  and  $G_2$  are determined from Pekeris and Shkoller's equations (22), (23), and (24). By substituting equations (44), (45), and (46) into (42) one can obtain an expression of the form (1) for the amplitude parameter,  $|A_1(t)|^2$ , i.e.,

$$\frac{d |A_1|^2}{dt} = k_1 |A_1|^2 + k_2 |A_1|^4 \quad (1)$$

The important point from our viewpoint is that according to the above analysis, the disturbance energy should be contained primarily in the  $f_1(y, t)$  mode and that the growth of this energy should behave according to equation (1). Assuming that the disturbance streamfunction can be adequately represented by  $f_1$  then we have from (44)

$$\psi'(x, y, t) = \epsilon_0 (A_1(t) \Phi_{11}(y) e^{-i\alpha x} + A_1^*(t) \Phi_{11}^*(y) e^{+i\alpha x}) \quad (47)$$

The disturbance kinetic energy as defined by equation (12c) (since we are neglecting the contribution from  $f_0$  the "disturbance" and "turbulent" kinetic energies are the same) becomes

$$\hat{E}(t) = \epsilon_0^2 I |A_1(t)|^2 \quad (48)$$

where

$$I = \int_0^1 \left\{ |\Phi'_{11}|^2 + \alpha^2 |\Phi_{11}|^2 \right\} dy \quad (49)$$

It was pointed out in part 2 of this paper that the constant,  $k_1$ , in (1) is related to the amplification factor of linear theory ( $k_1 = -2J \beta_{11}$ ) and if  $k_2 < 0$  then the growth of an unstable disturbance is limited so that

$$|A_1|^2 \rightarrow k_1/k_2 \quad (50)$$

Pekeris and Shkoller found that these conditions are satisfied for  $\alpha$  and  $R_e$  inside the lower portion of the neutral curve. For example, at  $R_e = 6667$  and  $\alpha = .90$  their calculations give

$$|A_1|^2 \rightarrow 1/9$$

Our solutions to the linear eigenvalue problem at  $R_e = 6667$  and  $\alpha = .875$  gives  $\beta_{11} = -.00394$  and  $I = 1.848$ . Hence,

$$\hat{E}(t) \rightarrow (1.848)(.00394)/9.0 = 8.08 \times 10^{-4}$$

Figure 13 shows the energy growth for modes  $E_0$ ,  $E_1$ ,  $E_2$ , and  $E_3$  for a run with the initial disturbance given by (38) with  $\alpha = .875$ ,  $R_e = 6667$ ,  $\epsilon = .005$ , and  $f_1(y,0) = \Phi_{11}(y)$  where  $\Phi_{11}$  is the unstable eigenfunction for  $\alpha = .875$ . The disturbance is, indeed dominated by  $E_1(t)$  and the mode shape,  $f_1(y,t)$ , normalized so that  $f_1(0,t) = 1.0$ , never departed from the initial shape given by  $\Phi_{11}(y)$ . A longer calculation was made using the same initial conditions except in this case  $\alpha = 1.0$ . Again the energy remained predominately in the  $n = 1$  mode and again the mode shape for  $f_1(y,t)$  never departed from the initial  $\Phi_{11}(y)$  shape indicating that (44) and (47) do indeed adequately represent the flow as far as the overall disturbance energy is concerned.

Although this latter calculation required 34.5 hours of computer time, we can see that the energy growth is still within the linear range. This demonstrates that, as was pointed out in part 2, it is impractical using the present techniques to follow the disturbance through the linear and into the non-linear range of amplitudes. For this reason we have been unable to establish whether or not the "supercritical" equilibrium states as predicted by (1) and (50) do, in fact, exist for our exact treatment. Our calculations, as shown in Figures 13 and 14, do indicate, however, that there is no significant

difference between cases for which  $\alpha = .875$  or  $\alpha = 1.0$  in equation (38).

The calculation of Pekeris and Shkoller, however, show that "super-critical" equilibrium states are possible for  $\alpha = .875$  but not for  $\alpha = 1.0$ . All our calculations for both low and high amplitude disturbances have shown no strong dependence on  $\alpha$  as far as the final result is concerned.

Although this last run was entirely within the linear energy growth range we will see that there were very interesting non-linear features to the calculations. The appearance of energy in modes  $E_0$ ,  $E_2$ , and  $E_3$  as shown in Figure 14 is, of course, due to the presence of the non-linear terms in equation (5a). In identical calculations for which the non-linear terms in (5a) were deliberately omitted the primary ( $n=1$ ) mode grew according to linear theory while the energy in the other modes remained constant or decreased and the energy levels (due to numerical "noise") were twelve to fifteen orders of magnitude lower than that of the primary mode. Figure 14 shows that the energy in the other modes ( $n = 0, 2, 3$ ) grows very rapidly at first and then seems to follow an exponential growth rate, i.e.,

$$E_n(t) \sim e^{2\beta_n t} \quad n = 0, 1, 2, 3$$

for large  $t$ . From the data shown in Figure 14 the values for  $\beta_n$  are  $\beta_0 = .0114$ ,  $\beta_1 = .0050$ ,  $\beta_2 = .0080$ , and  $\beta_3 = .0117$ .

The most interesting feature is the shape of the modes,  $f_2$ ,  $f_3$ , with respect to  $y^*$ . These shapes are shown in Figure 15 where the modes are normalized so that  $f_n(0,t) = 1.0$  for even modes and for odd modes the maximum real and imaginary parts of  $f_n(y)$  are unity. The phase velocities for these modes averaged between  $t = 65$  and  $t = 71$  were  $c_2 = .362$  and  $c_3 = .363$ . These phase velocities are the same as the phase velocity of the primary mode predictable from linear theory (i.e.,  $\beta_{11} = .363$ ).

The striking feature is the strong resemblance between these modes and the modes calculated from the Orr-Sommerfeld equation. Indeed, it appears that the non-linear solution has spontaneously generated modes that can be predicted from the linear theory even though the linear solution indicates that these are stable modes and would decay with time. This means that if we represent each mode by an expression of the form of (43) i.e.,

$$f_n(y,t) = \sum_{m=1}^{\infty} A_m(t) \Phi_{nm}(y) \quad (51)$$

\*From equation (15c) we see that  $g_n$  has the same symmetry or anti-symmetry as does  $f_n$ ; i.e. if  $f_n(y)$  is an even function of  $y$  then  $g_n$  is also even. Then from equation (42) we can establish that if  $\psi'(x,y,0)$  is given by (38) and  $f_1(y,0)$  is even in  $y$  then  $f_0(y,t)$  is odd,  $f_2(y,t)$  is odd,  $f_3(y,t)$  is even,  $f_4(y,t)$  is odd, etc. Likewise if  $f_1(y,0)$  is odd then  $f_0(y,t)$  is odd,  $f_2(y,t)$  even,  $f_3(y,t)$  odd,  $f_4(y,t)$  is even, etc. For example, let  $f_1(y,0)$  be even. Then since  $f_n(y,0) = 0$   $n \neq 1$

$$\frac{\partial g_2}{\partial t} \Big|_{t=0} = -i\alpha H_2 \Big|_{t=0} = -i\alpha [f_1' g_1 - g_1' f_1] \\ = \text{odd function of } y.$$

At the next time step,  $t = \delta t$

$$g_2(y, \delta t) = (\partial g_2 / \partial t) \delta t = \text{odd function of } y$$

then one mode seems to dominate the expansion. It is interesting to notice that in each case the dominant mode is one for which there exist a step gradient near the wall. Most of the stable modes that we have computed from linear theory are similar to the ones shown in Figure 9 which have a detailed structure near the center of the channel rather than near the wall.

A series of higher energy runs with various initial disturbance amplitudes was made at  $R_e = 6667$  using as initial conditions a disturbance with wave number  $\alpha = 1.0$  and that mode shape given by Thomas (see Figure 3). The total energy growth (or decay) is shown in Figure 16 for several different initial energy levels. A further energy breakdown is given in Figure 17 for the cases  $\epsilon = (.05)\sqrt{5}$ . For this case the total energy remains almost constant while there is a continual exchange of energy between the mean flow and the turbulence. The turbulent kinetic energy oscillates about a value of  $\hat{E}(t) = .03$  which is roughly ten times the equilibrium value predicted from equation 50. From Figure 14a it seems that there is a tendency towards some common energy equilibrium state for the different initial conditions. A more detailed inspection of the flow structure shows that there are significant differences between the three flows. Starting with the high energy run we summarize the structure of the flow by presenting plots of the mean velocity profile, Reynolds stresses, and energy spectrum at various times throughout the run (Figures 18, 19, and 20). Also, in Figure 21 the shape of the primary ( $n = 1$ ) mode at the end of the calculations is shown for each of the three energy levels. For the high energy run (although the time parameter is comparatively small) there are drastic

alterations of the mean velocity profile and primary mode shape and considerable energy transfer from the primary mode to the higher harmonics. For the two lower energy runs there is little alteration of the parabolic velocity profile and only small amounts of energy transfer to higher wave numbers. For the lowest initial energy level ( $\epsilon = .05 / \sqrt{2}$ ) the primary mode shape remains essentially unchanged throughout the entire calculation. More details of this low energy run are shown in Figure 22 where the growth of the total turbulent energy in the first three spectral components (equation 19b) is shown. The phase velocities (equation 40) were computed near the end of the run and are summarized below:

$$c_1 = .492, \quad c_2 = .484, \quad c_3 = .473$$

The measured  $C_n$  were independent of  $y$  and all are roughly 40% higher than the wave velocity ( $R_{B_{11}}$ ) of the primary unstable mode predicted by linear theory. This low energy run has some qualitative similarities to the predictions of the non-linear theory which was outlined at the beginning of this section. That is, there appears to be an asymptotic energy level, the primary mode shape is only slightly altered and the energy in the primary mode remains dominant.

In order to investigate the influence of initial wavenumber on the flow two runs were made at  $R_e = 6667$  with  $\alpha = .875$  (near the lower branch of the neutral curve) and with  $\alpha = 1.05$  (near the upper branch). For both cases the initial mode shape was determined from the eigenvalue solution to the linear equations and the initial energy was chosen to be slightly lower than that of the run ( $\epsilon = .05/\sqrt{5}$ ,

Figure 16) which seemed to remain in an energy equilibrium state. The energy variation for these cases is shown in Figure 23. There is no obvious qualitative difference between the three wavenumbers; the initial high energy level, however, apparently causes oscillations of the disturbance kinetic energy and makes any direct comparison with non-linear theory rather difficult.

Another important question which arises in the consideration of non-linear aspects in the stability of plane Poiseuille flows is whether or not a flow which is stable to infinitesimal disturbances might be unstable to disturbances of some finite amplitude. Such instabilities are generally referred to as "subcritical" instabilities. To investigate this aspect of the problem several runs were made using as initial conditions a disturbance that is known to be stable in the linear range. The case chosen was for  $\alpha = .78$ ,  $R_e = 6667$  for which  $\beta_{11} = .249 + i .00124$  for the least stable eigenfunction determined from the linear solution described in Section 5. Again the initial disturbance was given by equation 38 with the function  $f_1(y,0) = \Phi_{11}(y)$  determined from the linear solution. For a small amplitude disturbance ( $\epsilon = .005$ ) the disturbance energy decreased with time according to linear theory while for a larger amplitude ( $\epsilon = .0635$ ). The energy variation was as shown in Figure 24. The familiar oscillation of the turbulent kinetic energy which is associated with an initially high disturbance energy is present in this case; while the total kinetic energy appears to remain approximately constant after an initial decrease.

We now address ourselves to the question posed at the end of Section 2 concerning the character of a two dimensional "turbulence"

in channel flows. For all the runs discussed above the computational grid length ( $2L$ ) was equal to the wavelength of the initial unstable disturbance (i.e.  $2L = 2\pi/\alpha$ ). In any finite difference representation of the equations of motion there are only discrete wavelengths available to be excited by the non-linear interactions. Recall from equation 24a that the streamfunction is expressed as

$$\psi_{K,J} = \sum_{n=1}^M f_{n,J} e^{-i\theta_{n,k}} \quad (24a)$$

and since  $\psi_{K,J}$  is real

$$\Re f_{n,J} = \Re f_{M-n+2,J}$$

$$\Im f_{n,J} = -\Im f_{m-n+2,J}$$

i.e.,  $\Re f_{n,J}$  is even and  $\Im f_{n,J}$  is odd over the interval  $n = 1, 2, \dots, M/2, \dots, M$ . Therefore, there are  $M/2$  distinct Fourier modes "available" to the solution of the equations of motion. When the grid length equals the wavelength of the initial disturbance there is only one lower mode available to be excited; namely, the zero mode,  $f_{0,J}$ . It is known that two-dimensionality constrains the transfer of energy between the modes of which the disturbance is composed. For an isotropic two-dimensional turbulence there can be no systematic transfer of energy from lower to higher wave numbers without a corresponding transfer to still lower wavenumbers (Lilly (1968), Kraichnan (1967)). Hence, one may suspect that our discrete representation in which there are no available modes at lower wave numbers could force the disturbance energy to remain in the primary initial mode. The first

alternative to this dilemma would seem to be to increase the grid length,  $2L$ , thereby allowing modes with both higher and lower wave numbers to fit into the available grid length. However, if the initial disturbance energy is contained in, say, wave number  $n$  then the non-linear interaction of this mode with itself will initially excite wave numbers  $0$  and  $2n$ ; later modes  $0, 2n, 3n, 4n$ , etc. The modes that can be excited will be separated by a spacing of  $n$  in wave number space, resulting in a spectrum with "holes" or regions in which no energy can appear. Clearly, this is not a realistic case. The alternative to this situation is to initially perturb the flow with a disturbance in which at least two contiguous (in the discrete wave number space) modes are present. For example, if the initial disturbance contains modes  $n$  and  $n+1$  then the non-linear interaction will, at first, excite modes  $0, 1, 2n, 2n+1, 2n+2$ ; these in turn will excite modes  $0, 1, n-1, 2n-1, 4n$ , etc. until all possible wave numbers have been excited.

It seems reasonable to require that the wavelengths of these two initial modes should both fall within the unstable region in the  $(\alpha - R_e)$  plane. If we set the grid length so that  $2L=16\pi$  (or  $\alpha = 1/8$ ) then modes with wavenumbers  $7\alpha$  and  $8\alpha$  will both fall within the unstable region. Hence

$$\psi'(x, y, 0) = \epsilon \{ f_7 e^{-i7\alpha x} + f_8 e^{-i8\alpha x} + f_7^* e^{+i7\alpha x} + f_8^* e^{+i8\alpha x} \}$$

A lengthy numerical integration of the vorticity equations using the initial conditions just described is summarized in Figures 25 and 26 which show the turbulent kinetic energy time variation and the energy spectrum at various times during the run. For this run the turbulent kinetic energy initially grows and then appears to vary randomly about a value of  $\hat{E}(t) = .019$ . The energy spectrum is quite different from the other cases presented in that there is a gradual transfer of significant amounts of energy to other wavenumbers. Although it is not shown here, the mean velocity profile again differed only slightly from the parabolic distribution. Although, there are significant differences between this run and the others presented, all the examples that have been discussed are qualitatively similar in that most of the energy remains in modes whose wavelength approximately equals that of the primary (unstable) mode.

## 7. Conclusion

Our numerical technique for integrating the vorticity equation has been shown to be stable and predicts results that are consistent with linear solutions to the vorticity equation.

The influence of the finite difference representation on the linear eigenvalue solution to the equations of motion was investigated and some interesting conclusions resulted. The size of the  $\delta y$  increment significantly influences the stability of the equations and for grids with  $\delta y > .05$  (approximately) the equations are stable to all disturbance. Because of the DuFort-Frankel representation of the diffusion term, the growth rate of an unstable disturbance is strongly influenced by the  $\delta t$  increment. The growth rate increases

rapidly with  $\delta t$  even though the time step increment may still be small enough to satisfy ordinary numerical stability requirements.

The  $\delta x$  increment has the smallest effect on the linear solution and seems to be significant only when  $\delta x$  is approximately equal to the channel half-width.

Because of the long computing time required we were unable to follow the growth of an unstable disturbance through the linear and into the non-linear range of disturbance amplitudes. This precluded any direct comparison of our results with those predicted by the non-linear theories of Stuart and Watson and Reynolds and Potter. We can, however, make some general comparisons. We find qualitative agreement in the sense that the unstable primary mode dominates the disturbance and there is little distortion of the mean flow. The calculations presented indicate the existence of a disturbance energy equilibrium state which seems to be common (for a given Reynolds number) to all unstable disturbances despite their initial energy or wavenumber. Indeed, we have found no outstanding differences in the behaviour of disturbances with varying initial wave numbers (at a constant  $R_e$ ) which is not in agreement with the non-linear theories. The distortion of the primary mode shape is significant when the initial energy is high enough to be well beyond the linear range but for lower initial energies the distortion of the mode shape is less important.

The computed flows which have been discussed in this paper show little resemblance to actual turbulent shear flows. In a true three dimensional flow one would expect an initial unstable disturbance

with a length scale approximately  $2\pi$  times the channel half width to grow in amplitude and through non-linear interactions the energy of the disturbance would be transferred to higher wavenumbers with length scales comparable to the channel half width. The corresponding situation for a two dimensional turbulent channel flow is not clear. However, for two dimensional homogeneous turbulence the energy would cascade to the lower wavenumbers while mean square vorticity is transferred to higher wavenumbers when the turbulent energy is continually fed into the flow in a narrow band of spectral components. Neither of these processes was observed for the present calculations.

One can speculate that our calculated "quasi-equilibrium" states in which most of the energy remains in one or two spectral components with little alteration of the parabolic velocity profile represent two dimensional solutions to the equations of motion which are, in some sense, highly unstable flows and, for this reason, are not observed experimentally.

#### REFERENCES

1. Arakawa, A., 1966 "A Computational Design for Long Term Numerical Integration of the Equations of Fluid Motion: Two Dimensional Incompressible Flow, Part 1." J. Comp. Physics, 1, 1, pp. 119-143.
2. Cooley, J. W. and Tukey, J. W., 1965. "An Algorithm for the Machine Calculation of Complex Fourier Series," Math Comp., 19, 90, pp. 297-301.
3. DuFort, E. G. and Frankel, S. P., 1953. "Stability Conditions in the Numerical Treatment of Parabolic Differential Equations," Math Tables and Other Aids to Computation, 7, pp. 135-152.
4. Emmons, H. W., 1970. "Critique of Numerical Modeling," in Annual Review of Fluid Mechanics, Vol 2, Palo Alto, California: Annual Reviews, Inc.
5. Fair, G., 1971. "Allmat: A TSS/360 Fortran IV Subroutine for Eigenvalues and Eigenvectors of a General Complex Matrix," NASA TN D-7032.
6. Gawain, T. H. and Clark, W. H., 1971. "Tables of Eigenvalues and Eigenfunctions of the Orr-Sommerfeld Equation," to be published as Naval Postgraduate School Report, Monterey, California.
7. Kraichnan, R. H., 1967. "Inertial Ranges in Two-Dimensional Turbulence," Phys Fluids. 10, 7.
8. Lilly, D. K., 1970. "The Numerical Simulation of Three-Dimensional Turbulence with Two Dimensions." V. VII, SIAM-AMS Proceedings, American Mathematical Society, pp. 41-53.
9. O'Brien, G. D., 1970. "A Numerical Investigation of Finite-Amplitude Disturbances in a Plane Poiseuille Flow," Naval Postgraduate School, Ph.D. thesis.
10. Pekeris, C. L. and Shkoller, B., 1967. "Stability of Plane Poiseuille Flow to Periodic Disturbances of Finite Amplitude in the Vicinity of the Neutral Curve," JFM 29, 1.
11. Reynolds, W. C. and Potter, M. C., 1967. "Finite Amplitude Instability of Parallel Shear Flows," JFM 27, 3.
12. Schensted, I. V., 1961. "Contributions to the Theory of Hydrodynamic Stability," University of Michigan, Ph.D. Thesis.

13. Stuart, J. T., 1960. "On the Non-linear Mechanics of Wave Disturbances in Stable and Unstable Parallel Flows," part 1. JFM 9, 2.
14. Thomas, L. H., 1953. "The stability of Plane Poiseuille Flow," Phys Rev., 91, 4, pp. 780.
15. Watson, J., 1960. "On the Non-linear Mechanics of Wave Disturbances in Stable and Unstable Parallel Flows," part 2. JFM 9, 2.
16. Wilkinson, J. A., 1965. The Algebraic Eigenvalue Problem, pp. 485-569, Clarendon Press.

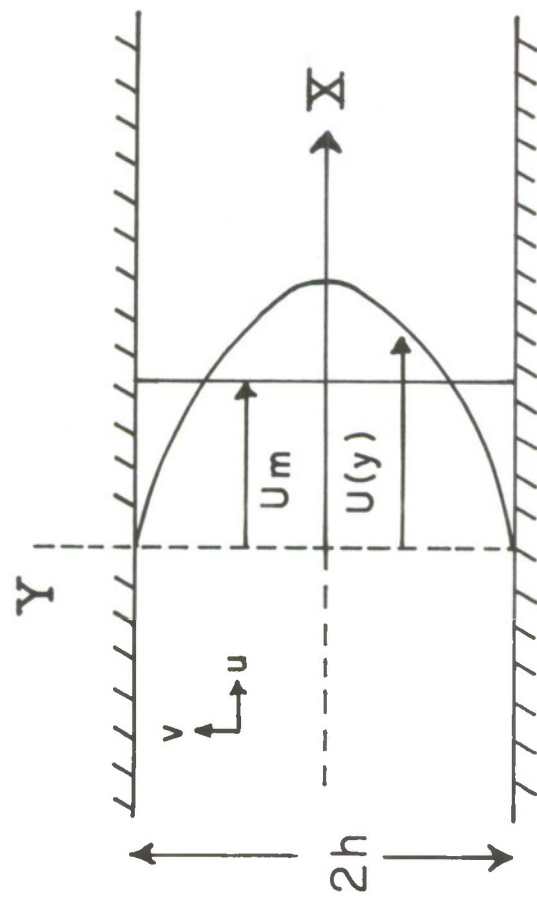


Figure 1.  $R_e = U_m / v ; \quad y = Y/h , \quad x = X/h$   
 $U(y) = 3/2 (1 - y^2)$

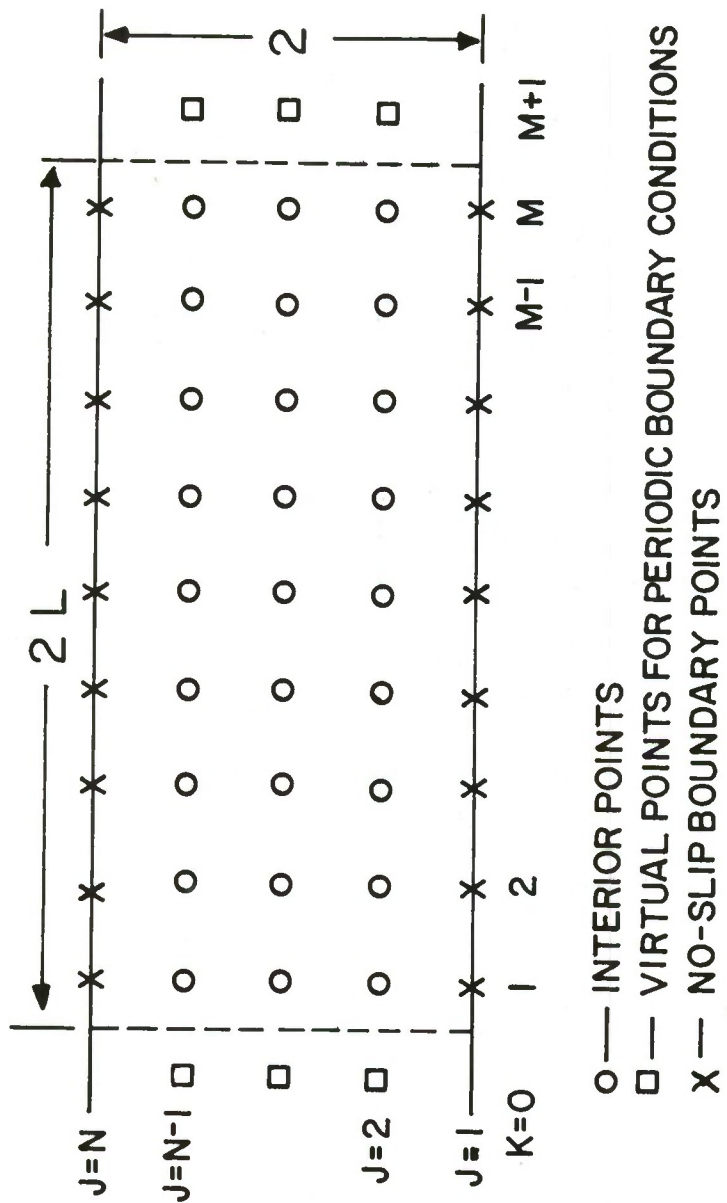


Figure 2. Finite Difference Mesh

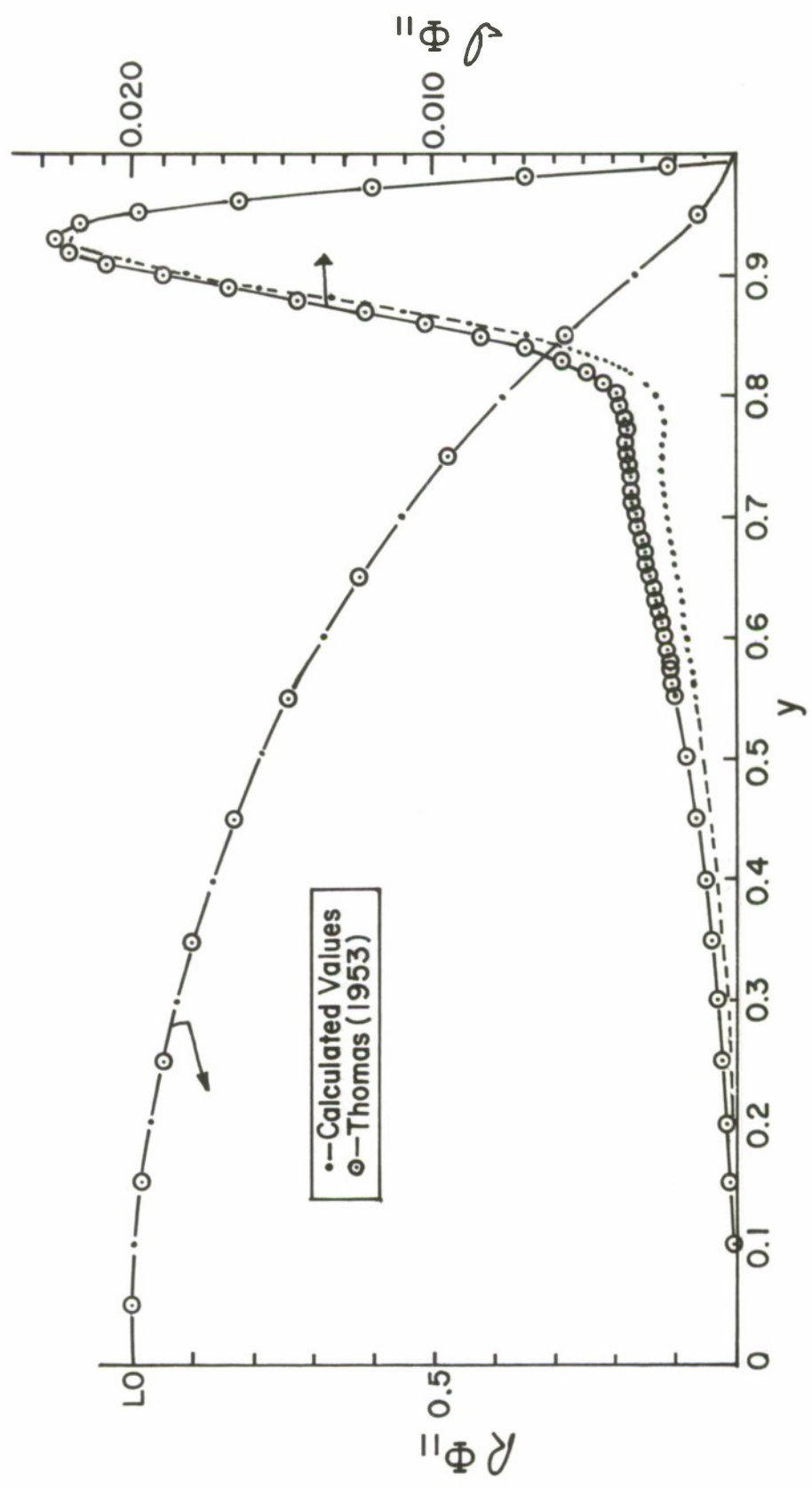


Figure 3. Comparison of the Eigenfunction,  
 $\Phi_{11}$ , for  $R_e = 6667$ ,  $\alpha = 1.0$ .

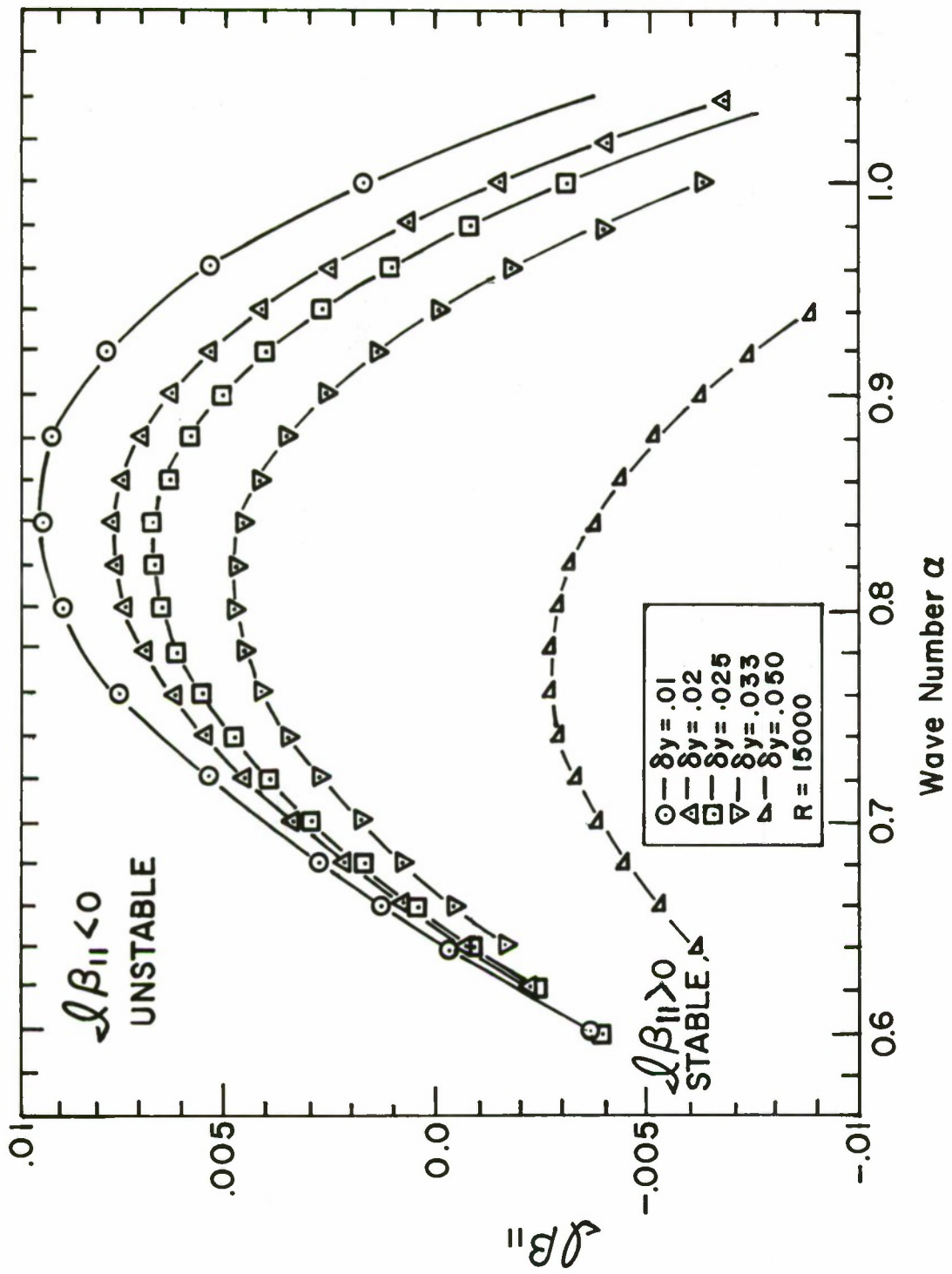


Figure 4. Effect of Grid Parameter,  $\delta y$ , on the Disturbance Growth Rate

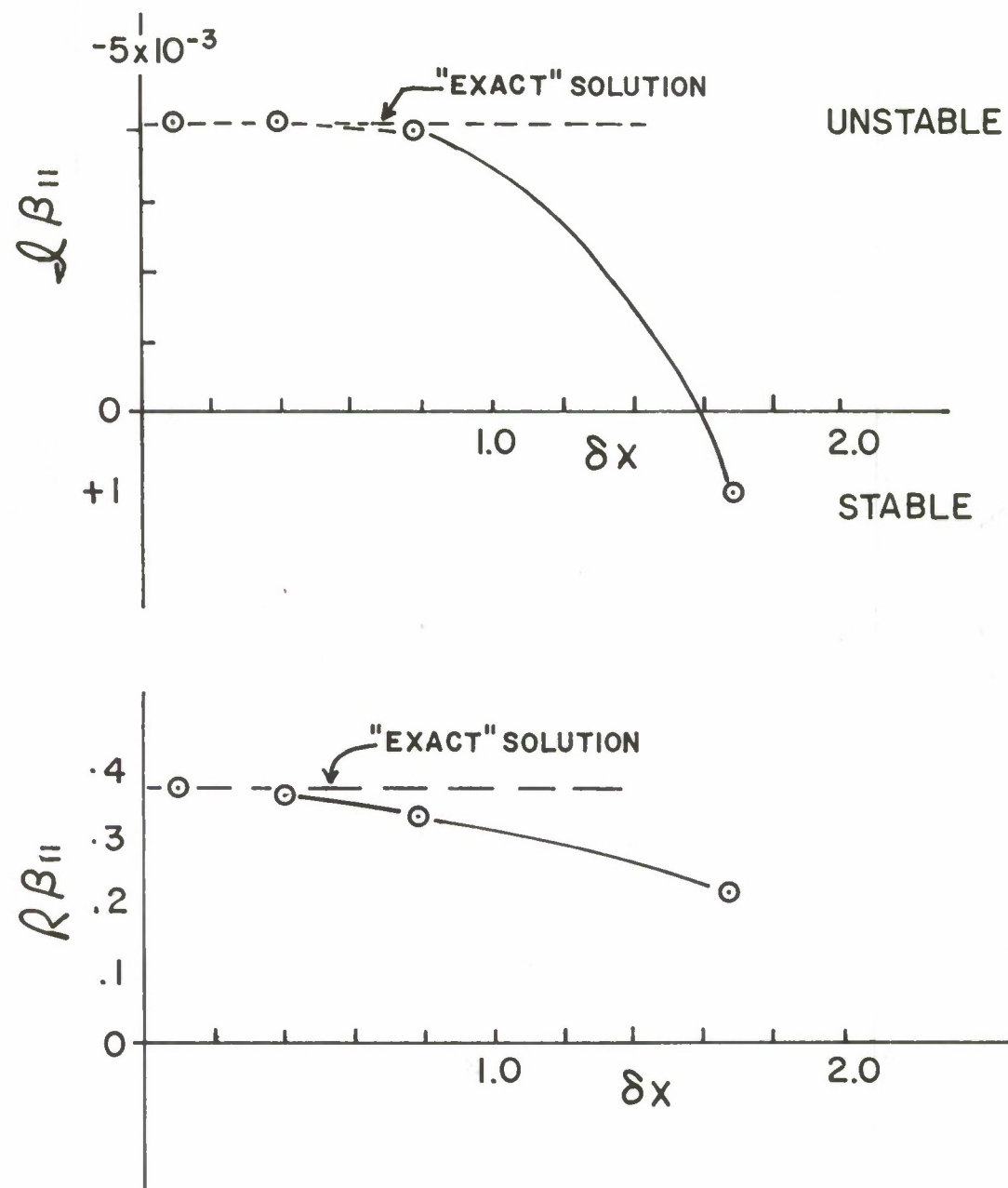


Figure 5. Effect of Grid Parameter,  $\delta x$ ,  
on the Eigenvalue,  $\beta_{11}$

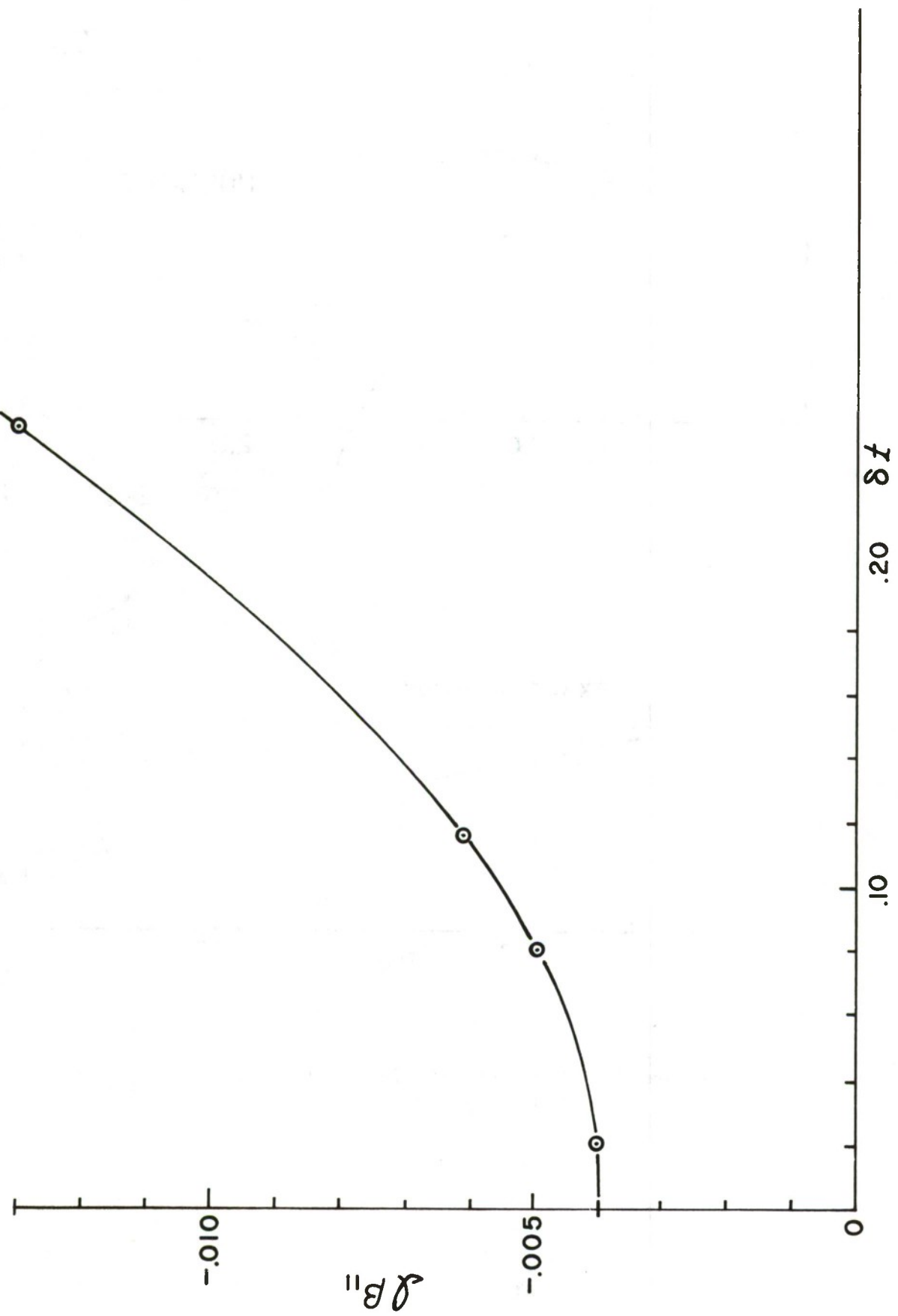


Figure 6. Effect of Grid Parameter,  $\delta t$ , on the Disturbance Growth Rate,

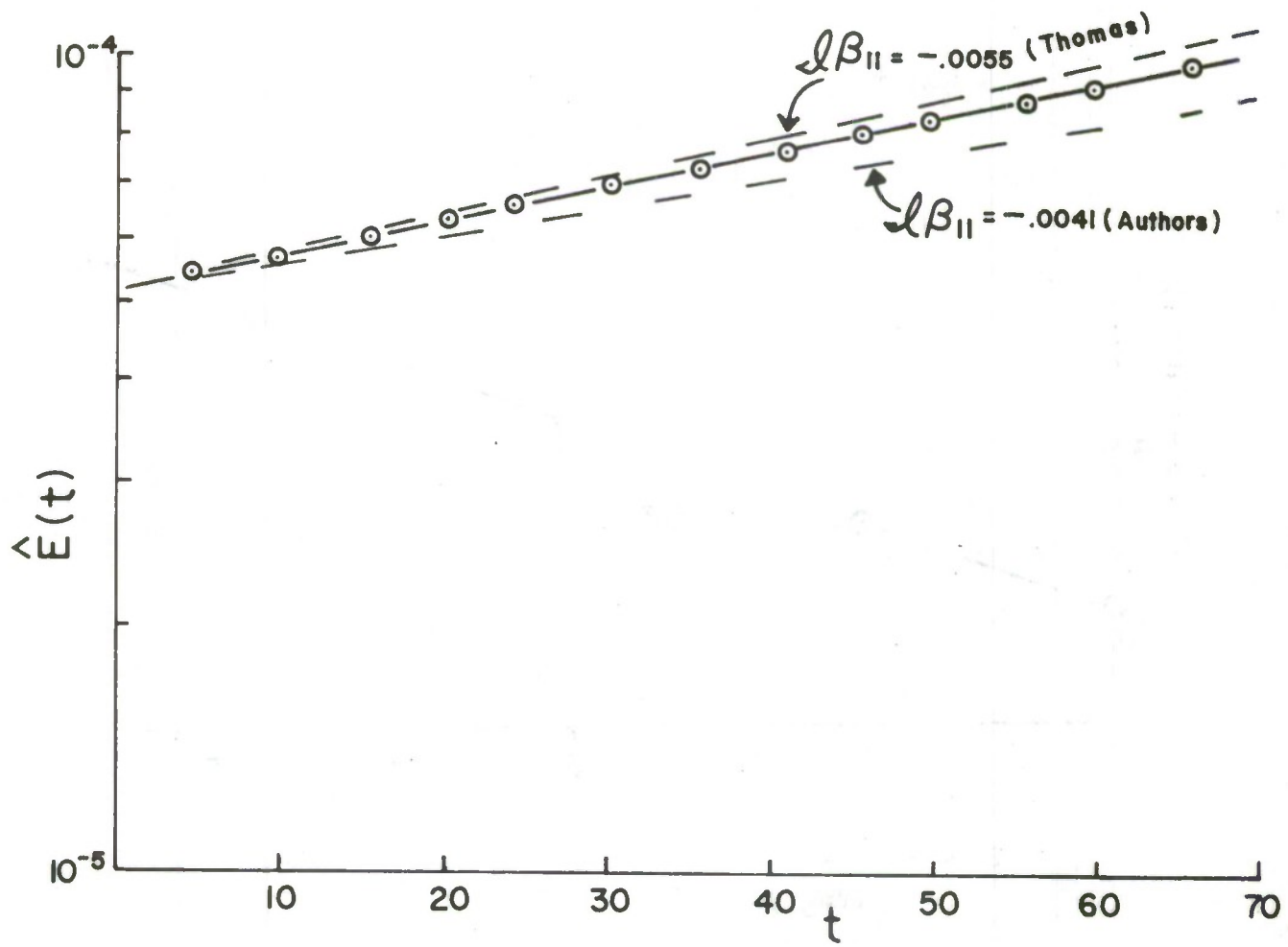


Figure 7. Energy Growth for a Low Amplitude Run.  
 $R_e = 6667$ ,  $\alpha = 1.0$

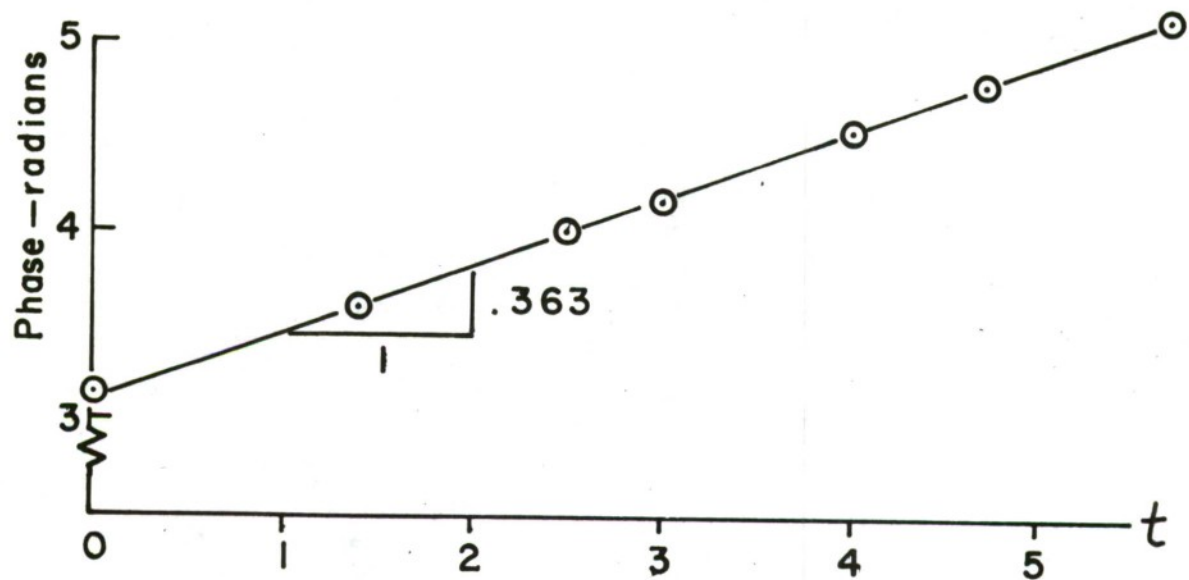


Figure 8. Phase,  $\varphi_1$ , Variation for a Low Amplitude Run.  $R_e = 6667$ ,  $\alpha = 1.0$

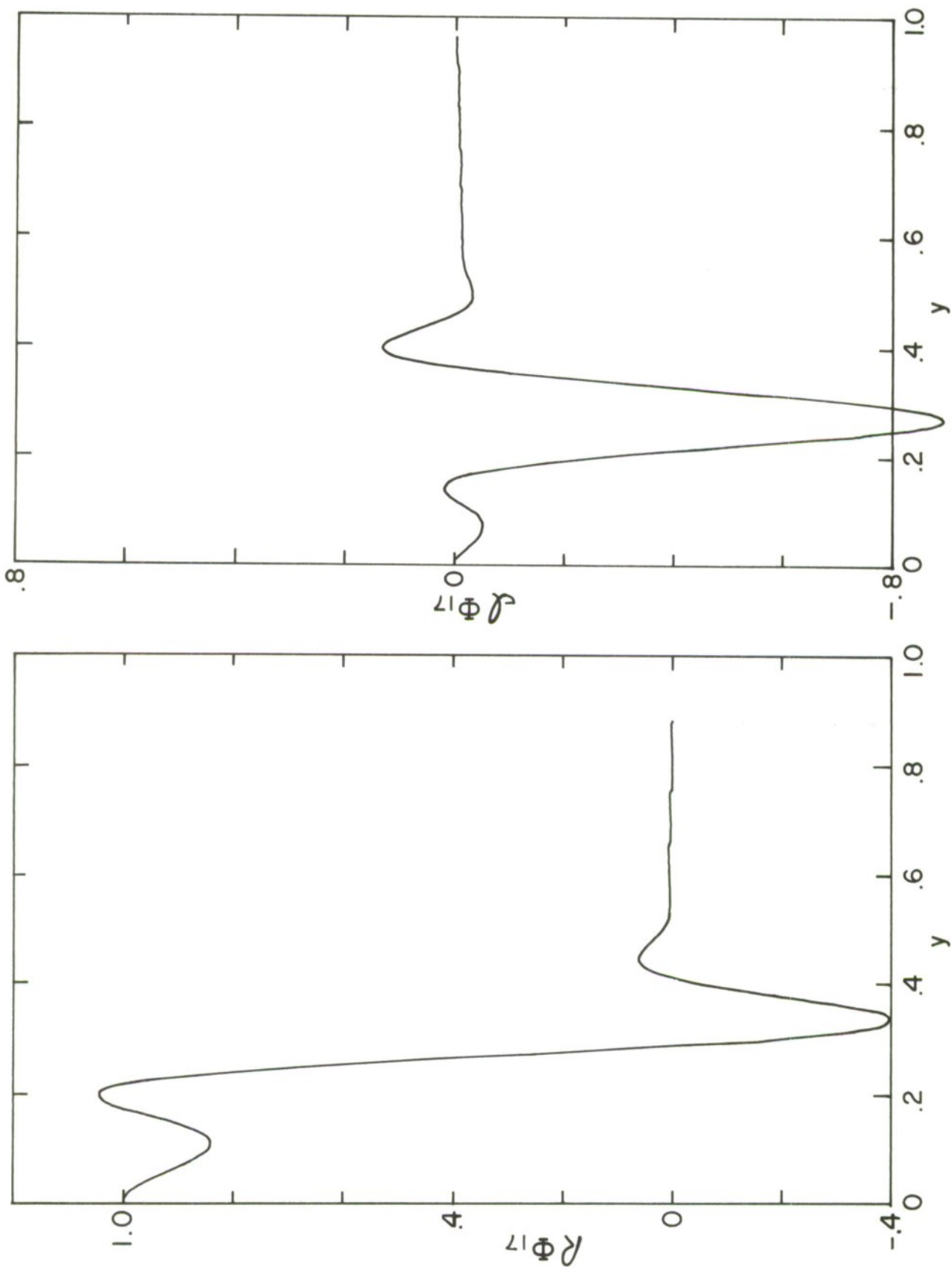


Figure 9a. Eigenfunction,  $\psi_{17}$ (even), for  $R_e = 6667$ ,  
 $\alpha = 1.0$

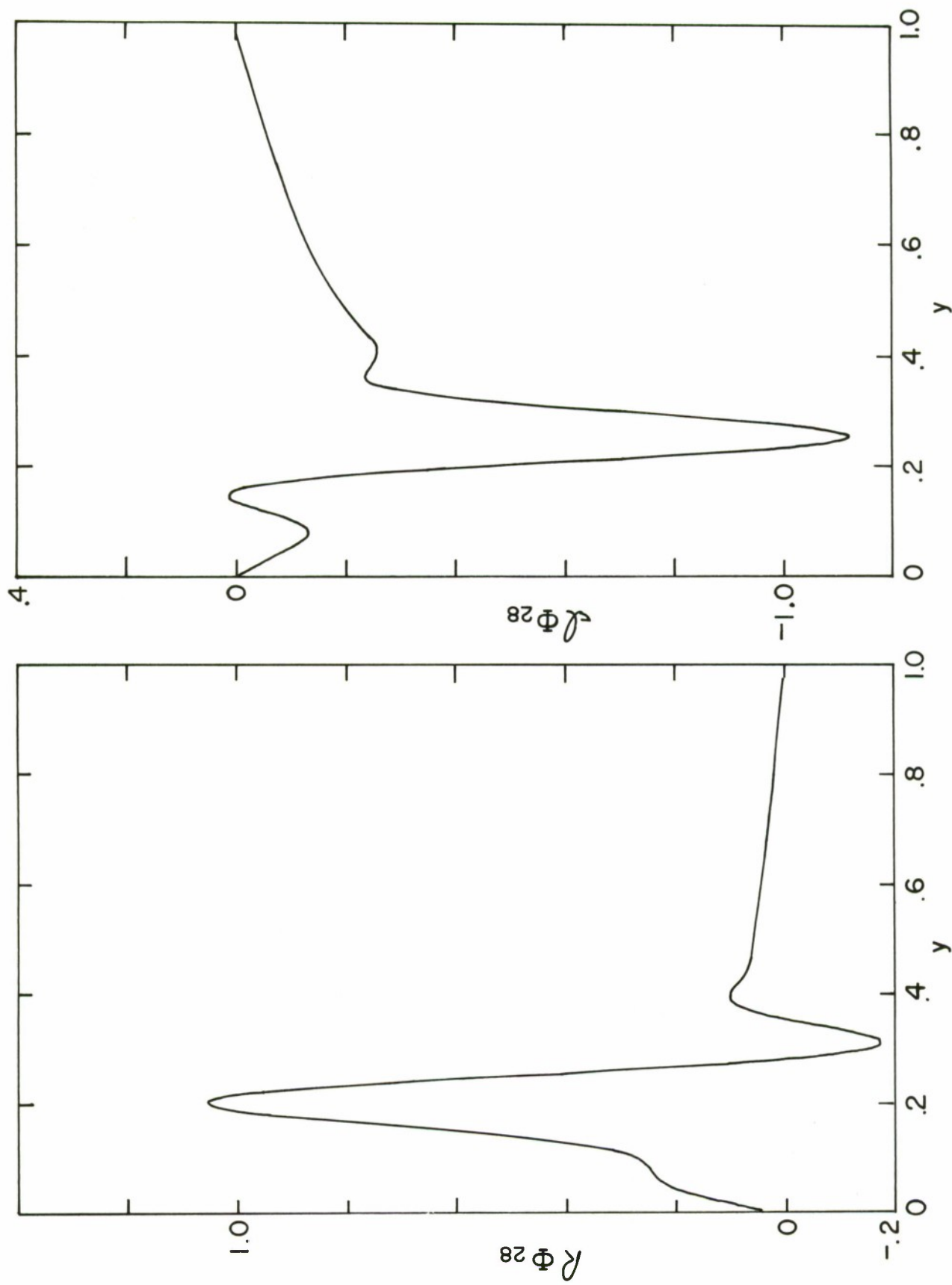


Figure 9b. Eigenfunction,  $\Phi_{28}$  (odd), for  $R_e = 6667$ ,  
 $\alpha = 1.0$

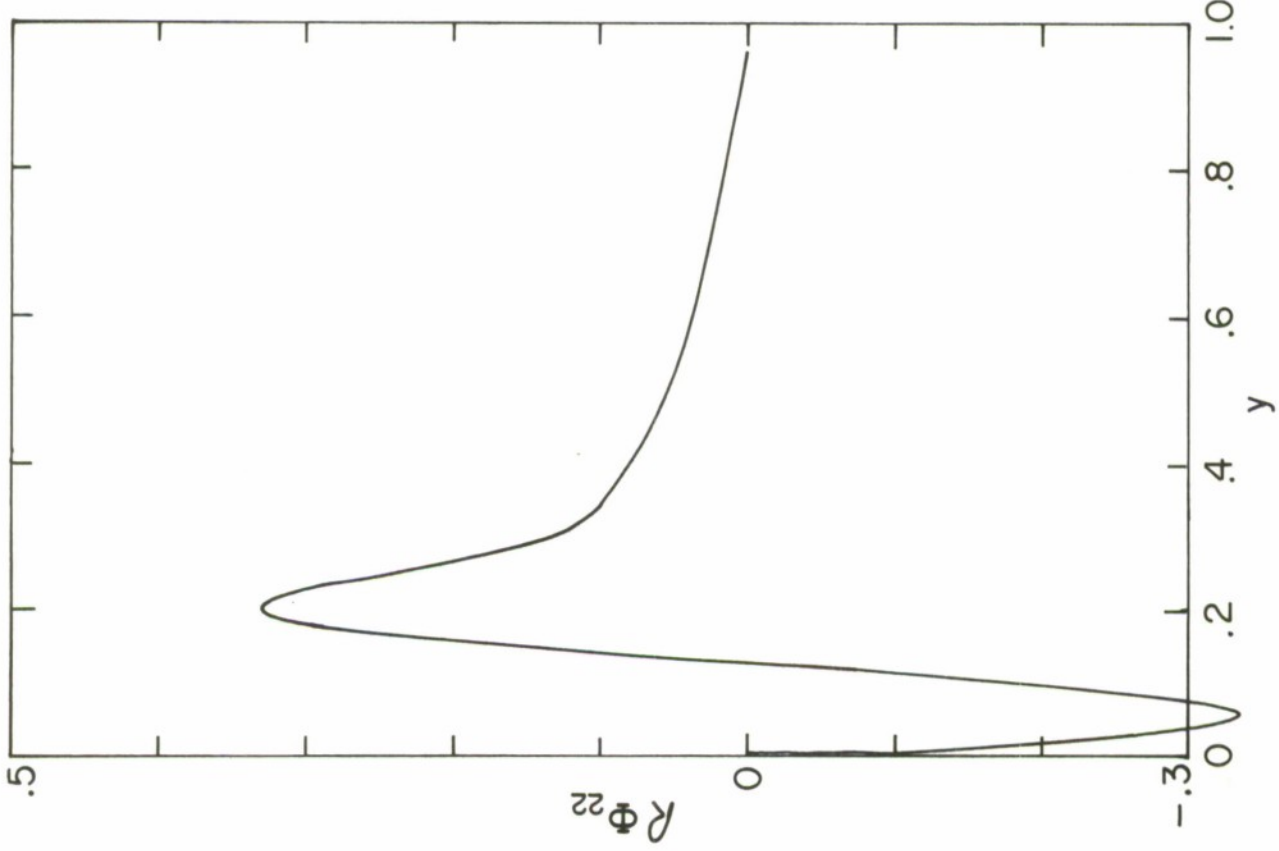
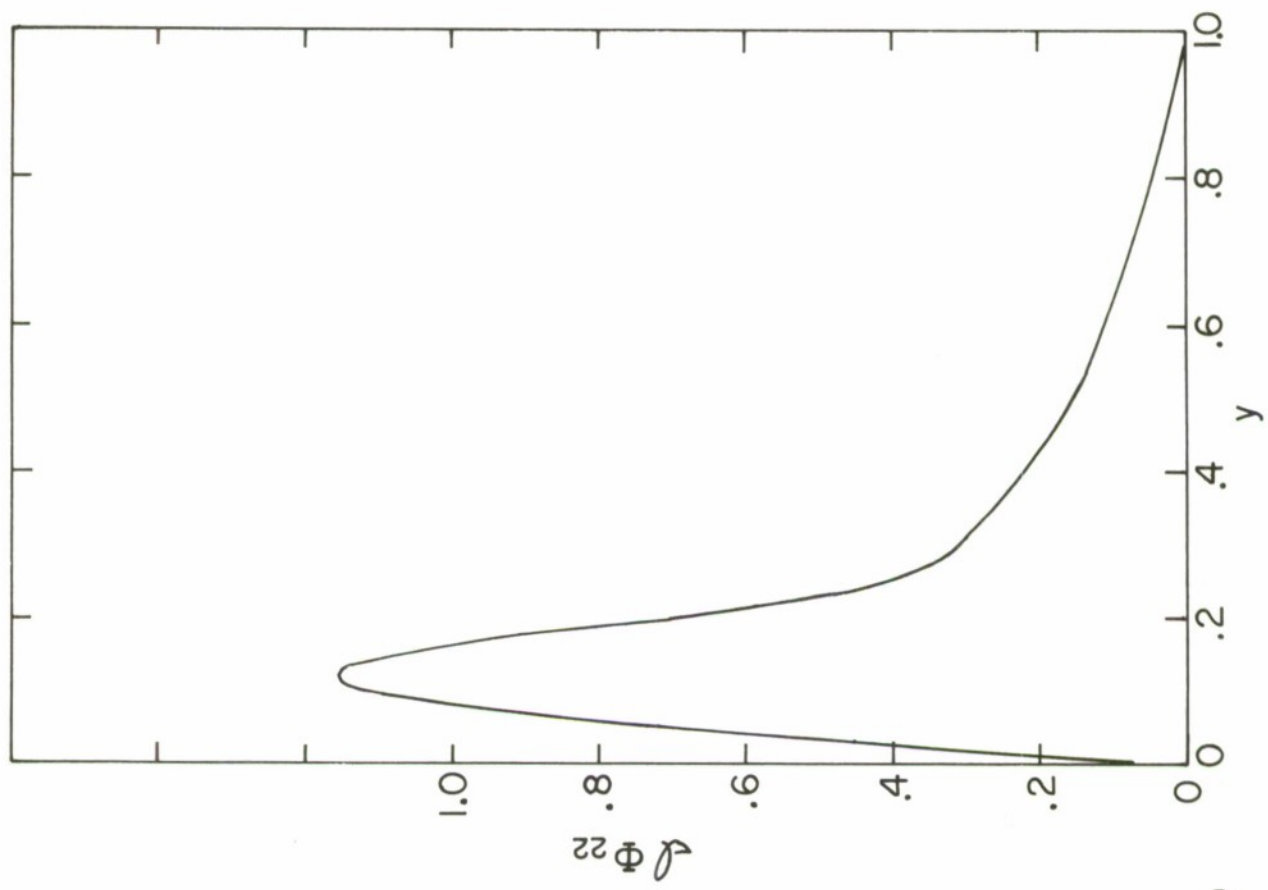


Figure 9c. Eigenfunction,  $\Phi_{22}$  (odd), for  $R_e = 6667$ ,  
 $\alpha = 1.0$

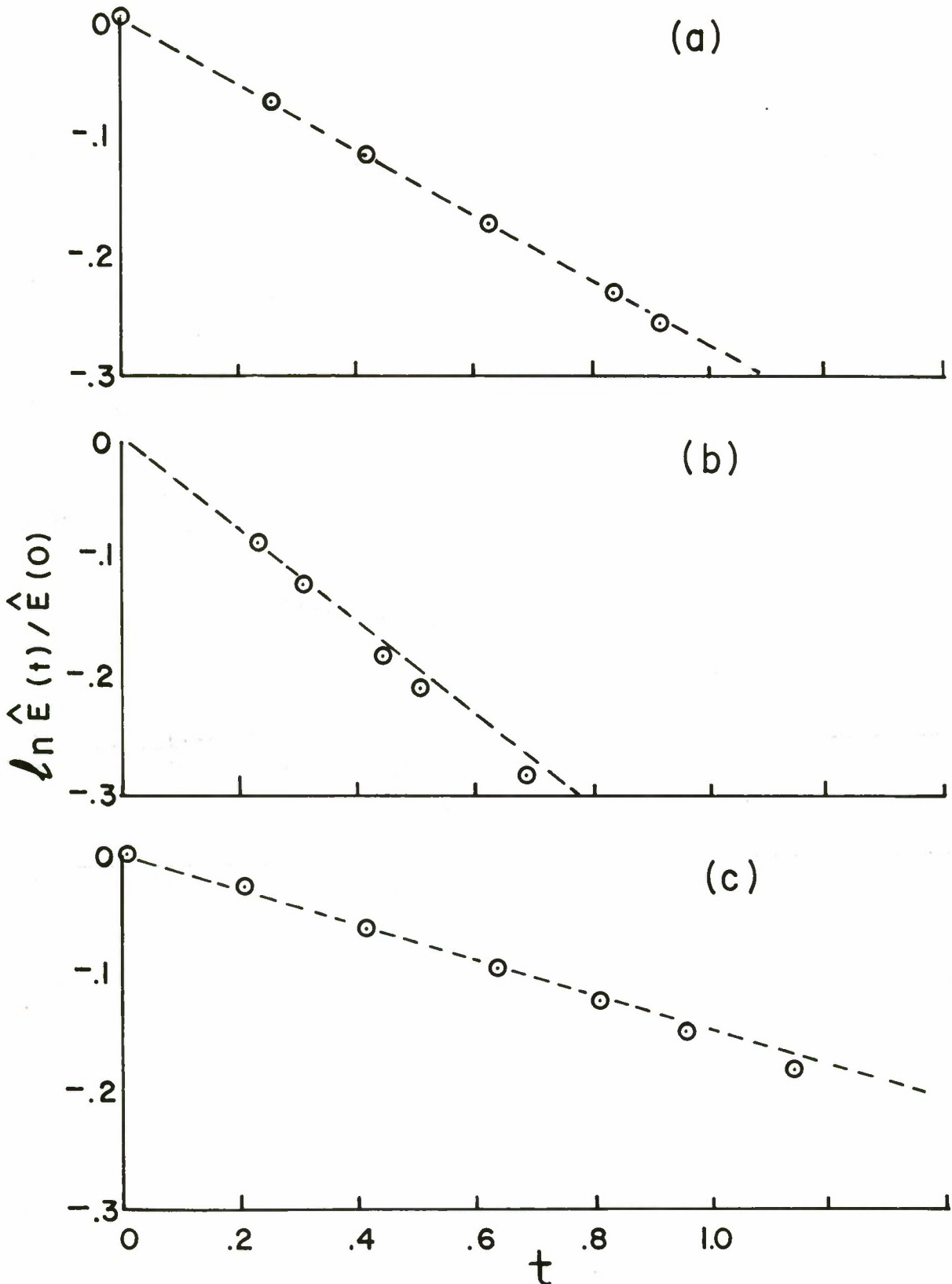


Figure 10. Computed Energy Decay for (a)  $\phi_{17}$ , (b)  $\phi_{28}$ ,  
 (c)  $\phi_{22}$ . Dashed line represents decay rate  
 predicted from linear theory

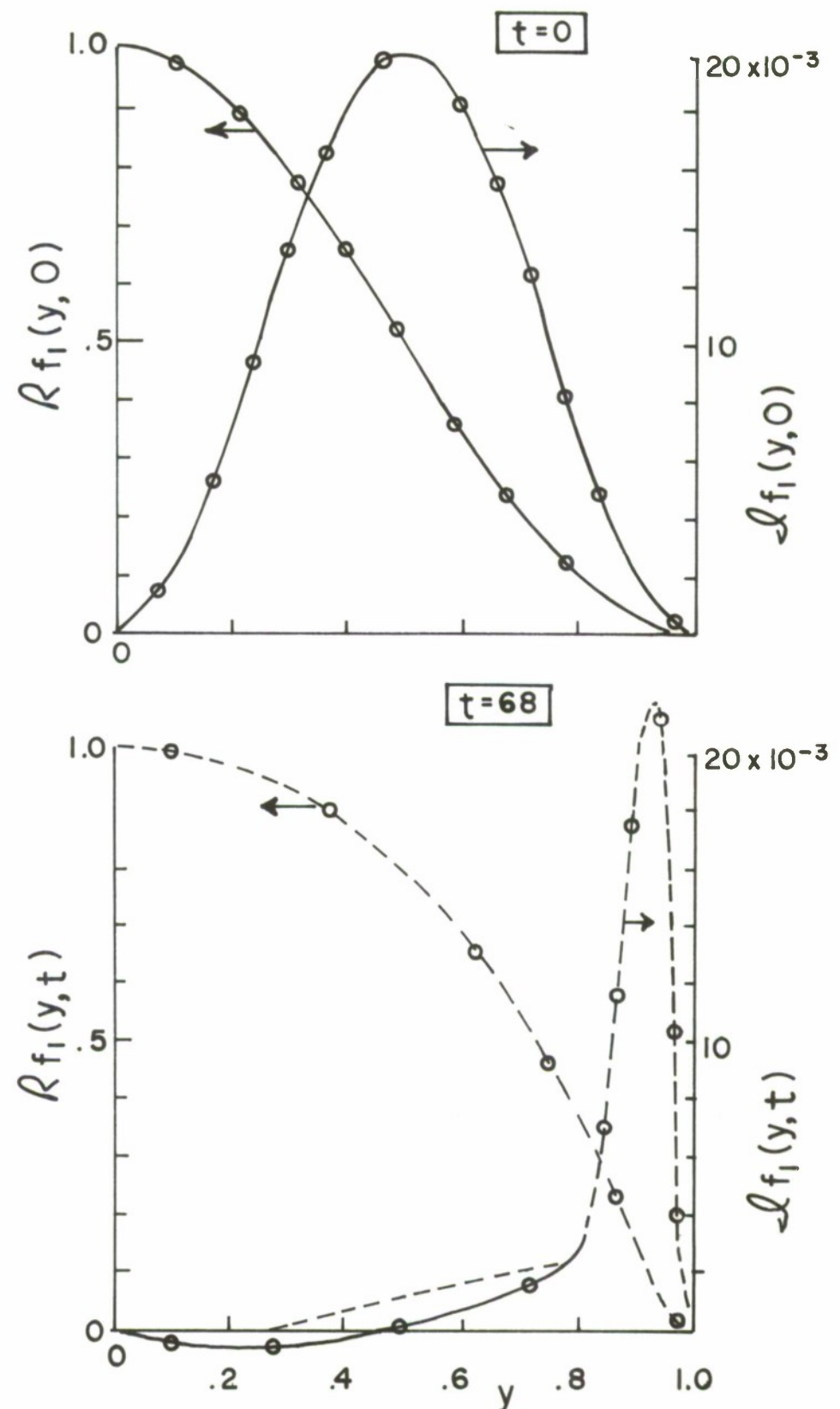


Figure 11. Primary Mode Shape,  $f_1$ , for a Low Energy (Linear) Run at Times  $t=0$  and  $t=68$ .  
Dashed Line Represents  $\Phi_{11}$

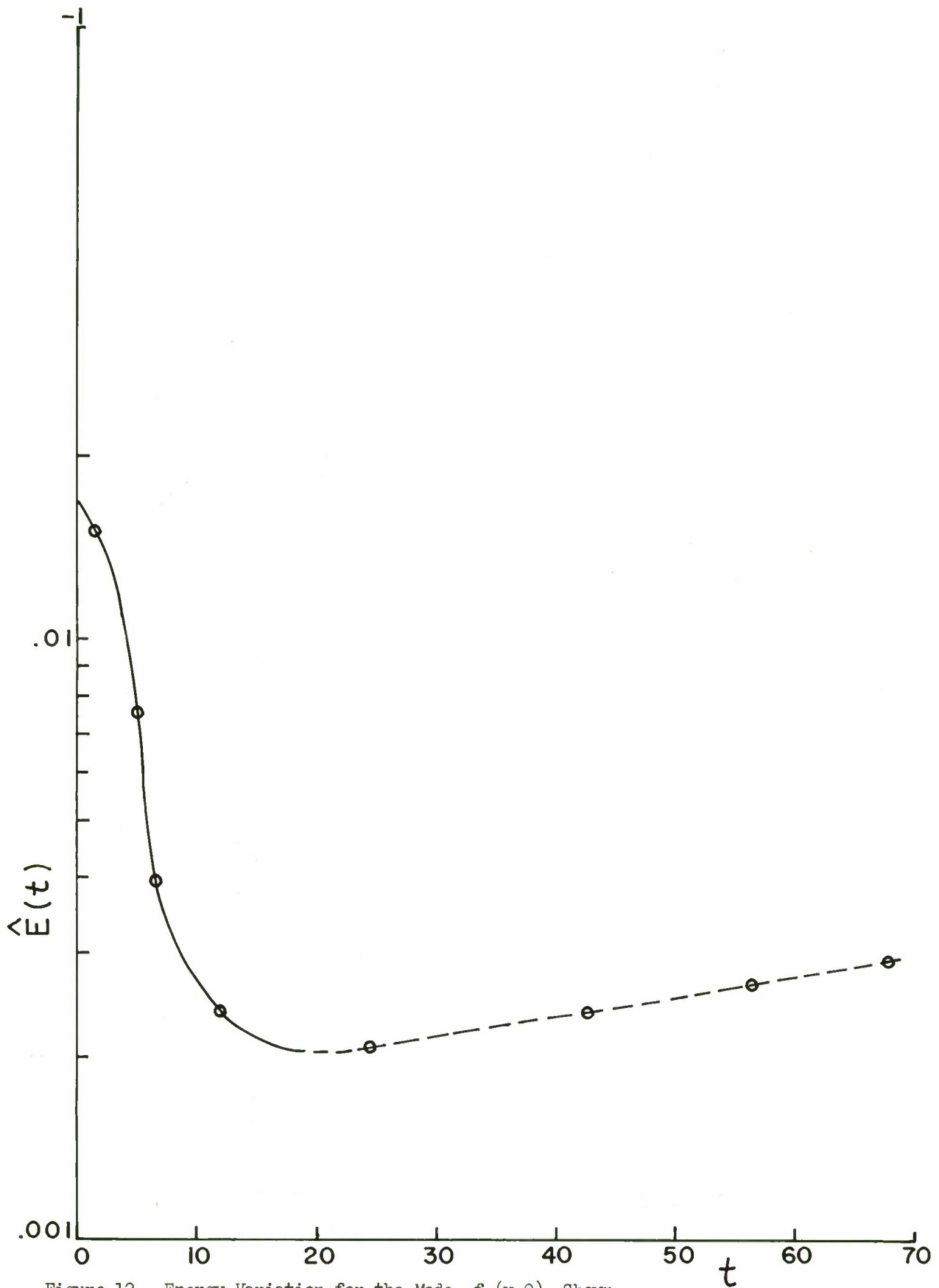


Figure 12. Energy Variation for the Mode,  $f_1(y,0)$ , Shown  
in Figure 11. Dashed Line Represents Predicted  
Growth Rate for  $f_{11}$

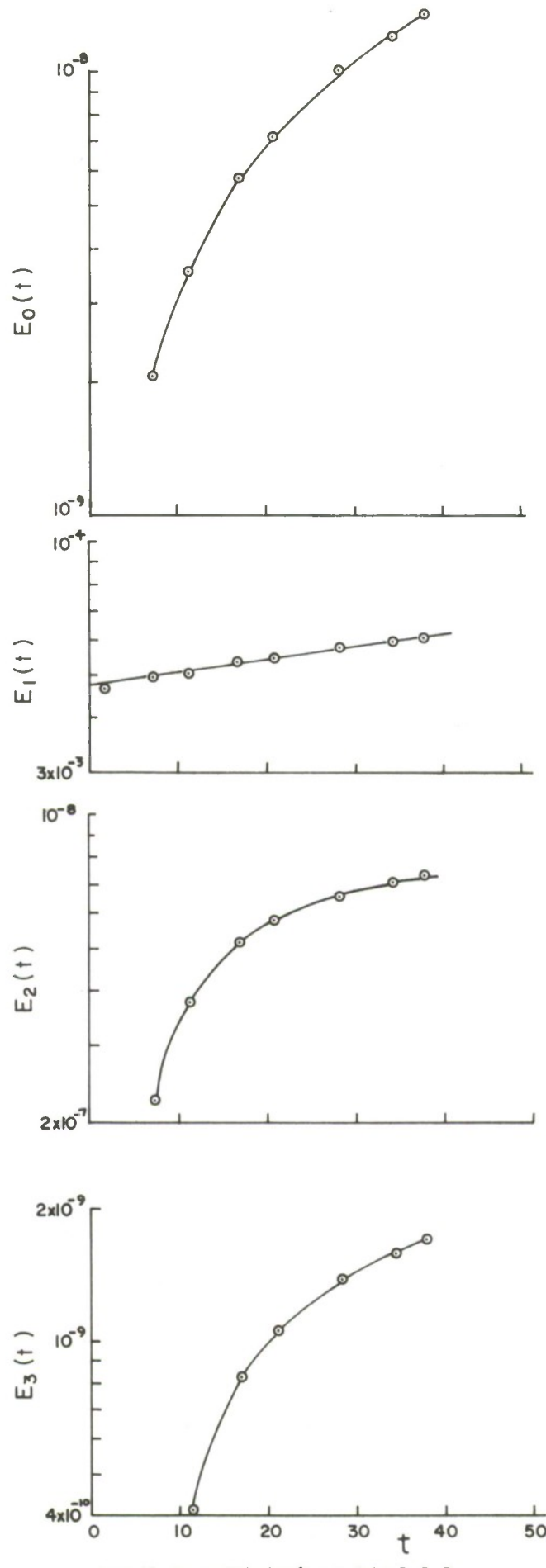


Figure 13. Energy Variation for the Modes  $E_0, E_1, E_2$  and  $E_3$ .  $R_e = 6667$ ,  $\alpha = .875$

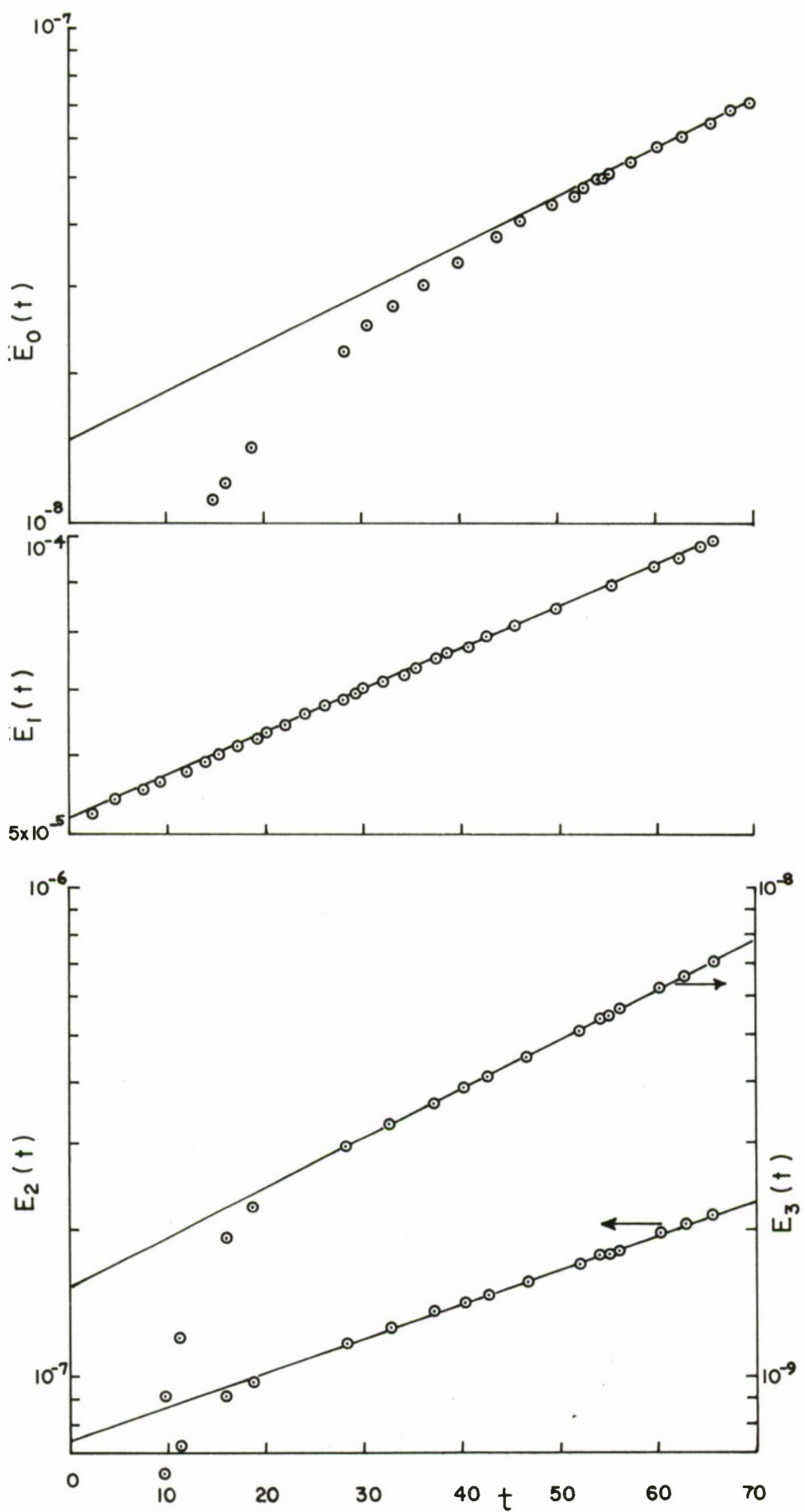


Figure 14. Energy Variation for the Modes  $E_0$ ,  $E_1$ ,  $E_2$  and  $E_3$ ,  $R_e = 6667$ ,  $\alpha = 1.0$

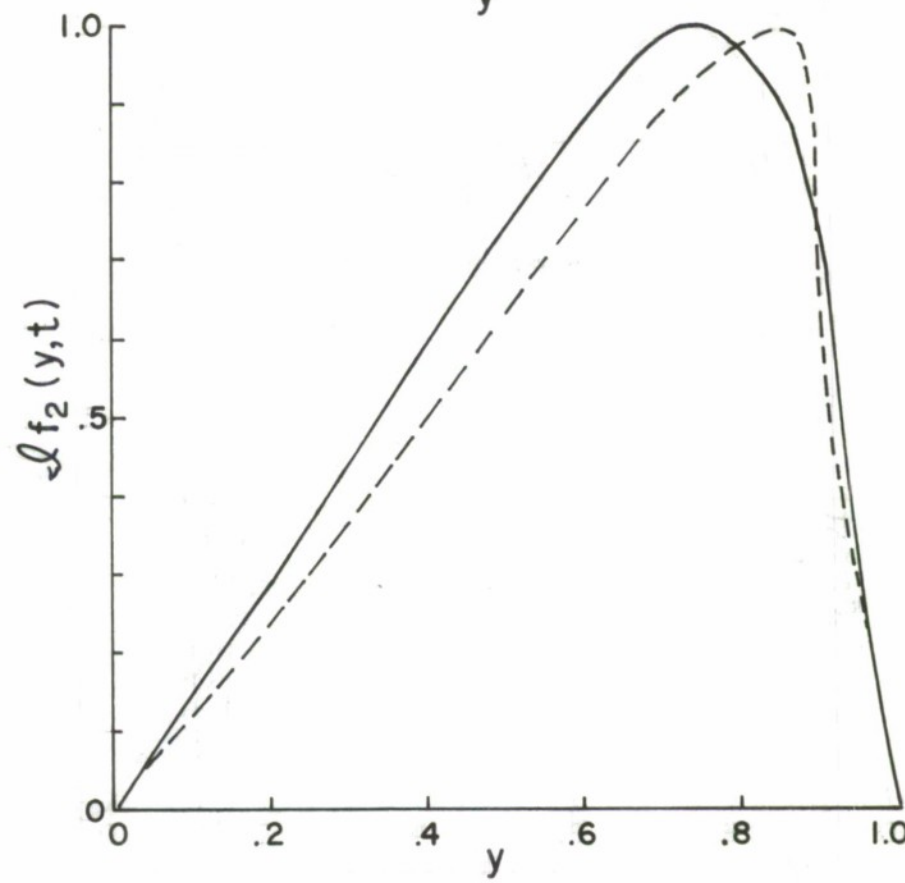
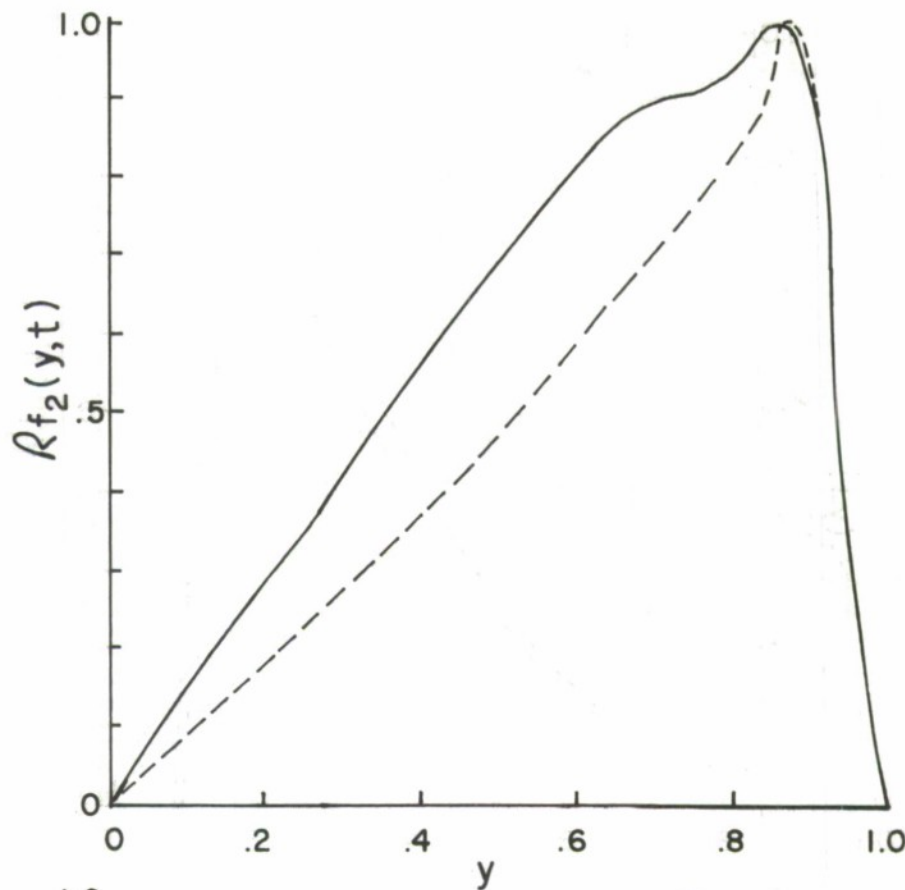


Figure 15a. Mode Shape for  $f_2(\text{odd})$  at  $t = 85$ .  $\alpha = 1.0$ ,  
 $R_e = 6667$ .  
Dashed Line Represents  $\Phi_{26}(\text{odd})$

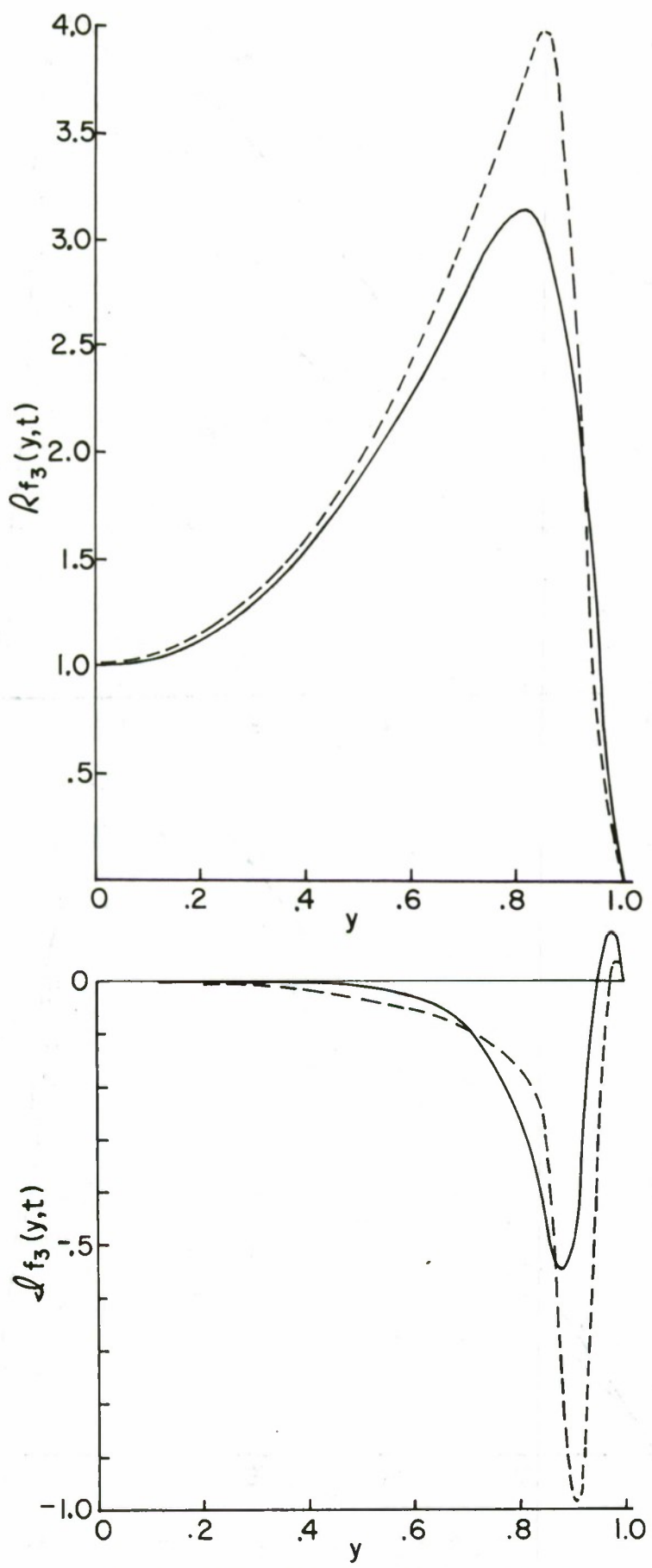


Figure 15b. Mode Shape for  $f_3(\text{even})$  at  $t = 85$ .  $\alpha = 1.0$ ,  
 $R_e = 6667$ .

Dashed Line Represents  $\phi_{33}(\text{even})$

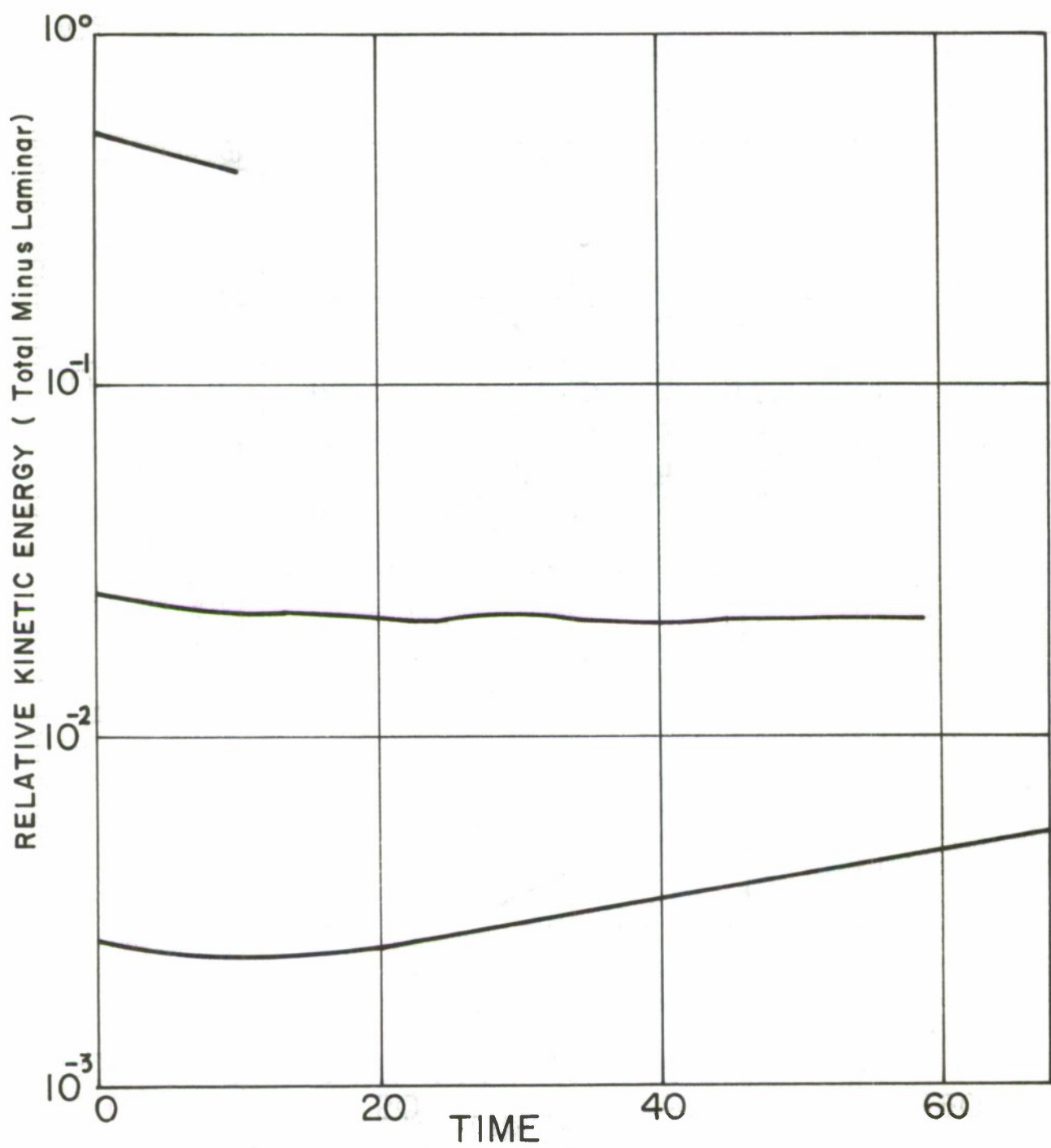


Figure 16. Total Kinetic Energy (Mean plus Turbulent)  
for Three Different Initial Energy Levels.  
The Laminar Energy (.600) has been Subtracted  
for Convenience.

Top Curve,  $\epsilon = .5$   
 Middle Curve  $\epsilon = .05\sqrt{5}$  }  
 Bottom Curve  $\epsilon = .05/\sqrt{2}$  }  $\alpha = 1.0, R_e = 6667$

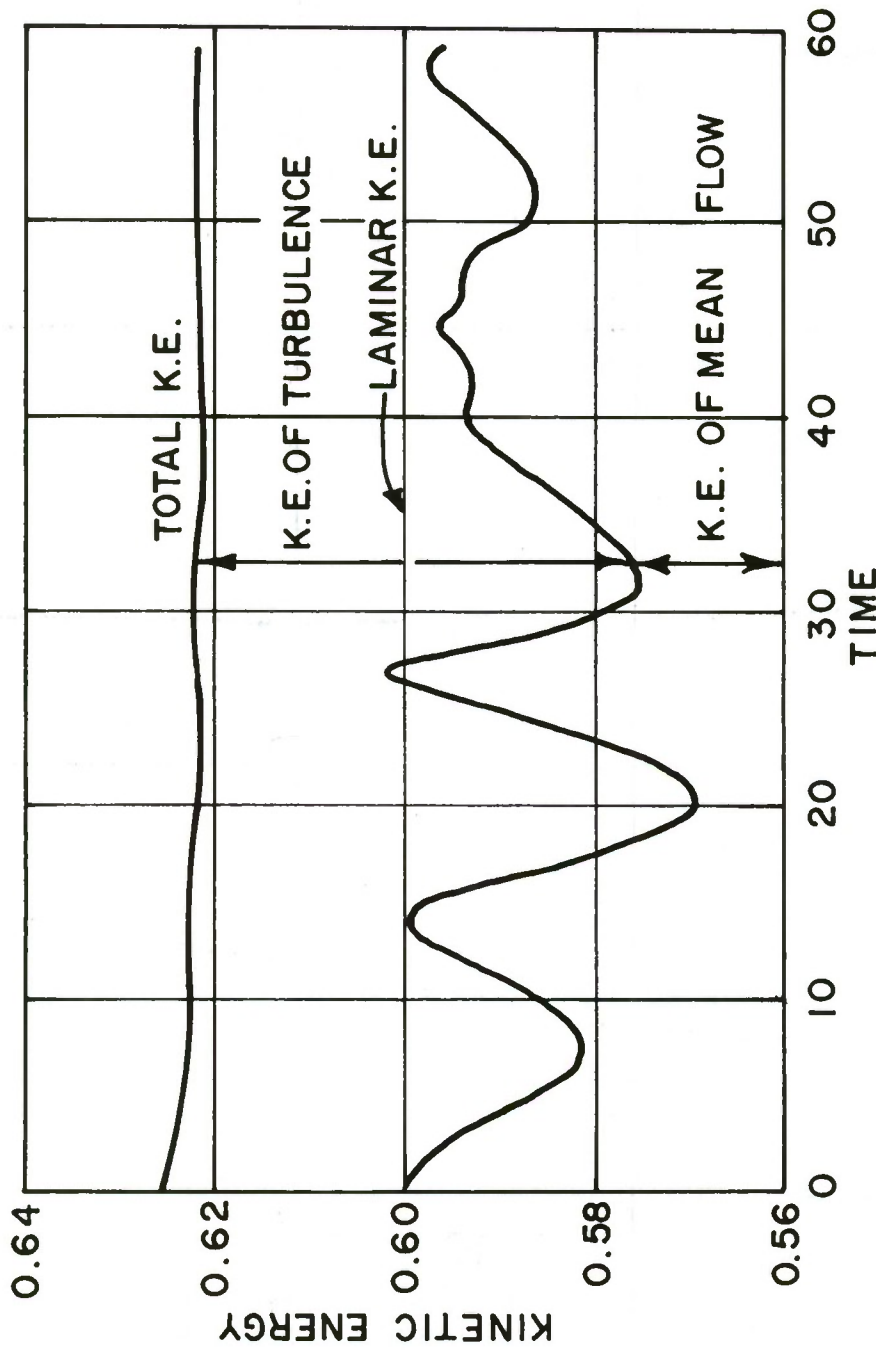


Figure 17. Energy Variation for the Run  $\epsilon = .05 \sqrt{5}$

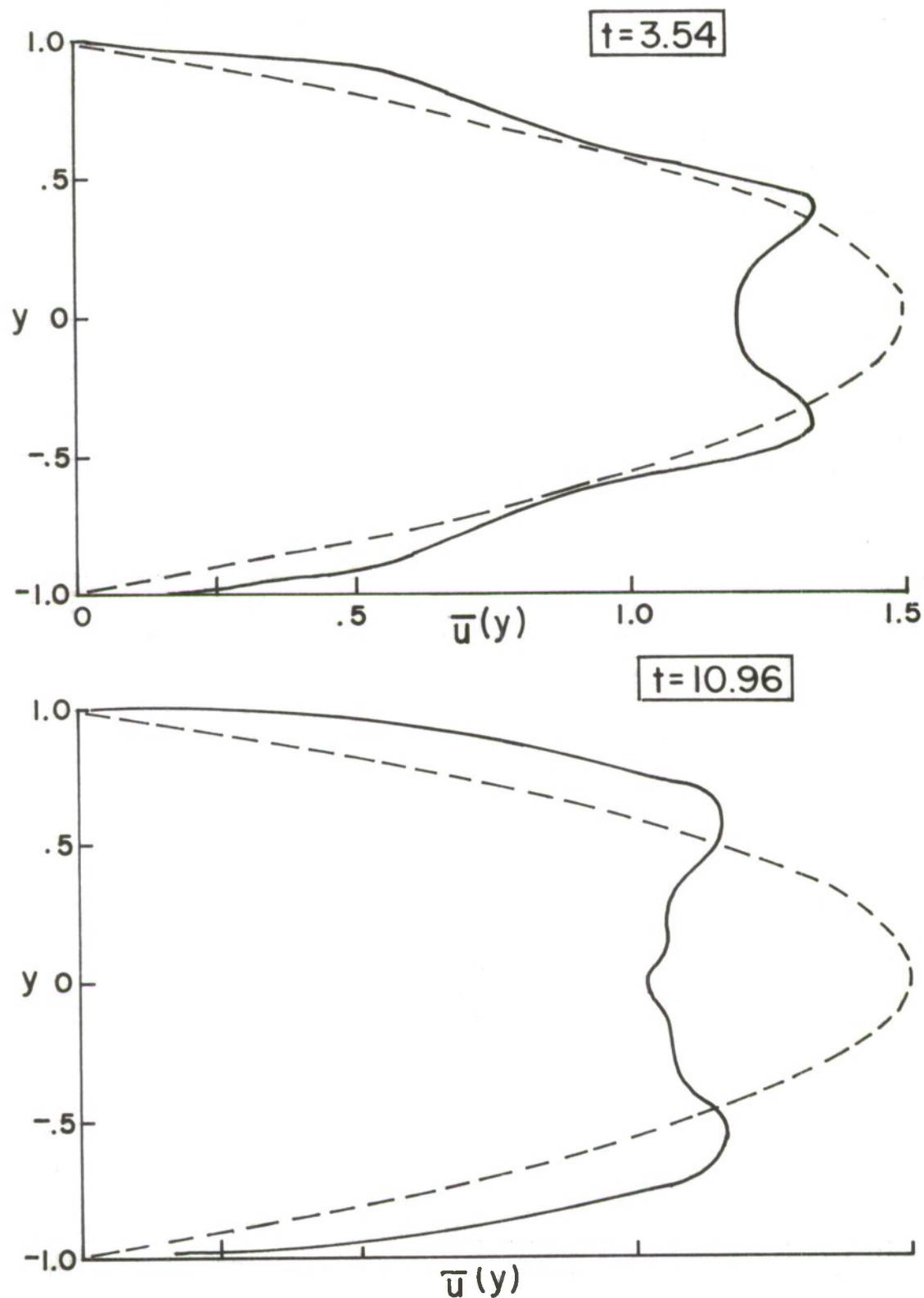


Figure 18a. Mean Velocity Profiles for the Run  $\epsilon = .5$ ,  
 $\alpha = 1.0$ ,  $R_e = 6667$   
Dashed Line is  $U(y) = 3/2(1 - y^2)$

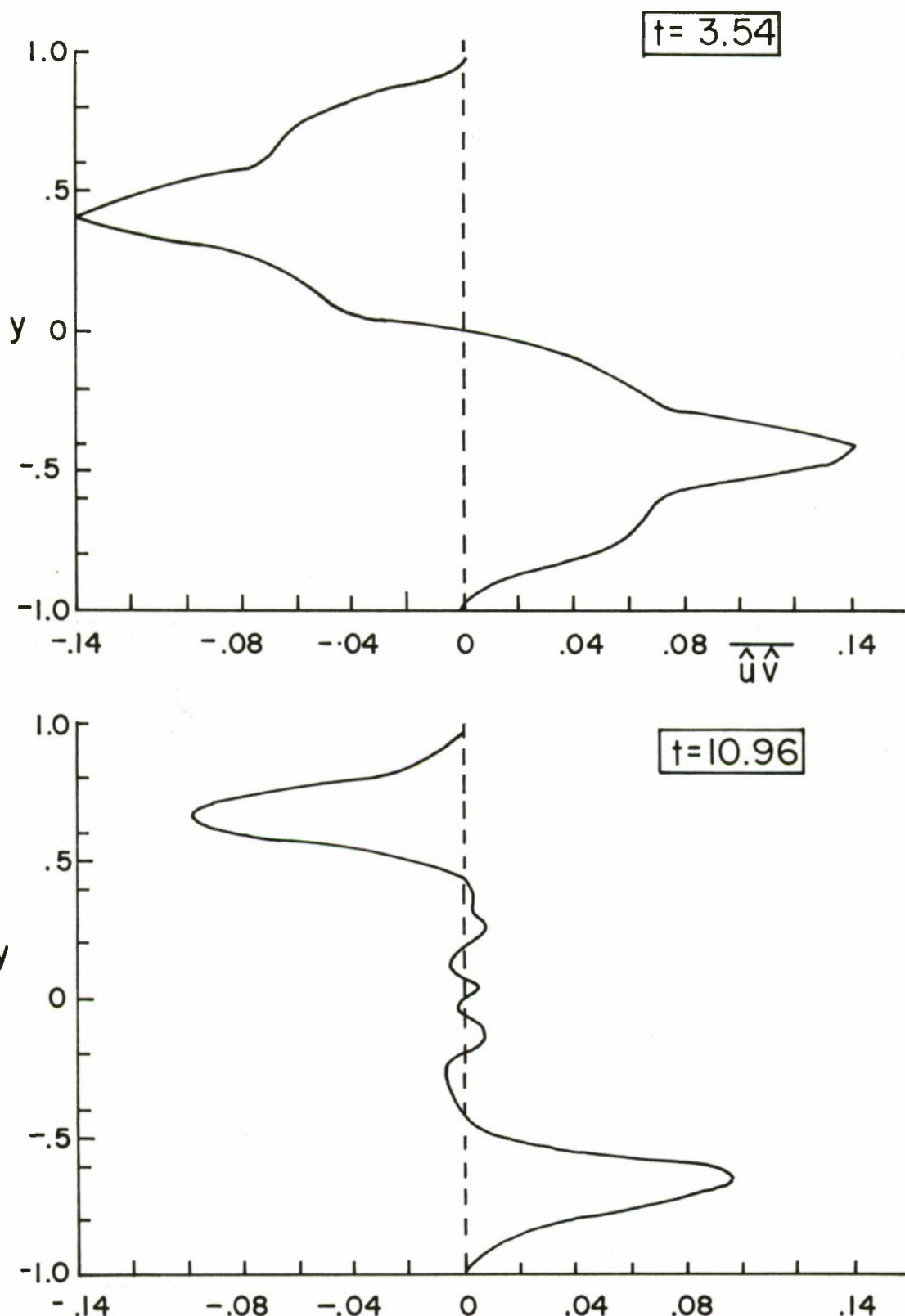


Figure 18b. Reynolds Stresses for the Run  $\epsilon = .5$ ,  $\alpha = 1.0$   
 $R_e = 6667$

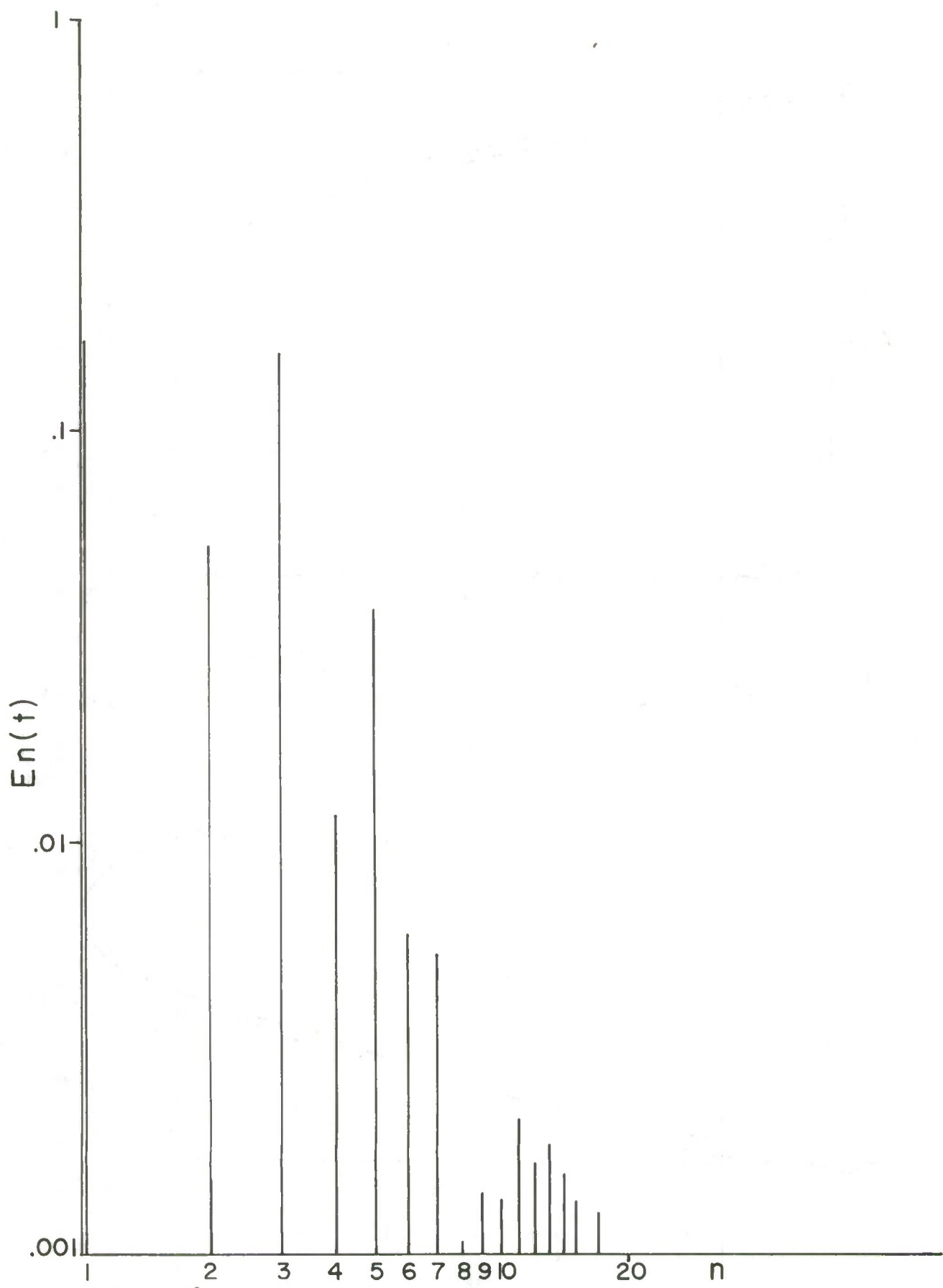


Figure 18c. Energy Spectrum for the Run  $\epsilon = .5$ ,  $\alpha = 1.0$ ,  
 $R_e = 6667$  at  $t = 11$

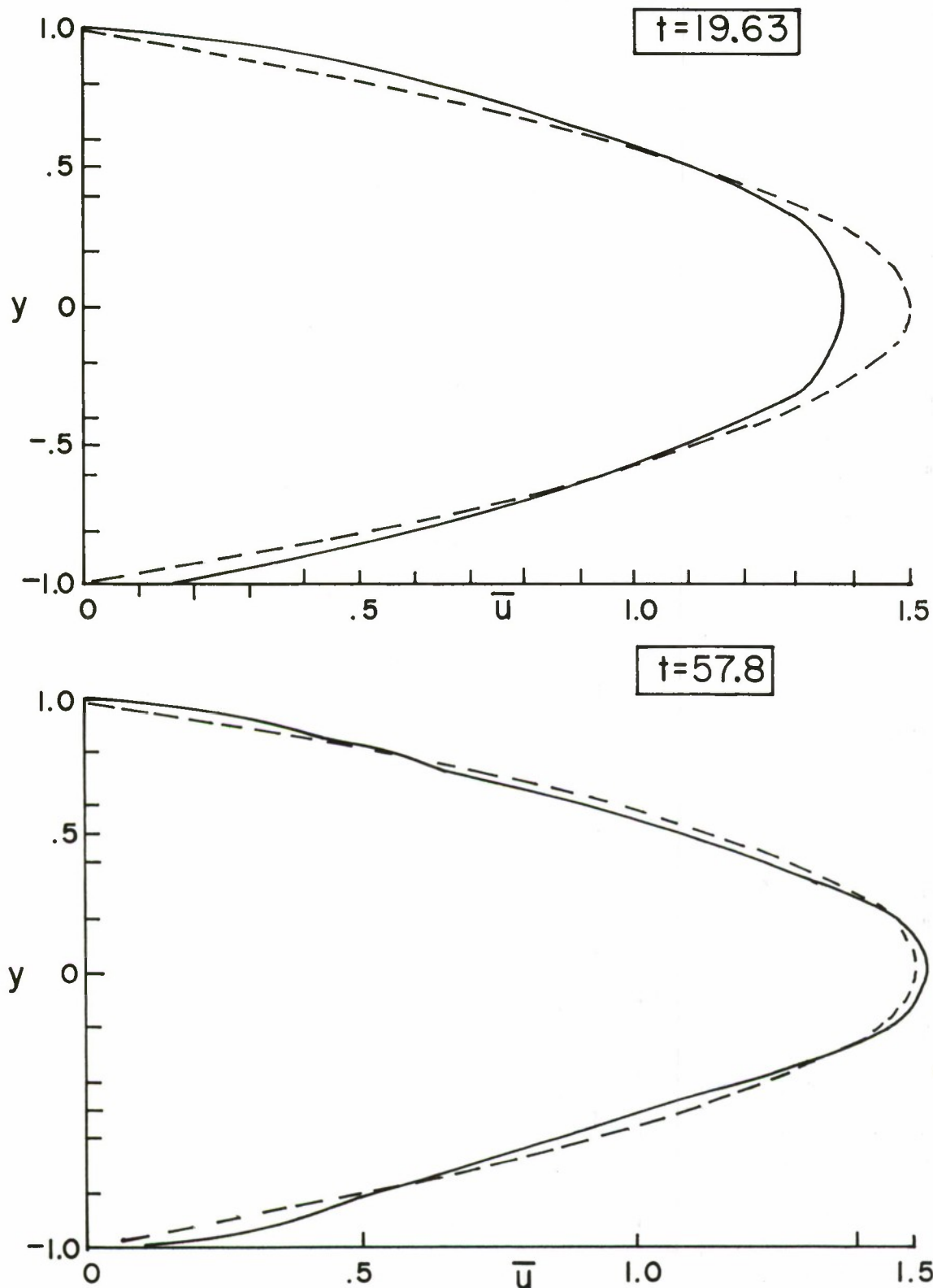


Figure 19a. Mean Velocity Profiles for the  
Run  $\epsilon = .05\sqrt{5}$ ,  $\alpha = 1.0$ ,  $R_e = 6667$   
Dashed Line is  $U(y) = 3/2(1-y^2)$

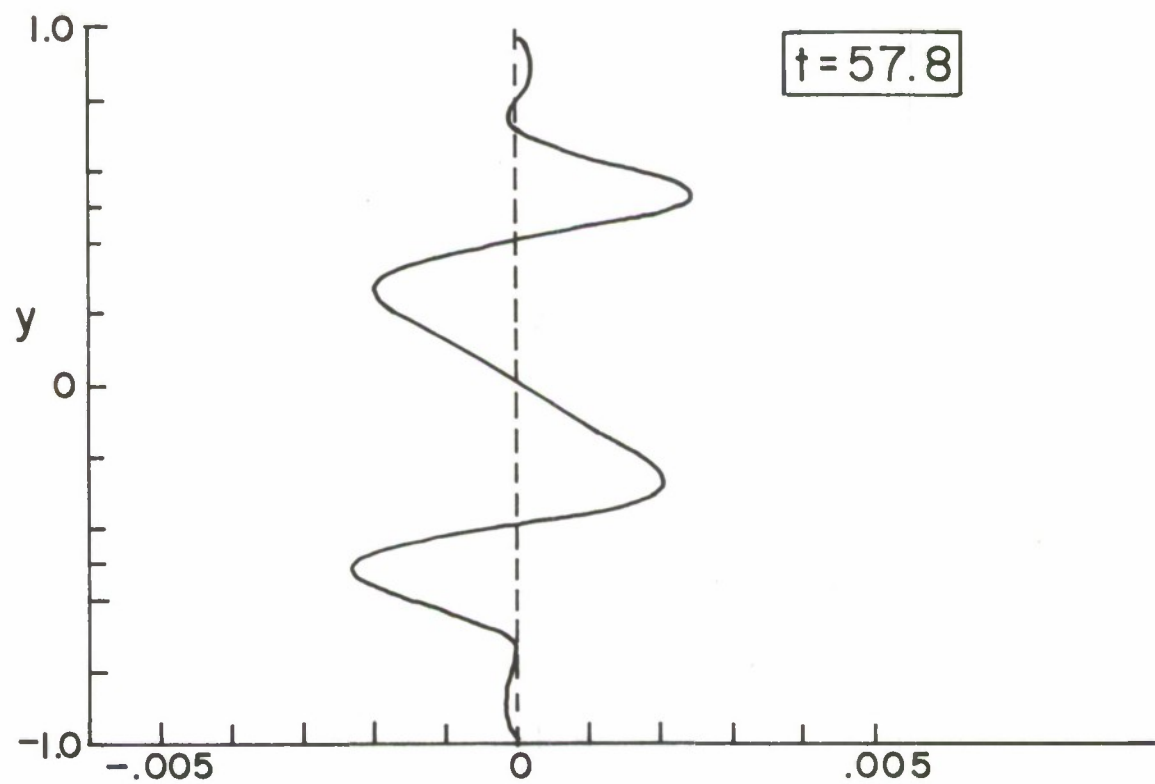
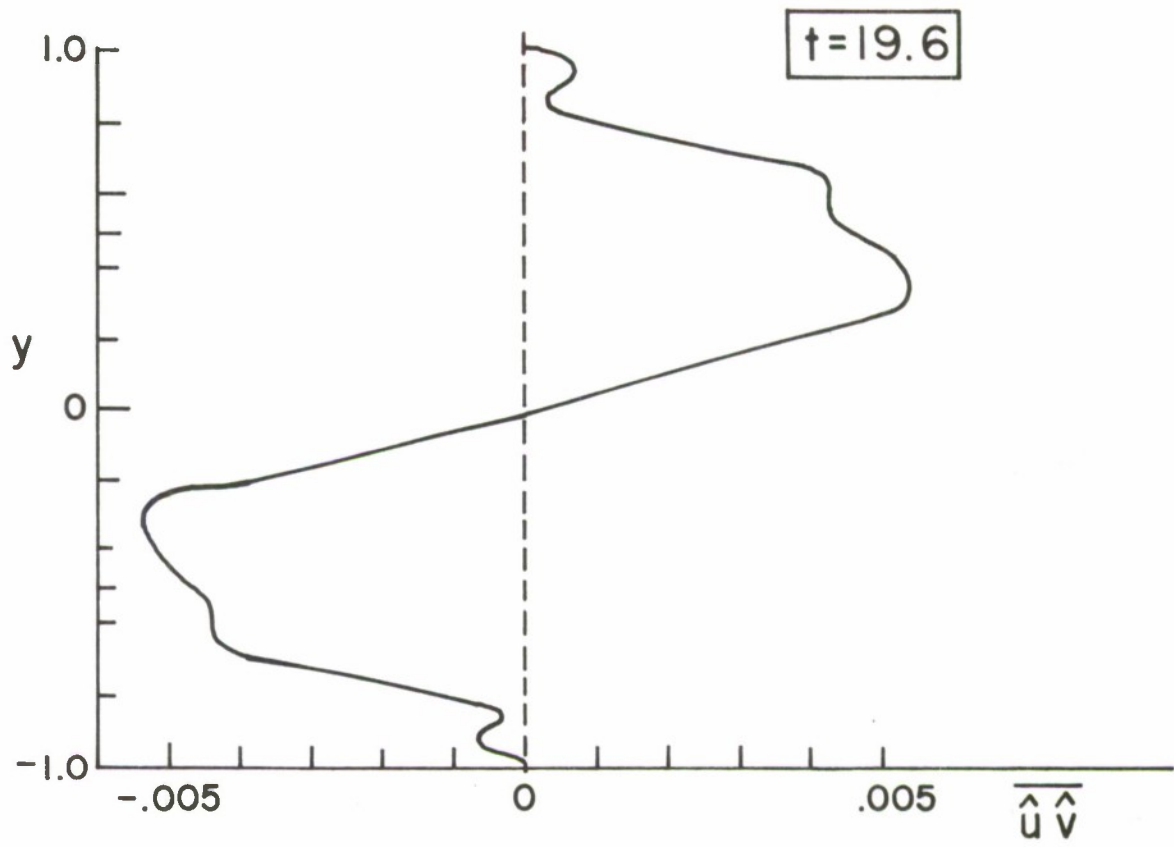


Figure 19b. Reynold's Stresses for the Run

$$\epsilon = .05\sqrt{5}, \alpha = 1.0, R_e = 6667$$

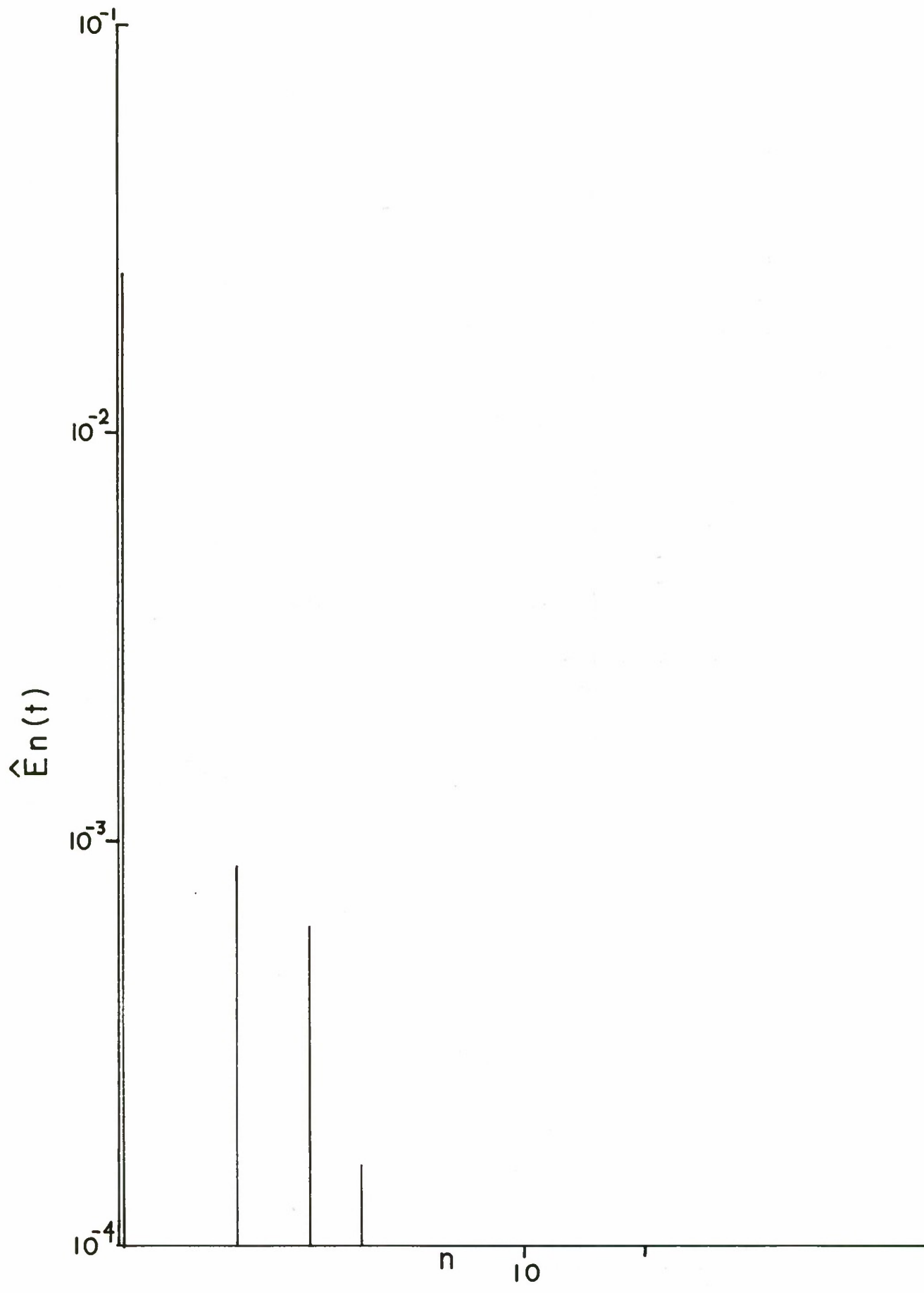


Figure 19c. Energy Spectrum for the Run  $\epsilon = .05\sqrt{5}$ ,  
 $\alpha = 1.0$ ,  $R_e = 6667$  at  $t = 59$

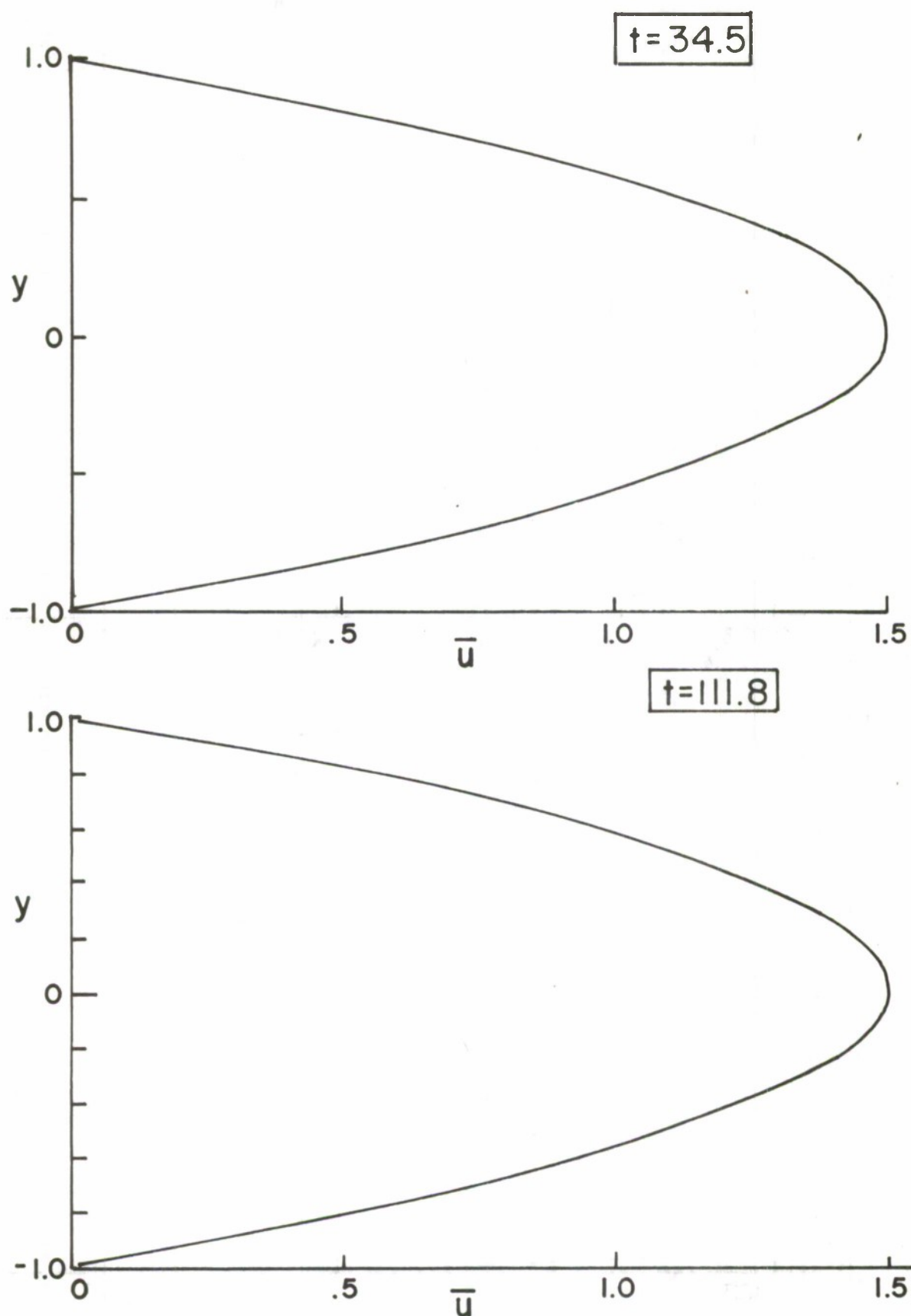


Figure 20a. Mean Velocity Profiles for the Run  
 $\epsilon = .05/\sqrt{2}$ ,  $\alpha = 1.0$ ,  $R_e = 6667$

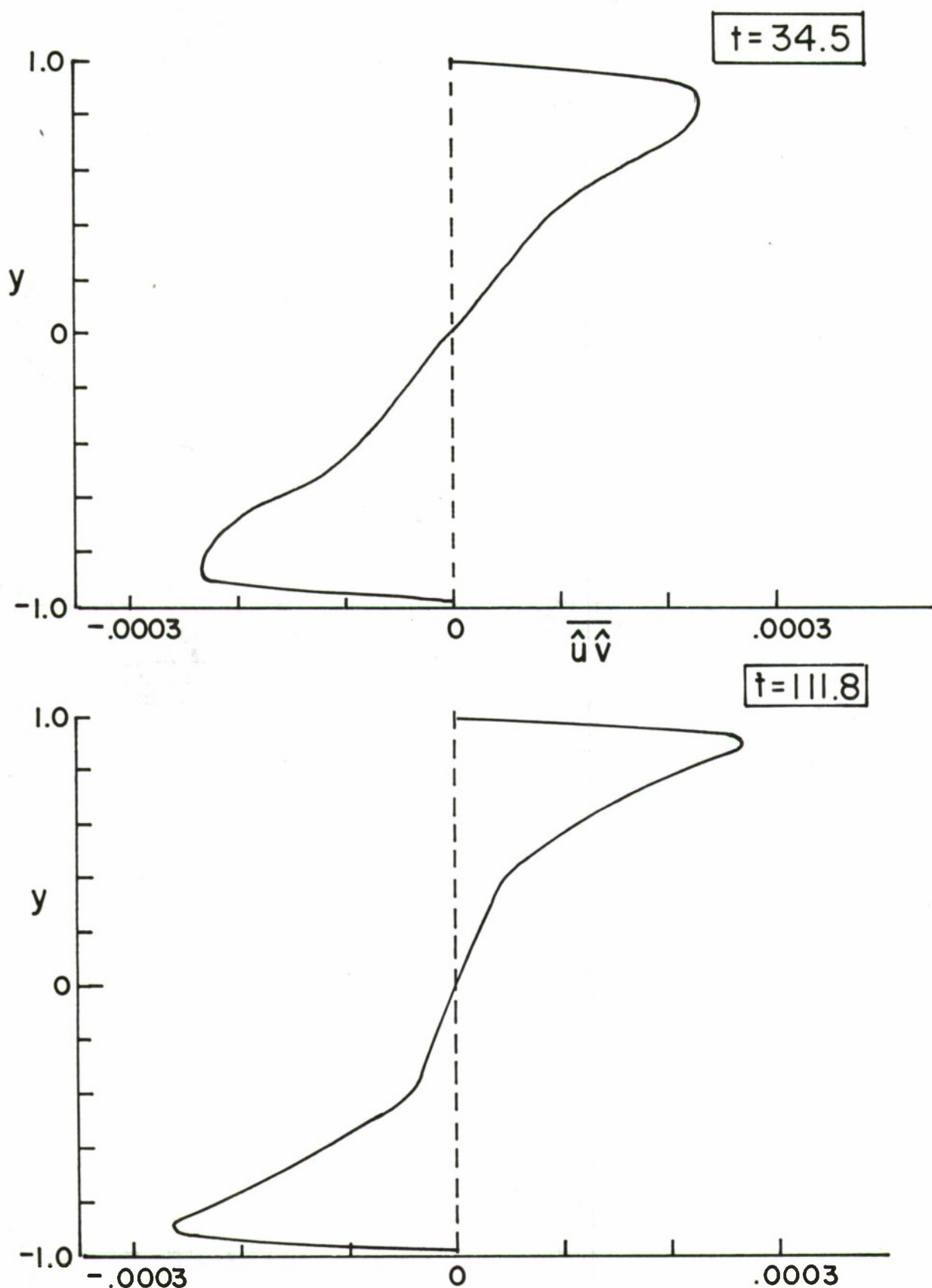


Figure 20b. Reynold's Stresses for the Run  $\epsilon = .05/\sqrt{2}$   
 $\alpha = 1.0, R_e = 6667$

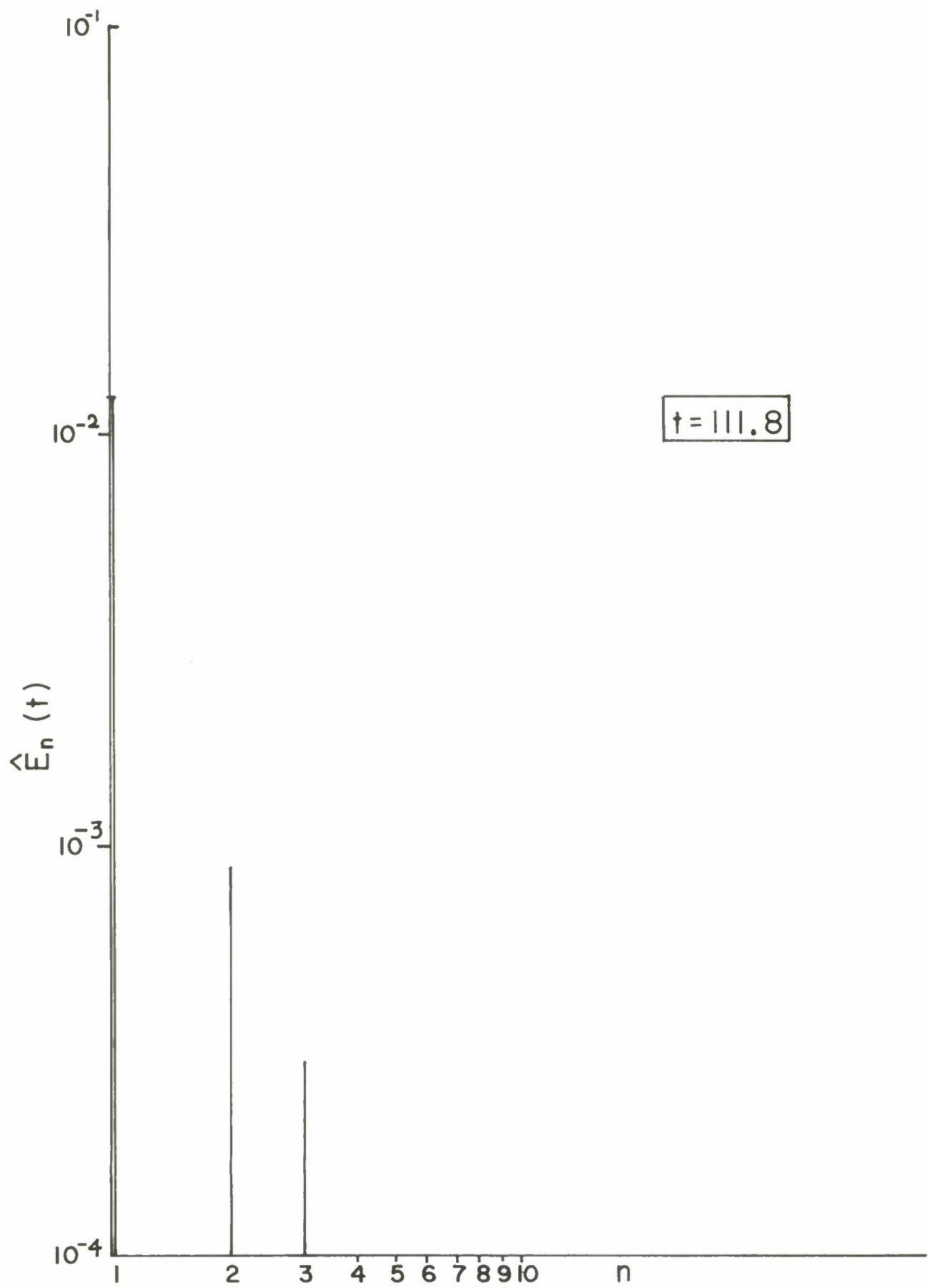


Figure 20c. Energy Spectrum for the Run  $\epsilon = .05/\sqrt{2}$ ,  
 $\alpha = 1.0$ ,  $R_e = 6667$  69

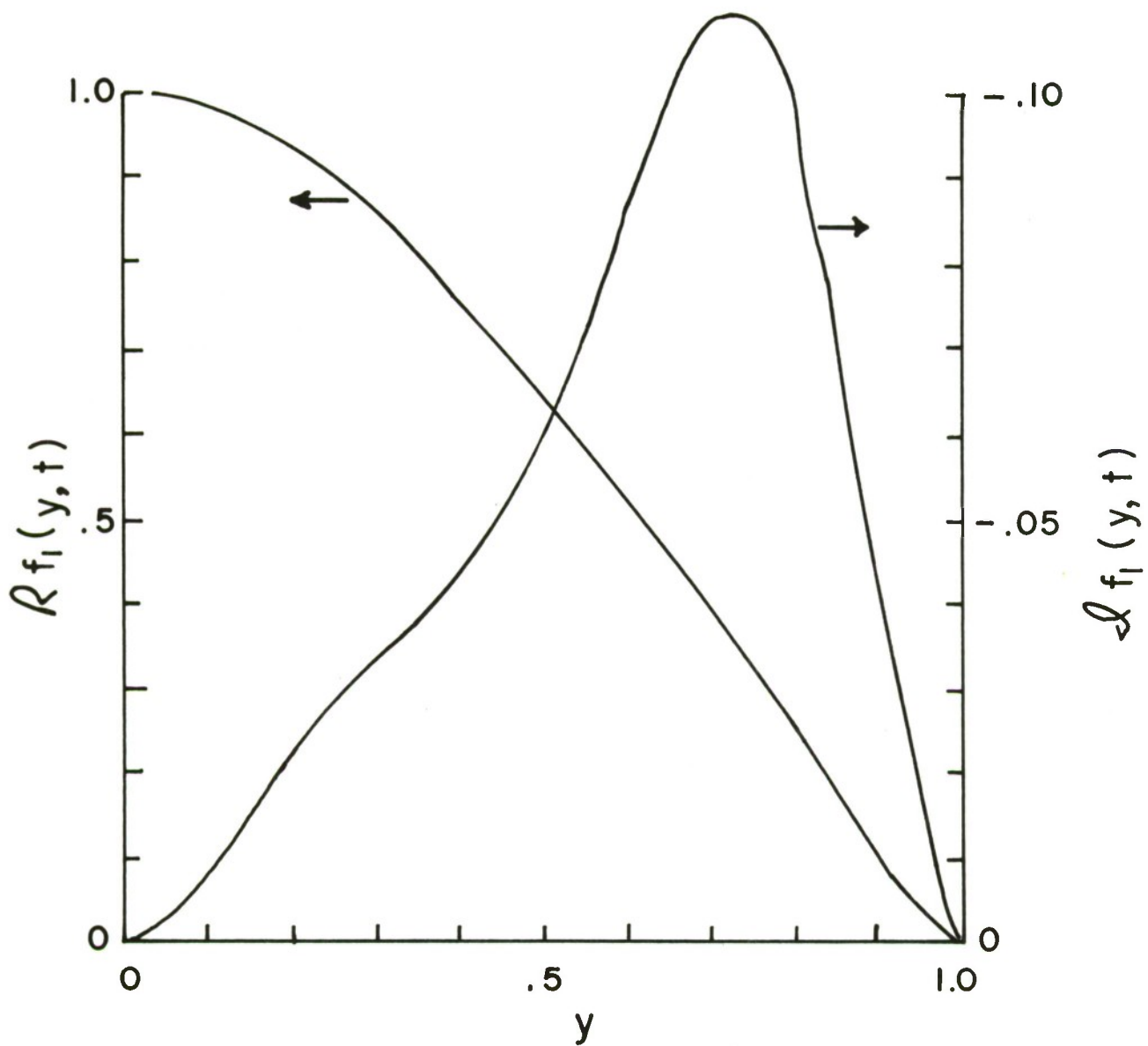


Figure 21a. Primary Mode Shape,  $f_1$ , for the Run  $\epsilon = .5$   
at  $t = 11$

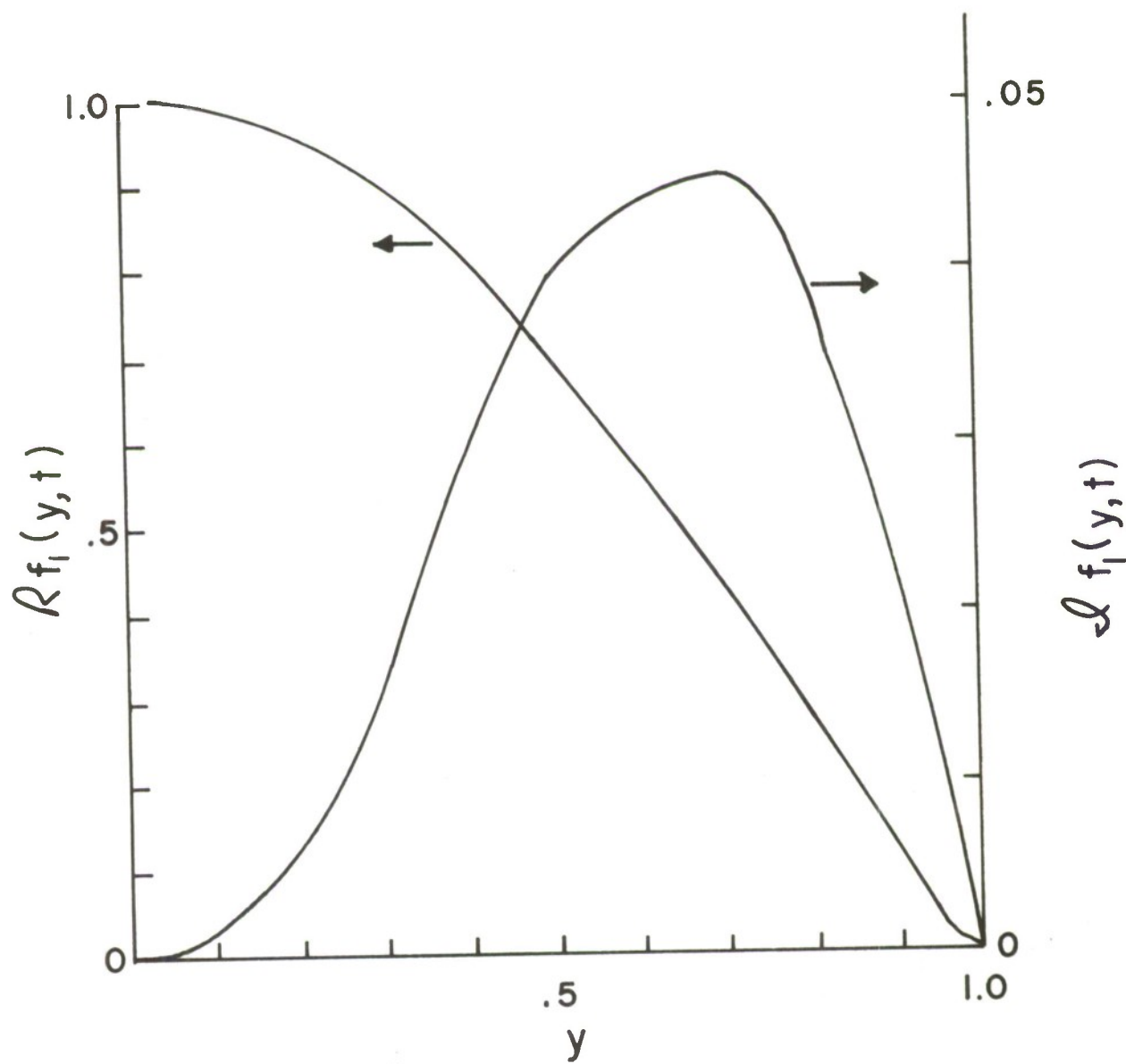


Figure 21b. Primary Mode Shape,  $f_1$ , for the Run  
 $\epsilon = .05\sqrt{5}$  at  $t = 59$

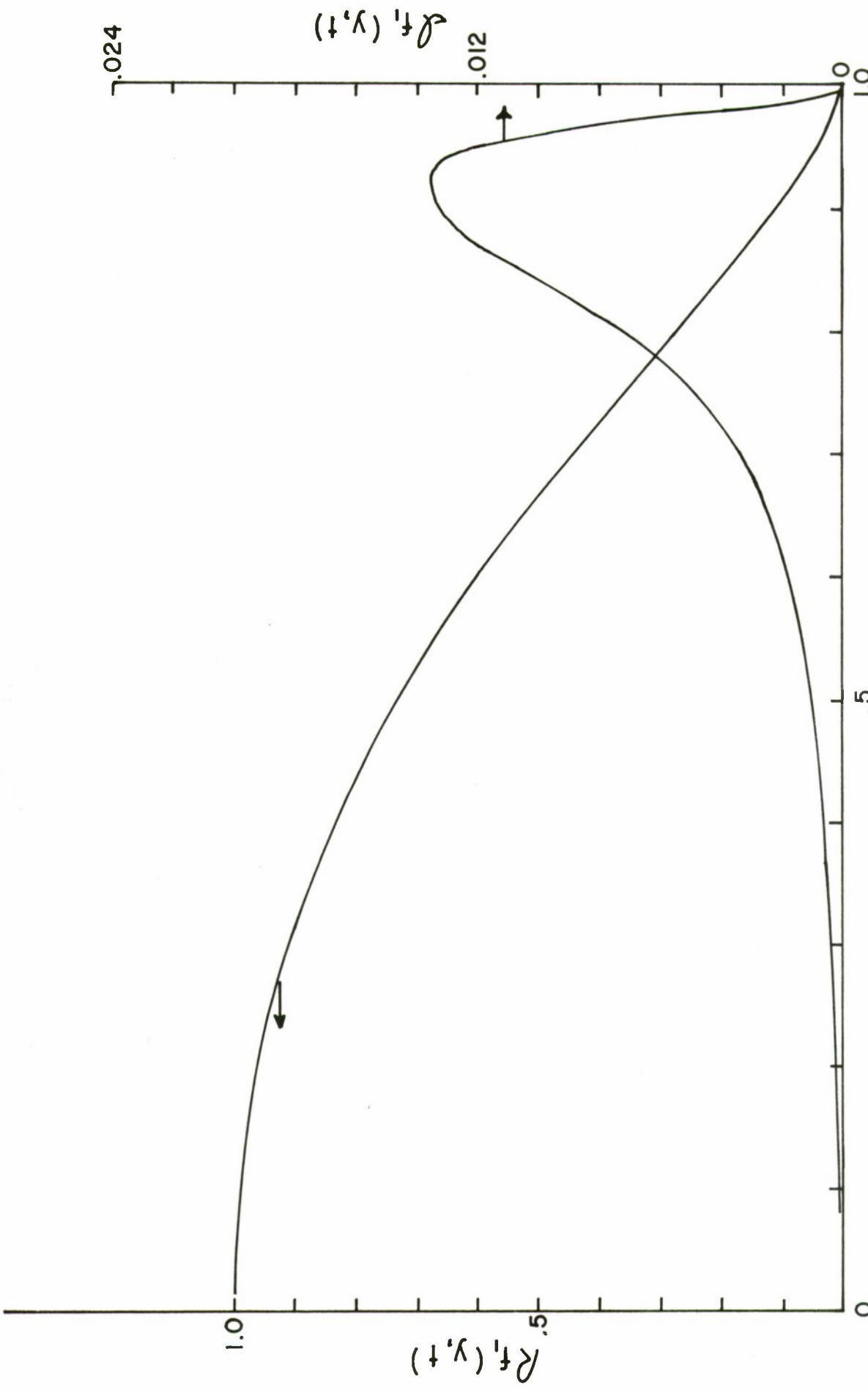


Figure 21c. Primary Mode Shape,  $f_1$ , for the Run  
 $\epsilon = .05/\sqrt{2}$  at  $t = 112$

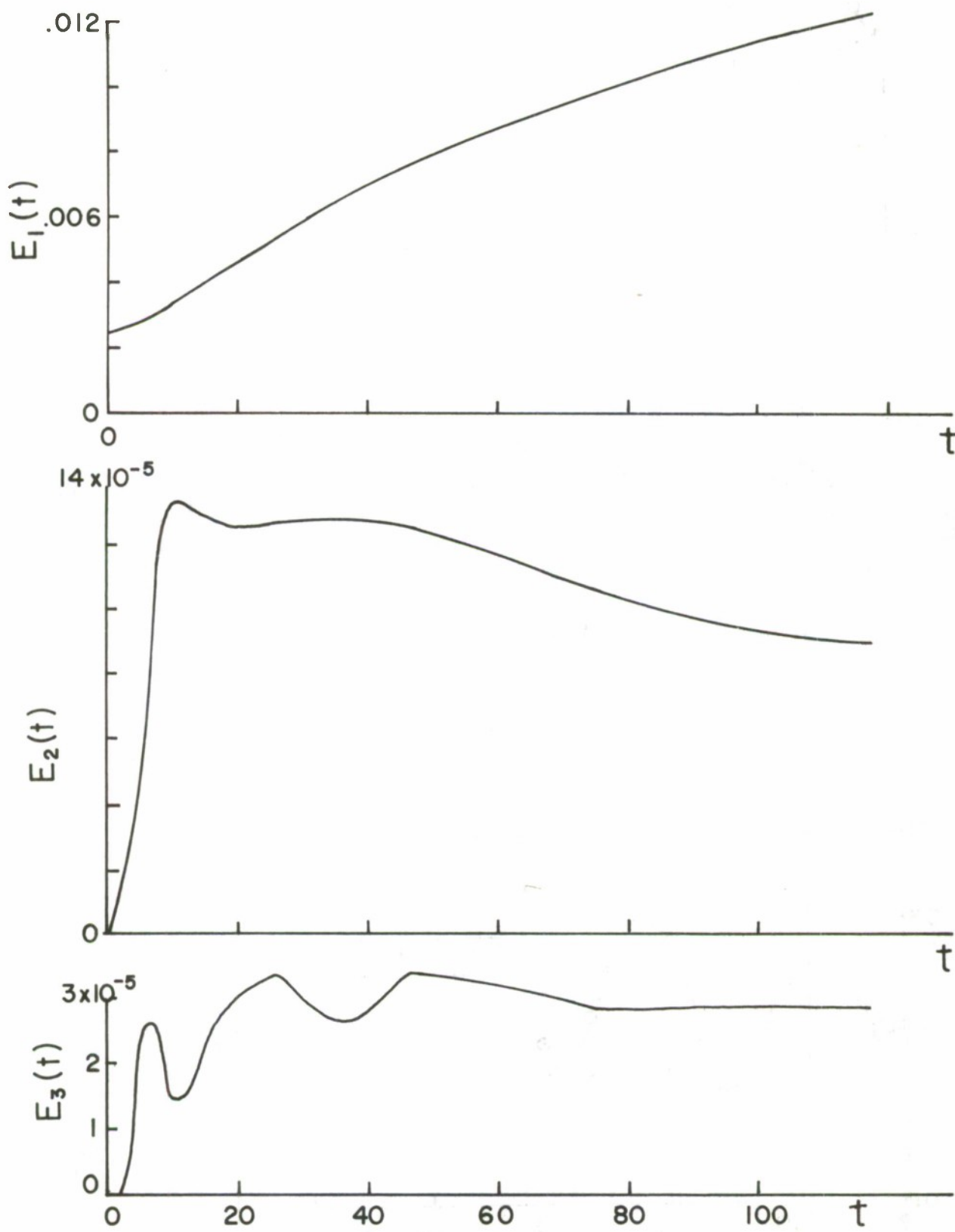


Figure 22. Energy Variation in  $E_1$ ,  $E_2$ , and  $E_3$  for the Run  $\epsilon = .05/\sqrt{2}$

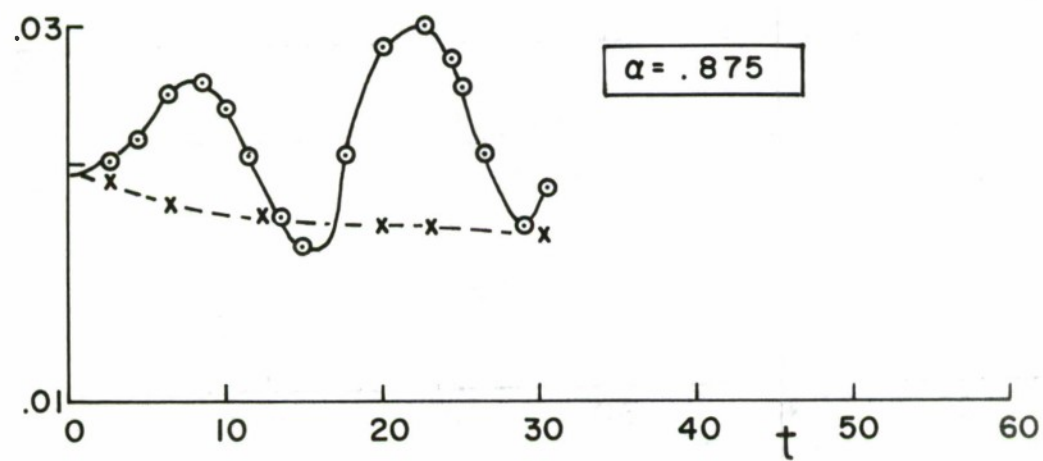
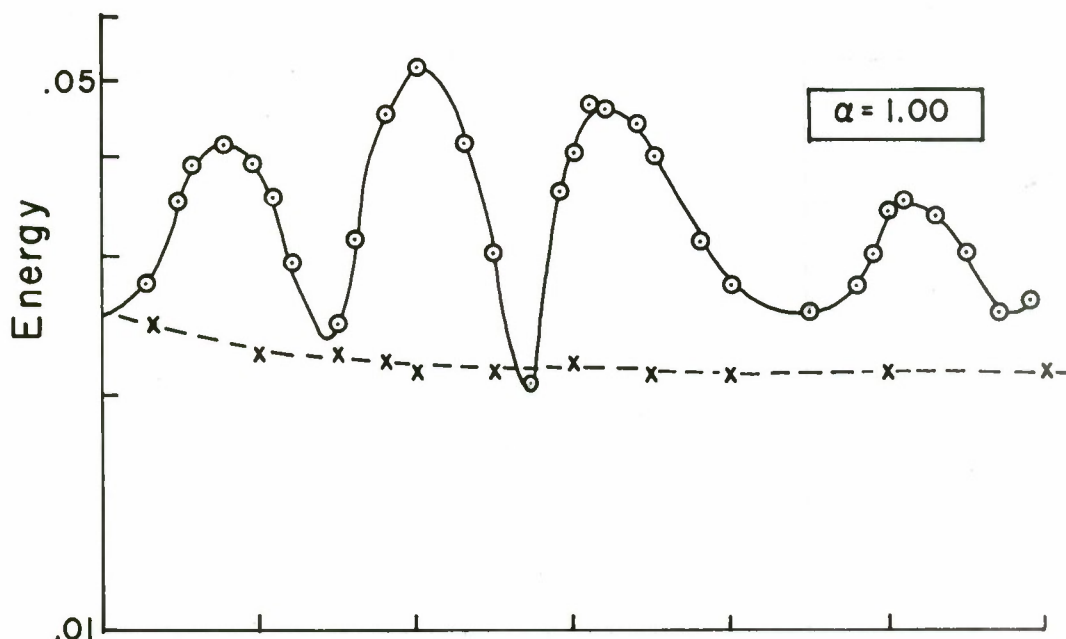
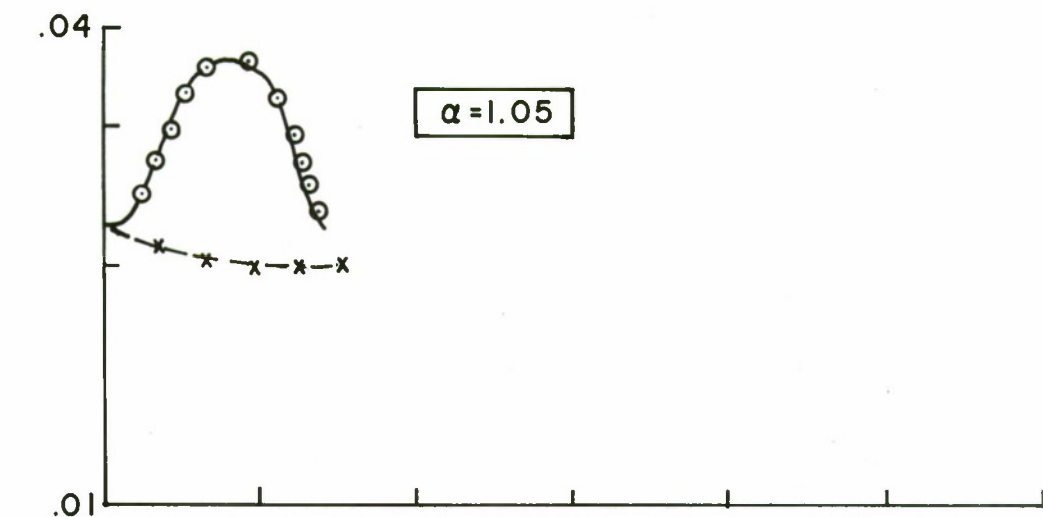


Figure 23. Energy Variation at  $R_e = 6667$  for Three Different Wavenumbers.

-○- Turbulent Kinetic Energy  
 -x- Total Kinetic Energy

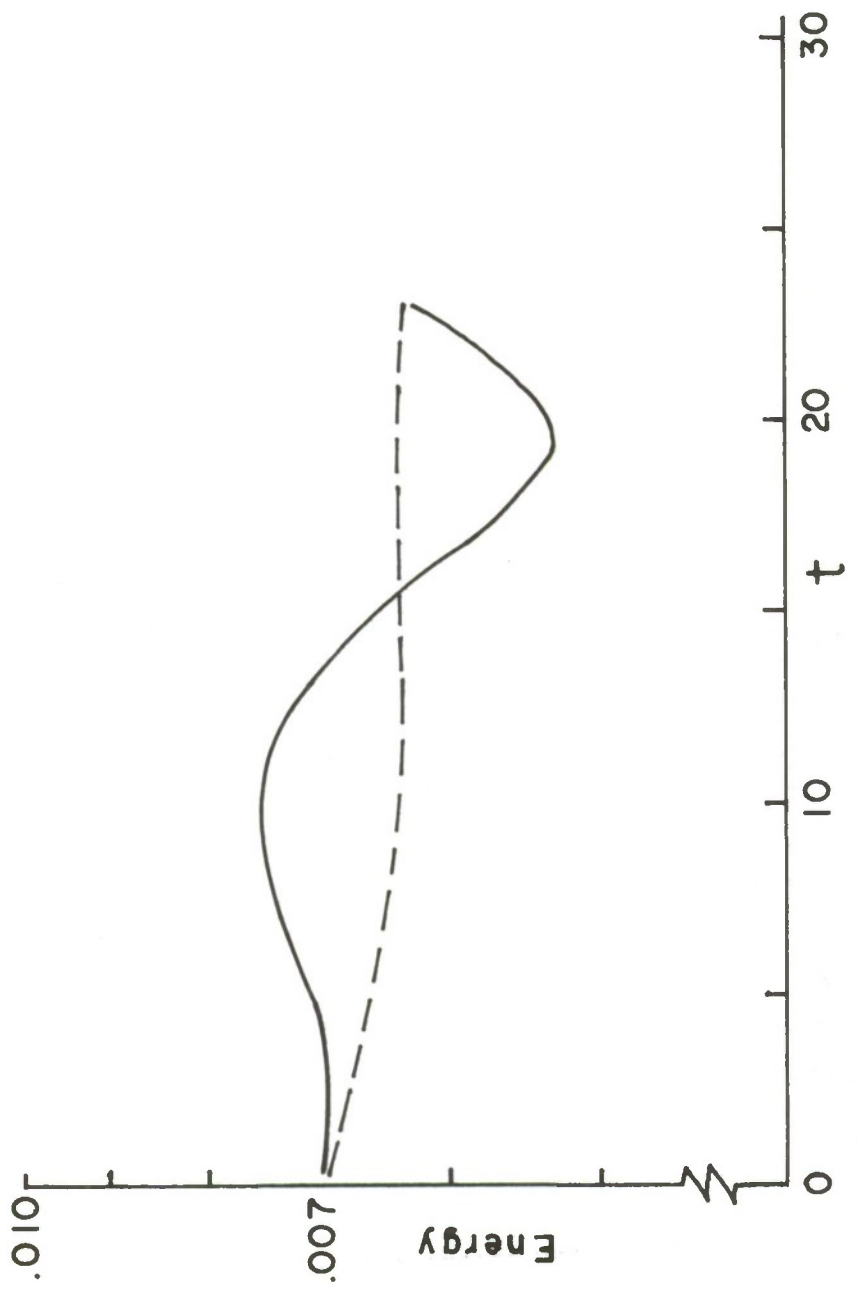


Figure 24. Energy Variation for  $\alpha = .78$   
 $R_e = 6667$ ,  $\epsilon = .0635$ . Dashed  
line is the total kinetic energy  
while solid line is turbulent  
kinetic energy.

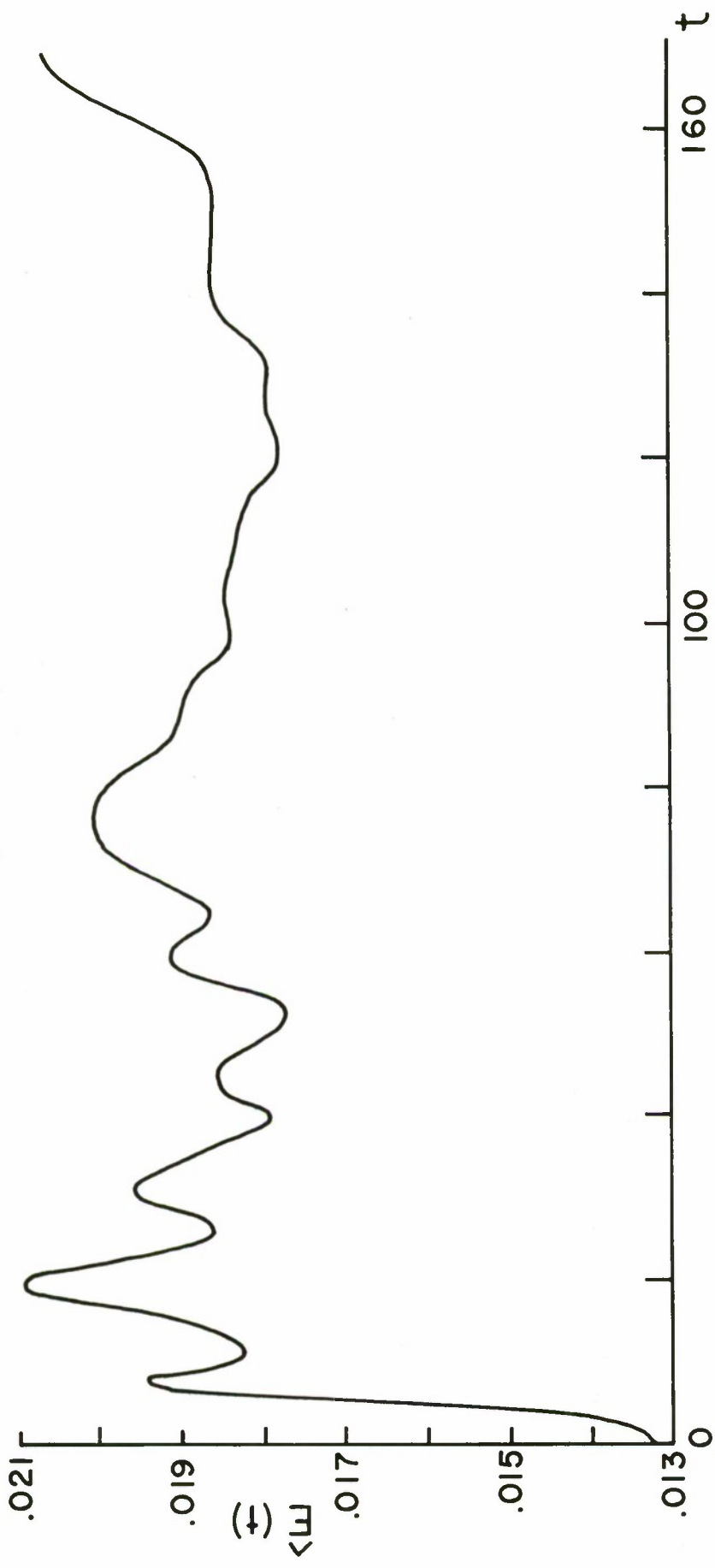


Figure 25. Turbulent Kinetic Energy for the Run with Modes  $f_7$  and  $f_8$  Initially Present  $R_e = 6667$ ,  $\epsilon = .059$

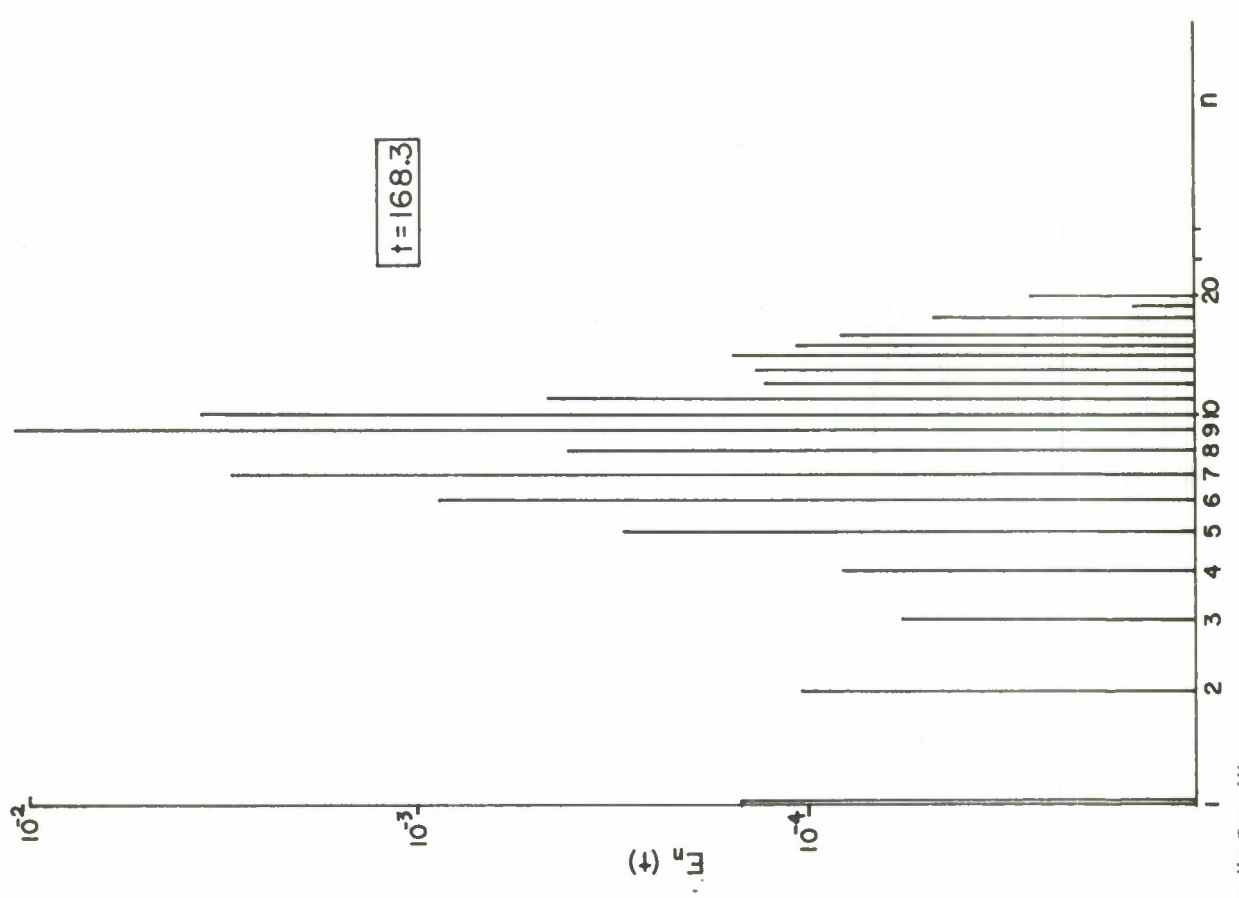


Figure 26. Energy Spectrum for the Run with Modes  $f_7$  and  $f_8$  Initially Present,  
 $R_e = 6667$ ,  $\epsilon = .059$

## APPENDIX

### LISTING OF THE FORTRAN CODE



```

* * * * * * * * * * * * * * * * * * * * * * * * * * * *
DIMENSIONS OF ARRAYS
DPHI,GAMMA,FG,GAMOLD,---,MXN
UMEAN,TEMP,TURBKE,U,PHILAM,T,PHMEAN,GAMEAN,Y --- N
XALPHA,X,IPO,IM0,INV,IAO,IAP --- M
S,INV --- M/2
A --- 2M

```

THE FOLLOWING ARRAYS CONTAIN FIXED QUANTITIES AND SHOULD NEVER BE USED FOR TEMPORARY STORAGE.

U,PHILAM,S,XALPHA,X,Y,IPO,IM0,INV,IAP,IAO  
 OTHER ARRAYS MAY BE USED FOR TEMPORARY STORAGE AT CERTAIN PARTS OF THE PROGRAM. ARRAYS T AND A ARE MOST SUITABLE FOR THIS PURPOSE.

\* \*

#### SUBROUTINE

SETUP	FUNCTION
START	ESTABLISH VALUES OF VARIOUS QUANTITIES WHICH REMAIN CONSTANT THROUGHOUT THE INTEGRATION
TITLE	ESTABLISH INITIAL VALUES OF STREAM FUNCTION AND VORTICITY
STEP	WRITES OUTPUT TITLE
ADVANC	TIME STEP BY MODIFIED EULER IMPLICIT TIME DIFFERENCING
PRESUR	SOLVES DELSQUARE(PHI)=GAMA FOR PHI BY FINITE FOURIER TRANSFORM
TRISOL	SOLUTION OF A SPECIAL TRIDIAGONAL SYSTEM OF LINEAR EQUATIONS BY GAUSS-ELIMINATION.
	CALLED BY SUBROUTINE PRESUR
TIMER	COMPUTES A NEW VALUE OF DT
MEANS	COMPUTES MEAN VALUES OF DISTURBANCE STREAM FUNCTIONS AND VORTICITY --- PHMEAN AND GAMEAN
ENERGY	COMPUTES THE MEAN KINETIC ENERGY OF THE TURBULENCE AS A FUNCTION OF Y, THE INTEGRAL OVER Y OF THAT QUANTITY AND THE MEAN KINETIC ENERGY OF THE MEAN FLOW
EDDYS	COMPUTES TURBULENCE STREAM FUNCTION AND CALL EDDYS(+1) --- PUTS PHI-PHMEAN IN FG

STRESS  
PRINT  
PLOT  
SPCTR M

000001000  
000001010  
000001020  
000001030  
000001040  
000001050  
000001060  
000001070  
000001080  
000001090  
000001100  
000001110  
000001120  
000001130  
000001140  
000001150  
000001160  
000001170  
000001180  
000001190  
000001200  
000001210  
000001220  
000001230  
000001240  
000001250  
000001260  
000001270  
000001280  
000001290  
000001300  
000001310  
000001320  
000001330  
000001340  
000001350  
000001360  
000001370  
000001380  
000001390  
000001400  
000001410  
000001420  
000001430  
000001440

CALL EDDYS(-1) ---- PUTS GAMMA-GAMMEAN IN FG  
COMPUTES TURBULENT REYNOLDS STRESS  
PRINTS OUTLINE LINE GRAPHS OF MEAN VELOCITY, VORTICITY  
TURBULENT KINETIC ENERGY AND REYNOLDS STRESS  
COMPUTES SPECTRAL DENSITY OF TURBULENT  
KINETIC ENERGY OR SQUARED VORTICITY AS  
FUNCTIONS OF Y AND THE MEAN OVER Y.  
CALLED BY PRESUR .  
CALL SPCTR M(1) ---- KINETIC ENERGY  
CALL SPCTR M(-1) ---- SQUARED VORTICITY  
COMPUTES AND PRINTS MODAL VECTORS  
CALL MODES(MOD1,MOD2,1) PRINTS VECTORS FOR  
FOURIER MODES MOD1 AND MOD2 NORMALIZED  
SO THAT AT Y=0 REAL PART = 1 AND IMAGINARY  
PART=0. CALL MODES(MOD1,MOD2,2) PRINTS  
MODULUS AND PHASE  
PRINTS ONLINE GRAPHS ---- GENERAL  
CALL PLOTSP(A,B,N) PRINTS GRAPHS OF  
POSITIVE N-DIMENSIONAL VECTORS A AND B  
PRINTS CONTOUR PLOT  
PRINTS TWO DIMENSIONAL ARRAYS.  
CALL OUTPUT(1) ---- PRINTS PHI  
CALL OUTPUT(2) ---- PRINTS GAMMA  
CALL OUTPUT(3) ---- PRINTS FG  
READS DATA FROM TAPE OR DISC  
WRITES DATA ON TAPE OR DISC  
COMPUTES FINITE FOURIER TRANSFORM.  
DHARM IS INCLUDED IN THE IBM SCIENTIFIC LIBRARY  
OF PRE COMPILED PROGRAMS AVAILABLE AT NPS.  
COMPUTES PHASES OF FIRST FIVE MODES AT SEVERAL  
LATERAL STATIONS  
\* \* \* \* \*

PLOTSP  
CPLT  
OUTPUT  
LOAD  
RELOAD  
DHARM  
PRMTRS  
LOGICAL INDICES ---- NUMBER OF COMPLETED TIME STEPS  
ICOUNT INT  
ISCI P  
MCOMP  
MSCIP  
KSTEP  
KINT

CONTROLS DEPLETED OUTPUT--WHEN ICOUNT=INT  
MAIN CALLS PRINT, PRESUR CALLS SPCTR M ETC.  
INCREMENT FOR INT  
CONTROLS SINGLE LINE OUTPUT---WHEN ICOUNT=MCOMP  
MAIN CALLS PRINT  
INCREMENT FOR MCOMP  
CONTROLS CALL OF SUBROUTINE STEP. IF ICOUNT=  
KSTEP TIME STEP IS PERFORMED BY STEP  
INCREMENT FOR KSTEP. IF KINT=1 THEN INTEGRATION  
IS BY MOD EULER TIME DIFFERENCING.

```

C MRLOAD    CCNTROLS FREQUENCY AT WHICH DATA IS WRITTEN ON DISK
C             THIS IS INCLUDED AS A PRECAUTION TO PREVENT LOSING
C             A LENGTHY COMPUTATION DUE TO MACHINE FAILURE NEAR
C             END OF COMPUTATION * * * * * * * * * * * * * * * * *
C             * * * * * * * * * * * * * * * * * * * * * * * * * * * *
C
C     READ(5,11) NPROB, NCYCLS, LINR
C     ITAPE=10          00001490
C     CALL ERSET(255,1000,-1,1) 00001500
C     IF(NPROB.LT.0) GO TO 2 00001510
C   1   READ(5,12) NMISCIP,MSCIP 00001520
C     READ(5,13) REYNLD,FRACEL,XLAMDA 00001530
C     READ(5,19) DOT,BLANK,XXX 00001540
C     INT=0            00001550
C
C     ISTART=0          00001560
C     KSTEP=0           00001570
C     MCOMP=0           00001580
C     TIME=0.           00001590
C     NITOT=0           00001600
C     MRLLOAD=200        00001610
C     CALL SETUP          00001620
C     CALL START          00001630
C     WRITE(6,14) NPROB,NCYCLS,N,M,NITMAX,ISCIP,MSCIP 00001640
C     GO TO 3           00001650
C
C   2   CALL LOAD          00001660
C     MCOMP=ISTART
C     ISCIP=55
C     CALL TITLE          00001670
C     WRITE(6,15)
C     WRITE(6,16)
C     IFIG=1
C     CALL PRINT          00001680
C     CALL PLOT            00001690
C
C     DO 10 ICOUNT=ISTART,NCYCLS 00001700
C     IF(ICOUNT.NE.MCOMP) GO TO 5 00001710
C   4   MCOMP=MCOMP+MSCIP 00001720
C     CALL PRINT          00001730
C     IF(ICOUNT.NE. INT) GO TO 7 00001740
C   5   INT=INT+ISCIP 00001750
C     CALL PLOT            00001760
C   6   CALL ADVANC          00001770
C     IF(ICOUNT.NE.MRLLOAD) GO TO 8 00001780
C     MRLLOAD=MRLLOAD+200 00001790
C     ISTART=ICOOUNT+1      00001800
C     CALL RELOAD          00001810
C
C   8   CONTINUE

```

```

10  CCNTINUE
    ISTART=NCYCLS+1
    CALL PRINT
    WRITE(6,17)
    17 FORMAT(6,18)
    WRITE(6,18)
    18 FORMAT(3I10)
    19 FORMAT(5I10)
    20 FORMAT(7I10)
    21 FORMAT(10X,'INITIAL VALUES OF STREAM FUNCTION'//)
    22 FORMAT(10X,'INITIAL VALUES OF VORTICITY'//)
    23 FORMAT(10X,'STREAM FUNCTION'//)
    24 FORMAT(10X,'VORTICITY'//)
    25 FORMAT(3A1)
    CALL RELOAD
    STOP
    END

```

```

SUBROUTINE SETUP
COMMON / FIELDS / PHI,GAMA,FG,GAMOLD
COMMON / VECTOR / T,A,S,XALPHA,PHMEAN,GAMEAN,UMEAN,TEMP,TURBKE,
1 COMMON / ARRAYS / U,PHILAM,FF,ETA,GAP,X,Y
2 COMMON / PARAMS / IPO,IMO,INV,IAO,IAP,MM(3)
3 COMMON / FACTOR / NM,NP1,NP2,NM2,NM3,NM4,NH,MPI1,MP2,MP3,MM1,
4 COMMON / SYMBOL / M2M,MH,MHP,ICOUNT,ITEL,INT,KSTEP,ISTART,P,ISCIPI,MSCIPI,ITAPE,NITER,NITOT,NITMAX,IFIG,MCOMP,KINT
5 COMMON / DOUBLE PRECISION / DXDX2,DXSQR,DXSQR4,DXSQR8,DY,DY2,DYSQR,R1RSQR,R2RSQR,RSRCP,REYNLD,REY,FRACEL,XLAMDA,TIMEDT,DT,PI,H,EKMEAN,EKTURB,UVBAR,ATERM,BTERM,ALPHA,BETA,XM,XN,XNM1,UMNFL0,UFLO,TOL,FA,FB,FC,F1,F2,F3,F4,F5,F6,BLANKXXX,DOT,DX2,DQSQR,DQSQR4,DQSQR8,DY,DY2,DYSQR,R1RSQR,R2RSQR,RSRCP,REYNLD,REY,FRACEL,XLAMDA,TIMEDT,DT,PI,H,EKMEAN,EKTURB,UVBAR,ATERM,BTERM,ALPHA,BETA,XM,XN,XNM1,UMNFL0,UFLO,TOL,FA,FB,FC,F1,F2,F3,F4,F5,F6
6 DIMENSION PHI(64,201),GAMA(64,201),FG(64,201),GAMOLD(64,201)
7 DOUBLE PRECISION UMEAN(201),TEMP(201),TURBKE(201),U(201),S(32),XALPHA(64),Y(201),Y(201),FF(32),
8 DIMENSION ETA(201),GA(201)
9 IPO(64),IMO(64),INV(32),IAO(64),IAP(64)
*
```

CCCCC

### MISCELLANEOUS PARAMETERS

P1=3.1415926535898  
H=3.1415926535898

C C

```
ALPHA=1.0D0
H=H/ALPHA
KINTMAX=15
NP1=N+2
NP2=N+1
NN1=N-1
NN2=N-2
NN3=N-3
NN4=N-4
NH=N/2+1
NM(1)=N
NM(2)=0
NM(3)=0
NM(4)=0
MH=M/2
MH=M+1
MP1=M+1
MP2=M+2
MP3=M+3
M2M=M+N-1
MN1=M-1
XN=DFLQAT(N)
XNM1=DFLOAT(NM1)
XN=DFLOAT(M)
DX=2.0*D0*X
DX2=2.0*D0*DX
DXSQR=DX*SQR
DXSQR4=4.0*D0*DXSQR
DXSQR8=8.0*D0*DXSQR
DY=2.0*D0/XNM1
DY2=2.0*D0*DY
DYSQR=DY*DY
R=DX/DY
RSQR=R*R
RSQRP=RSQR+1.0D0
REY=1.0D0/REYNLD
TOL=0.0002DC
ATERM=1.0D0/(2.0*D0*DYSQR)
BTERM=XM*D2Y2
FA=1.0D0/(XM*X)
FB=1.0D0/(DY2**2)
FC=1.0D0/(8.0D0*(XM*DY)**2)
```

```

      THETA=2.*DO*PI/XM
      WRITE(6,100)R,RSQR,RSQRP
      FORMAT(8X,F12.8,3X,F12.8,3X,F12.8)
100
C      SET UP PERIODIC COUNTERS
C      SET UP INDEXING COUNTERS, IAU & IAP.
C
C      JC=0
      DO 10 I=1,M
      IPO(I)=I+1
      IMO(I)=I-1
      IAO(I)=I+JC
      IAP(I)=IAO(I)+1
      JC=JC+1
10     CONTINUE
      IPO(M)=1
      IMO(1)=M
C      SET UP COORDINATES
      DO 20 J=1,N
      Y(J)=DFLOAT(J-1)*DY-1.0D0
20     CONTINUE
      DO 30 I=1,M
      X(I)=DFLOAT(I-1)*DX-H+DX/2.*DO
30     CONTINUE
C      SET UP MODAL CONSTANTS. ---- ALPHA & FF .
      ALPHAF=DYSQR/DXSQR
      XALPHA(1)=2.*DO
      FF(1)=0.*DO
      DO 35 I=2,MH
      IM=I-1
      IA=IAP(IM)
      IP=IA+1
      XNN=DFLOAT(IM)
      XALPHA(IA)=2.*DO*(1.*DO-ALPHA*(DCOS(THETA*XNN)-1.*DO))
      XALPHA(IP)=XALPHA(IA)
      FF(I)=1.*DO/DXSQR*(DSIN((2.*DO*PI*XNN)/XM))**2
35     CONTINUE
      XNN=DFLOAT(MH)
      XALPHA(M)=2.*DO*(1.*DO-ALPHA*(DCOS(THETA*XNN)-1.*DO))
C      SET UP S AND INV TABLES FOR DHARM.
C      CALL DHARM(A,MM,INV,S,O,IFERR)

```

```

00002760
00002770
00002780
00002790
00002800
00002810
00002820
00002830
00002840
00002850
00002860
00002870
00002880
00002890
00002900
00002910
00002920
00002930
00002940
00002950
00002960
00002970
00002980
00002990
00003000
00003010
00003020
00003030
00003040
00003050
00003060
00003070
00003080
00003090
00003100
00003110
00003120
00003130
00003140
00003150
00003160
00003170
00003180
00003190
00003200
00003210
00003220
00003230

```



```

DO 10 I=1,M
PHI(I,1)=0.
PHI(I,N)=0.
10 CCNTINUE
C ESTABLISH INITIAL VALUES OF STREAM FUNCTION
C USE ARRAYS UMEAN AND TEMP FOR TEMPORARY STORAGE
C A1,B,D,D,E,F ARE DUMMY VARIABES
DO 60 J=1,NH
PHMEAN(J,C)=PHMEAN(J)
READ(5,11) PHMEAN(J),GAMEAN(J),A1,B,C,D,E,F
FORMAT(8F10.0)
11 CCNTINUE
NHM=NH-1
DO 65 J=1,NHM
JC=N-J+1
PHMEAN(JC)=PHMEAN(J)
GAMEAN(JC)=GAMEAN(J)
65 CCNTINUE
FORMAT(10X,3(F12.6),3X)
EPS=1D0/D$QRT(2.D0)
EPS*=EPS*1.8D0
EPS=1.D0
EPS=.2D0
EPS=0.1D0
DO 71 J=1,N
C=PHMEAN(J)
B=GAMEAN(J)
DO 70 I=1,M
THETA=X(I)
PHI(I,J)=EPS*(C*DCOS(THETA)+B*DSIN(THETA))
70 CCNTINUE
CONTINUE(6,12) Y(J),C,B
71 CONTINUE
C COMPUTE INITIAL VALUES OF VORTICITY
DO 15 I=1,M
IP=IP0(I)
IM=IMO(I)
GAMA(I,N)=(8.*DO*PHI(I,NM1)-PHI(I,NM2))*ATERM
GAMA(I,1)=(8.*DO*PHI(I,2)-PHI(I,3))*ATERM
GAMA(I,N)=(1.5*PHI(I,NM2)-4.*PHI(I,3))/9.*DYSQR
GAMA(I,1)=(1.5*PHI(I,3)-4.*PHI(I,4))/9.*DYSQR
GAMOLD(I,1)=GAMA(I,1)
GAMOLD(I,N)=GAMA(I,N)
DO 15 J=2,NM1
GAMA(I,J)=(RSQR*(PHI(I,J+1)+PHI(I,J-1))+PHI(IP,J)+PHI(IM,J))
15 CCNTINUE

```

```

1 GAMOLD(I,J)=GAMA(I,J)
15 CONTINUE
CALL MEANS
CALL TIMER
WRITE(6,99)
WRITE(6,100)(I,I=1,10)
DO 131 J=1,15
WRITE(6,101)J,Y(J),(GAMA(I,J),I=1,10)
131 CONTINUE
FORMAT(1H0,'3X','INITIAL DISTURBANCE GAMA NEAR WALL.')
99 FORMAT(1H,'5X';I=1,11X,10(13,8X))
100 FORMAT(1X,;I3,1X,;I3,1X,;I3,1X,;I3,1X,10(E10.3,1X))
101 RETURN
END
00004160
00004170
00004170

SUBROUTINE MEANS
COMMON / FIELDS / PHI,GAMA,FG,GAMOLD,
COMMON / VECTOR / T,A,S,XALPHA,PMEAN,GAMEAN,UMEAN,TEMP,TURBKE,
1 COMMON / ARRAYS / UPO,IMO,INV,IAP,MM(3),
COMMON / PARAMS / NM,NP1,NP2,NM1,NM2,NM3,NM4,NH,MP1,MP2,MP3,MM1,
1 M2M,MH,MHP,NPROB,ICOUNT,ITEL,IINT,KSTEP,ISTART,
2 ISCIP,MSCHIP,ITAPE,NITER,NITOT,NITMAX,IFIG,NCOMP,
KINT
3 COMMON / FACTOR / DX2,DXSQR,DXSQR4,DY2,DYSQR,R,RSQR,
RSQR,P,REYNLD,REY,FRACEL,XLAMDATIME,DT,DTT,PI,H,
EKMEAN,EKTURB,UUVBAR,ATERM,BTERM,ALPHA,BETA,XN
XNM1,UNMFLO,UFLO,TCL,FA,FB,FC,F1,F2,F3,F4,F5,F6
000012560
000012580
000012590
000012600
000012610
000012620
000012630
000012640
000012650
000012660
000012670
000012680
000012690
000012700
000012710
000012720
000012730
000012740
000012750

SUBROUTINE MEANS
COMMON / FIELDS / PHI,GAMA,FG,GAMOLD,
COMMON / VECTOR / T,A,S,XALPHA,PMEAN,GAMEAN,UMEAN,TEMP,TURBKE,
1 COMMON / ARRAYS / UPO,IMO,INV,IAP,MM(3),
COMMON / PARAMS / NM,NP1,NP2,NM1,NM2,NM3,NM4,NH,MP1,MP2,MP3,MM1,
1 M2M,MH,MHP,NPROB,ICOUNT,ITEL,IINT,KSTEP,ISTART,
2 ISCIP,MSCHIP,ITAPE,NITER,NITOT,NITMAX,IFIG,NCOMP,
KINT
3 COMMON / FACTOR / DX2,DXSQR,DXSQR4,DY2,DYSQR,R,RSQR,
RSQR,P,REYNLD,REY,FRACEL,XLAMDATIME,DT,DTT,PI,H,
EKMEAN,EKTURB,UUVBAR,ATERM,BTERM,ALPHA,BETA,XN
XNM1,UNMFLO,UFLO,TOL,FA,FB,FC,F1,F2,F3,F4,F5,F6
000012610
000012620
000012630
000012640
000012650
000012660
000012670
000012680
000012690
000012700
000012710
000012720
000012730
000012740
000012750

DIMENSION PHI(64,201),GAMA(64,201),FG(64,201),F6(64,201)
DIMENSION UMEAN(201),TEMP(201),TURBKE(201),U(201)
1 PHILAM(201),T(201),A(128),XALPHA(64)
2 PHMEAN(201),GAMEAN(201),X(64),Y(201),FF(32),
3 ETA(201),GA(201),IPO(64),IMD(64),INV(32),IAC(64),IAP(64)
* * * * * * * * * * * * * * * * * * * * * * * * * * * * * * * * * * *
THIS ROUTINE COMPUTES THE MEAN VALUES OF PHI AND GAMA
ARRAY A IS USED FOR TEMPORARY STORAGE.
DO 10 J=1,N

```

CCCCCCC

```

DO 20 I=1,M
A(1)=PHI(I,J)
CONTINUE
CALL ASUM(A,M,SUM)
PHMEAN(J)=SUM/XM
DO 30 I=1,M
A(I)=GAMA(I,J)
CONTINUE
CALL ASUM(A,M,SUM)
GAMEAN(J)=SUM/XM+3. DO*Y(J)
RETURN
END

```

```

SUBROUTINE TITLE
COMMON / FIELDS / PHI,GAMA,FG,GAMOLD,
COMMON / VECTOR / T,A,S,XALPHA,PHMEAN,GAMEAN,UMEAN,TEMP,TURBKE,
1 COMMON / ARRAYS / U,P,O,IM,O,INV,IAP,MM(3),
COMMON / PARAMS / NM,NM1,NM2,NM3,NM4,NH,MP1,MP2,MM1,
2 M2,M,MH,MHP,NPROB,ICOUNT,ITEL,INT,KSTEP,P,ISTART,
ISCIP,MSCIP,ITAPE,NITER,NITOT,NITMAX,IFIG,MCOMP,
KINT
DX,DX2,DXSQR,DXSQR4,DY2,DYSQR,R'SQR,
RSQR,REYNLD,REY,FACEL,XLAMDA,TIME,DT,DTT,P,I,H,
EKMEAN,EKTURB,UVBAR,ATERM,BTERM,ALPHA,BETA,XM,XN
XNM1,UINFL0,UFL0,TOL,FA,FB,FC,F1,F2,F3,F4,F5,F6
3 COMMON / SYMBOL / DOT,BLANK,XXX
DOUBLE PRECISION RSQR,REYNLD,REY,FACEL,XLAMDA,TIME,DT,DTT,P,I,H,
EKM,REYNLD,REY,FACEL,XLAMDA,TIME,DT,DTT,P,I,H,
XNM1,UINFL0,UFL0,TOL,FA,FB,FC,F1,F2,F3,F4,F5,F6
123 DIMENSION PHI(64,201),GAMA(64,201),GAMOLD(64,201)
DOUBLE PRECISION UMEAN(201),TEMP(201),U(201),
PHILAM(201),T(201),A(128),S(32),XALPHA(64),
PHMEAN(201),GAMEAN(201),X(64),Y(201),FF(32),
ETA(201),IGA(201)
123 DIMENSION IP0(64),IMO(64),INV(321),IAO(64),IAP(64),
* * * * * * * * * * * * * * * * * * * * * * * * * * *
C C
WRITE(6,11)
WRITE(6,22)
WRITE(6,12)NPROB
IF(NPROB.LT.0) WRITE(6,23)
WRITE(6,13)N
WRITE(6,14)REYNLD
* * * * * * * * * * * * * * * * * * * * * * * * * * *
00012760
00012770
00012780
00012790
00012800
00012810
00012820
00012830
00012840
00012850
00012860
00012870
00012880
00004180
00004190
00004200
00004210
00004220
00004230
00004240
00004250
00004260
00004270
00004280
00004290
00004300
00004310
00004320
00004330
00004340
00004350
00004360
00004370
00004380
00004390
00004400
00004410
00004420
00004430
00004440
00004450
00004460
00004470
00004480
00004490
00004500

```

```

      WRITE(6,15)DX
      WRITE(6,16)DY
      WRITE(6,18)TOL
      WRITE(6,19)XLAMDA
      WRITE(6,21)FRACEL
      HH=PI/H
      WRITE(6,24)HH,HH
      FORMAT(1H,'10X','H=','14X','F7.5X','ALPHA=','3X','F7.5)
      24 FORMAT(1H,'10X','TURBCODE MARK VI 16. D. O'BRIEN //')
      11 FORMAT(1H0,'10X','PROBLEM NUMBER: 13X',I4)
      12 FORMAT(1H0,'10X','MESSH SIZE NUMBER: 13X',BY,' ',I3)
      13 FORMAT(1H0,'10X','REYNOLDS NUMBER=:',F9.1)
      14 FORMAT(1H0,'10X','DX =:',13X,F7.6)
      15 FORMAT(1H0,'10X','DY =:',13X,F7.6)
      16 FORMAT(1H0,'10X','TOL =:',12X,F7.6)
      17 FORMAT(1H0,'10X','LAMDA=:',10X,F7.6)
      18 FORMAT(1H0,'10X','FRACEL =:',9X,F7.5)
      19 FORMAT(1H0,'10X','DUFORT FRANKEL CENTRAL TIME DIFFERENCING')
      20 FORMAT(1H0,'10X','CONTINUED')
      21 FORMAT(1H0,'10X','RETURN')
      22 FORMAT(1H+,32X,'END')

```

```

      SUBROUTINE PRINT
      COMMON / FIELDS /
      PHI,GAMA,FG,GAMMOLD
      T,A,S,XALPHA,PHMEAN,GAMEAN,UMEAN,TEMP,TURBKE,
      U,PHILAM,FF,ETA,GA,X,Y
      1 COMMON / ARRAYS /
      IPO,IMO,INV,IAO,IAP,MM(3)
      NM,NP1,NP2,NM1,NM2,NM3,NM4,NH,MP1,MP2,MP3,MM1,
      M2,M,MH,MHP,NPROB,ICOUNT,ITEL,INT,KSTEP,ISTART,
      ISCIP,MScip,ITAPE,NITER,NITOT,NITMAX,IFIG,NCOMP,
      KINT,DX2,DXSQR,DXSQR4,DXSQR8,DY,DY2,DYSQR,R1,R2,SQR,
      R2QRP,REYNLD,REY,FRACEL,XLAMDA,TIME,DT,DT1,PI,H,
      EKMEAN,REKTURB,UVRBAR,ATERM,BTERM,ALPHA,BETA,XN,
      XNM1,UMNFL0,UFL0,TOL,FA,FB,FC,FI,F4,F3,F5,F6
      12 COMMON / PARAMS /
      DOT,BLANK,XXX
      DX,DX2,DXSQR,DXSQR4,DXSQR8,DY,DY2,DYSQR,R1,R2,SQR,
      R2QRP,REYNLD,REY,FRACEL,XLAMDA,TIME,DT,DT1,PI,H,
      EKMEAN,REKTURB,UVRBAR,ATERM,BTERM,ALPHA,BETA,XN,
      XNM1,UMNFL0,UFL0,TOL,FA,FB,FC,F1,F2,F3,F4,F5,F6
      13 COMMON / SYMBOL /
      PHI(64,201),GAMA(64,201),GAMOLD(64,201),
      DOUBLE PRECISION UMEAN(201),TEMP(201),U(201),
      12 PHILAM(201),T(201),A(128),S(32),XALPHA(64),
      PHMEAN(201),GAMEAN(201),X(64),Y(201),FF(32),
      ETA(201),GA(201),
      13 DIMENSION IPO(64),IM0(64),INV(32),IA0(64),IAP(64),
      000122400,000122500,000122600

```

```

C * * * * * * * * * * * * * * * * * * * * * * * * * * * *
C THIS ROUTINE PRINTS THE VALUES OF ICOOUNT,T,CT,EKMEAN,EKTURB,UVBAR
C NITER AND NITOT
C CALL ENERGY

IF(IFIG .GT. 0) WRITE(6,11)
EKTOT=EKMEAN+EKTURB
WRITE(6,12) ICOOUNT,TIME,DT,EKMEAN,EKTURB,UFLO,EKTOT,UVBAR,UMNFLD,
11 FORMAT(3X,'CYCLE',6X,'TIME',9X,'DT',7X,'MEAN KE',5X,'TURB KE',7X,
1      ,LOG TURB KE,6X,'TOTAL KE',6X,'UVBAR',7X,'UMNFLD',3X,
2      ,NITOT,2X,'ITEL')
12 FORMAT(3X,15,3XF10.6,2(3X,F8.6),2(3X,F13.7),3X,F9.7,3X,E10.4,3X,
F8.6,2X,15,2X,14)
1 IFIG=-1
1 RETURN
END

```

```

THIS ROUTINE COMPUTES THE AVERAGE KINETIC ENERGIES OF BOTH THE
MEAN AND THE TURBULENT COMPONENTS OF THE FLOW
00013680
00013690
00013700
00013710
00013720
000013730
00000013740
00000013750
00000013760
00000013770
00000013780
00000013790
00000013800
00000013810
00000013820
00000013830
00000013840
00000013850
00000013860
00000013870
00000013880
00000013890
00000013900
00000013910
00000013920
00000013930
00000013940
00000013950
00000013960
00000013970
00000013980
00000013990
00000014000

CALL EDDYS(10)
CALL STRESS
MEAN FLOW. T IS USED FOR TEMPORARY STORAGE
DO 10 J=2,NM1
T(J)=UMEAN(J)**2
10 CONTINUE
T(1)=0
ASUM(T,NM1,SUM)
EKMEAN=SUM/(2.0*D0*XNM1)

C TURBULENT FLOW. TURBULENT COMPONENTS OF PHI ARE STORED IN FG BY
EDDYS. ARRAY A IS USED FOR TEMPORARY STORAGE.

XNM2=2.0*XNM
TURBKE(N)=0.
TURBKE(1)=0.
DO 30 J=2,NM1
DO 20 I=1,N
IP=IPO(I)
IM=IMO(I)
A(I)=(FG(I,J+1)-FG(I,J-1))/DY2)**2+(FG(IP,J)-FG(IM,J))/DX2)**2
20 CONTINUE
CALL ASUM(A,M;SUM)
TURBKE(J)=SUM/XNM2
30 CONTINUE
CALL ASUM(TURBKE,NM1,SUM)
EKTURB=SUM/XNM1
RETURN
END

```

```

SUBROUTINE EDDYS(INDEX)
COMMON / FIELDS /
T,A,S,XALPHA,PMEAN,GMEAN,UMEAN,TEMP,TURBKE,
COMMON / VECTOR /
U,PHILAM,FF,ETA,GAP,X,Y
1 COMMON / ARRAY S /
IPO,IMO,INV,IAO,IAP,MM(3)
COMMON / PARAMS /
N,M,NP1,NP2,NM1,NM2,NM3,NM4,NH,MP1,MP2,MP3,MM1,
M2,M,MH,MHP,NPROB,ICOUNT,ITEL,INT,KSTEP,ISTART,00012950
1 ISCIP,MSCI,ITAPE,NITER,NITOT,NITMAX,IFIG,MCOMP,00012960
2 KINT,DX2,DXSQR,DXSQR4,DXSQR8,DY,DY2,DYSQR,R,RSQR,00012970
3 COMMON / FACTOR /
RSQR,REYNLD'REYFRACEL,XLAMDA,TIME,DT,DTT,PI,H,00012980
EKMEAN,EKTURB,UVBAR,ATERM,BTERM,ALPHA,BETA,XM,XNO,00013000
12

```

```

3 COMMON / SYMBOL / 'XNM1,UMNFL0,UFLO,TOL,FA,FB,FC,F1,F2,F3,F4,F5,F6 00013010
DCUBLE PRECISION
1 DOT,BLANKXXX
DX,DXSQR,DXSQR4,DXSQR8,DY,DY2,DYSQR,R,RSQR,
2 RSQRP,REYNLD,REY,FRACEL,XLAMDA,TIME,DT,DTT,PI,H,
EKMEN,EKTURB,UVBAR,ATERM,BTERM,ALPHA,BETA,XN00013040
3 XNM1,UMNFL0,UFLO,TOL,FA,FB,FC,F1,F2,F3,F4,F5,F6
00013050 00013060 00013070 00013080 00013090 00013100
DIMENSION PHI(64,201),GAMA(64,201),GAMOLD(64,201)
1 DOUBLE PRECISION UMEAN(201),TEMP(201),TURBK(201),U(201),
2 PHILAM(201),T(201),A(128),S(32),XALPHA(64),
3 PHMEAN(201),GAMEAN(201),X(64),Y(201),FF(32),
ETA(201),GA(201)
1PO(64),IMO(64),INV(32),IAO(64),IAP(64)
* * * * * * * * * * * * * * * * * * * * * * * * * *
ASSUMES SUBROUTINE MEANS HAS GENERATED CURRENT VALUES OF PHMEAN
AND GAMEAN
00001312C 00001313C 00001314C 00001315C 00001316C 00001317C
00001318C 00001319C 00001320C 00001321C 00001322C 00001323C
00001324C 00001325C 00001326C 00001327C 00001328C 00001329C
00001330C 00001331C 00001332C 00001333C 00001334C 00001335C
00001336C 00001337C 00001338C

IF INDEX > 0 ROUTINE PUTS TURBULENT COMPONENTS OF STREAM
FUNCTION IN ARRAY FG
IF INDEX < 0 ROUTINE PUTS TURBULENT COMPONENTS OF VORTICITY
IN ARRAY FG

1 IF(INDEX .LT. 0) GO TO 15
2 DO 10 J=1,N
3 DO 10 I=1,M
4 FG(I,J)=PHI(I,J)-PHMEAN(J)
5 10 CONTINUE
6 DO 15 J=1,N
7 DO 20 I=1,M
8 FG(I,J)=GAMA(I,J)-GAMEAN(J)
9 15 CONTINUE
10 20 RETURN
11 END

SUBROUTINE STRESS
COMMON / FIELDS / PHI,GAMA,FG,GAMOLD,
COMMON / VECTOR / TA,S,XALPHA,PHMEAN,GAMEAN,Umean,TEMP,TURBKE,
1 COMMON / ARRAYS / T,PHILAM,FF,ETA,GAP,X,Y,MM(3),
COMMON / PARAMS / NM,NM1,NM2,NM3,NH,MP1,MP2,MP3,MM1,
12 M2,MH,MHP,NPROB,ICOUNT,ITEL,INT,KSTEP,ISTART,COC140700
1 SCIP,MSCLP,ITAPE,NITER,NITOT,NITMAX,IFIG,MCMP,OC140800

```

```

3 COMMON / FACTOR /
1   DX2*DXSQR,DXSQR4*DXSQR8,DY,DY2*DYSQR,R1RSQR,
2   DSQR,P1REYNLD,REY,FRACEL,XLAMDA,TIME,DT,DTT,PI,H
3   EKMEAN,EKTURB,UVBAR,ATERM,BTERM,ALPHA,BETA,XM,F6
1   XNML,UMNFLO,TOL,FA,FB,FC,F1,F2,F3,F4,F5,F6
2   00014100
3   00014110
1   00014120
2   00014130
3   00014140
1   00014150
2   00014160
3   00014170
1   00014180
2   00014190
3   00014200
1   00014210
2   00014220
3   00014230
1   00014240
2   00014250
3   00014260
1   00014270
2   00014280
3   00014290
1   00014300
2   00014310
3   00014320
1   00014330
2   00014340
3   00014350
1   00014360
2   00014370
3   00014380
1   00014390
2   00014400
3   00014410
1   00014420
2   00014430
3   00014440
1   00014450
2   00014460
3   00014470
1   00014480
2   00014490
3   00014500
1   00014510
2   00014520
3   00014530
1   00014540
2   00014550
3   00014560
1   00014570
C
3 COMMON / SYMBOL /
1   DCUBLE PRECISION
2   DOT,BLANK,XXX
3   DX2*DXSQR,DXSQR4*DXSQR8,DY,DY2*DYSQR,R1RSQR,
1   RSQR,P1REYNLD,REY,FRACEL,XLAMDA,TIME,DT,DTT,PI,H
2   EKMEAN,EKTURB,UVBAR,ATERM,BTERM,ALPHA,BETA,XM,F6
3   XNML,UMNFLO,UFL0,TOL,FA,FB,FC,F1,F2,F3,F4,F5,F6
1   00014100
2   00014110
3   00014120
1   00014130
2   00014140
3   00014150
1   00014160
2   00014170
3   00014180
1   00014190
2   00014200
3   00014210
1   00014220
2   00014230
3   00014240
1   00014250
2   00014260
3   00014270
1   00014280
2   00014290
3   00014300
1   00014310
2   00014320
3   00014330
1   00014340
2   00014350
3   00014360
1   00014370
2   00014380
3   00014390
1   00014400
2   00014410
3   00014420
1   00014430
2   00014440
3   00014450
1   00014460
2   00014470
3   00014480
1   00014490
2   00014500
3   00014510
1   00014520
2   00014530
3   00014540
1   00014550
2   00014560
3   00014570
C
3 DIMENSION PHI(64,201),GAMA(64,201),FG(201)
1   DCUBLE PRECISION UMEAN(201),TEMP(201),U(201),
2   PHILAM(201),T(201),A(128),S(32),XALPHA(64)
3   PHMEAN(201),GAMEAN(201),X(64),Y(201),FF(32),
1   ETA(201),GA(201),IPO(64),IMO(64),INV(32),IAO(64),IAP(64)
2   * * * * * * * * * * * * * * * * * * * * * *
3   * * * * * * * * * * * * * * * * * * * * * *
1   ASSUMES THAT FLUCTUATING CAMP. OF PHI IS STORED IN FG
2   COMPUTES REYNOLDS STRESSES AND MEAN VELOCITIES.
3
1   TEMP(1)=0.
2   TEMP(N)=0.
3   DO 20 J=2,NM1
1   DO 10 I=1,M
2   IP=IPO(I)
3   IM=IMO(I)
1   A(I)=(1.0*FG(I,J-1)-FG(I,J+1))*(1.0*FG(IP,J)-FG(IM,J))
2   10 CONTINUE
3   CALL ASUM(A,M,SUM)
1   TEMP(J)=SUM/BTERM
2   20 CONTINUE
3   CALL ASUM(TEMP,NM1,SUM)
1   UVBAR=SUM/XNM1
2
C   MEAN VELOCITY
3
1   DG 30 J=2,NM1
2   UMEAN(J)=PHMEAN(J-1)-PHMEAN(J+1)/DY2+U(J)
3   CONTINUE
1   UMEAN(1)=0.
2   30 UMEAN(N)=0.
3   CALL ASUM(UMEAN,NM1,SUM)
1   UNFL0=SUM/XNM1
2   UFL0=(2.0*DO+PHMEAN(2)-PHILAM(NM1)+PHILAM(2))/4.0*DO
3   RETURN
1   END

```

```

SUBROUTINE PLOT
COMMON / FIELDS /
 1 COMMON / VECTOR / PHI,GAMA,FG,GAMOLD,
    T,A,S,XALPHA,PHMEAN,UMEAN,TEMP,TURBKE,
    U,PHILAM,FF,ETA,GA,X,Y
    1PO,INV,IAO,IAP,M(3)
    NM,NP1,NP2,NM1,NM2,NM3,NM4,NH,MP1,MP2,MP3,M(1),
    M2,M,MH,MHP,NPROB,IOUNT,ITEL,INT,KSTEP,ISTART,
    ISCP,MSCP,ITAP,E,NITER,NITOT,NITMAX,IFIG,MCOMP,
    KINT,DX2,DXSQR,DXSQR4,DXSQR8,DY,DY2,DYSQR,R,RSQR,
    RSQR,P,REYNLD,REY,FACEL,XALMDA,TIME,DT,DTT,PI,H,
    EKMEAN,EKTURB,UVBAR,ATERM,BTERM,ALPHA,BETA,XN,F6
    XNM1,UMNFLT,UFLO,TOL,FA,FB,FC,F1,F2,F3,F4,F5,F6
    DOT'BLANK XXX
 1 COMMON / FACTOR / ALINE(49),BLINE(49),APLOT(201),BPLOT(201),
    DX2,DX2,DXSQR,DXSQR4,DYSQR,DY2,DYSQR,R,RSQR,
    RSQR,REYNLD,REY,FACEL,XALMDA,TIME,DT,DTT,PI,H,
    EKMEAN,EKTURB,UVBAR,ATERM,BTERM,ALPHA,BETA,XN,F6
    XNM1,UMNFLT,UFL0,TOL,FA,FB,F2,F3,F4,F5,F6
 1 2 3 COMMON / SYMBOL / ALINE(64),GAMA(64,201),FG(64,201),
    GAMOLD(64,201),U(201),U(201),A(128),S(32),XALPHA(64),
    PHMEAN(201),GAMEAN(201),X(64),Y(201),FF(32),
    ETA(201),GA(201),IP(64),INV(32),IAO(64),IAP(64)
 1 2 3 DIMENSION PHI(64,201),GAMA(64,201),FG(64,201),
    DOUBLE PRECISION UMEAN(201),TEMP(201),TURBKE(201),
    PHILAM(201),T(201),A(128),S(32),XALPHA(64),
    PHMEAN(201),GAMEAN(201),X(64),Y(201),FF(32),
    ETA(201),GA(201),IP(64),INV(32),IAO(64),IAP(64)
 1 2 3 DIMENSION
C THIS ROUTINE PRINTS ONLINE PLOTS OF MEAN VELOCITY,VORTICITY,
C TURBULENT KINETIC ENERGY AND REYNOLDS STRESS AS FUNCTIONS OF Y.
C * * * * * * * * * * * * * * * * * * * * * * * * * * * * * *
C IFIG=1
C III=-1
C PUT UMEAN IN APLOT , TEMP IN BPLOT
C DC 10 J=1,N
C APLOT(J)=UMEAN(J)
C BPLOT(J)=TEMP(J)
C 10 CONTINUE
C C TITLE
C C
C 11 WRITE(6,11)
C FFORMAT(IHO,4X,'UMEAN',25X,'UMEAN',34X,'UVBAR',28X,'UVBAR')
C 00015117
C 00015160
C 00015150
C 00015140
C 00015130
C 00015090
C 00015090
C 00015100
C 00015110
C 00015120
C 00015130
C 00015050
C 00015060
C 00015070
C 00015080
C 00015090
C 00015090
C 00015100
C 00015110
C 00015120
C 00015130
C 00014810
C 00014820
C 00014830
C 00014840
C 00014850
C 00014860
C 00014870
C 00014880
C 00014890
C 00014900
C 00014910
C 00014920
C 00014930
C 00014940
C 00014950
C 00014960
C 00014970
C 00014980
C 00014990
C 00015000
C 00015010
C 00015020
C 00015030
C 00015040
C 00015050
C 00015060
C 00015070
C 00015080
C 00015090
C 00015100
C 00015110
C 00015120
C 00015130

```

11 WRITE(6,11)  
FORMAT(IHO,4X,'UMEAN',25X,'UMEAN',34X,'UVBAR',28X,'UVBAR')  
00015117

C C

TITLE  
10 CONTINUE

C C

PUT UMEAN IN APLOT , TEMP IN BPLOT

DC 10 J=1,N  
APLOT(J)=UMEAN(J)  
BPLOT(J)=TEMP(J)

IFIG=1  
III=-1

```

C FIND LARGEST ELEMENTS IN APLOT AND BPLOT
C
C 15 ABIG=0.
DC 20 J=1 N
ABIG=AMAX1(ABIG,ABS(APLOT(J)))
BBIG=AMAX1(BBIG,ABS(BPLOT(J)))
CONTINUE
C SET UP TOP HORIZONTAL AXIS
C
C DO 30 I=1,49
ALINE(I)=DCT
BLINE(I)=DOT
CONTINUE
30 WRITE(6,12) ALINE,BLINE
12 FORMAT(14X,49A1,20X,49A1)
C BLANK ALINE AND BLINE AND PUT PLOTTING SYMBOL IN COMPUTED ELEMENT
C
C DO 40 I=1,49
ALINE(I)=BLANK
BLINE(I)=BLANK
CONTINUE
40 ALINE(1)=DOT
BLINE(25)=DCT
J=N
DO 50 JC=1,N**2
JA=APLOT(J)/ABIG*48.+1.
JB=BPLOT(J)/BBIG*24.+25.
ALINE(JA)=XX
BLINE(JB)=XX
WRITE(6,13) APLOT(J),ALINE(J),BPLOT(J),BLINE(J)
13 FORMAT(1X,E10.4,2X,49A1,2X,13,3X,E10.4,2X,49A1)
ALINE(JA)=BLANK
BLINE(JB)=BLANK
ALINE(1)=DOT
BLINE(25)=DOT
J=J-2
CONTINUE
C SET UP BOTTOM HORIZONTAL AXIS
C
C DO 60 I=1,49
ALINE(I)=DOT
BLINE(I)=DCT
CONTINUE
60

```

```

00015180
00015200
00015210
00015220
00015230
00015240
00015250
00015260
00015270
00015280
00015290
00015300
00015310
00015320
00015330
00015340
00015350
00015360
00015370
00015380
00015390
00015400
00015410
00015420
00015430
00015440
00015450
00015460
00015470
00015480
00015490
00015500
00015510
00015520
00015530
00015540
00015550
00015560
00015570
00015580
00015590
00015600
00015610
00015620
00015630
00015640
00015650

```

```

14 WRITE(6,14)ALINE,BLINE
      FCRMAT(14X,49A1,20X,49A1//)
      IF(III .GT. 0)GO TO 100
C   PUT TURBKE IN A PLOT , GAMEAN IN B PLOT
C
C   65 DO 70 J=1,N
      APLOT(J)=TURBKE(J)
      BPLOT(J)=GAMEAN(J)
      70 CONTINUE
      III=1
C   TITLE
      C   WRITE(6,16)
      16 FORMAT(1H0,4X,'TURBKE',25X,'TURBKE',32X,'GAMEAN',26X,'GAMEAN')
      GO TO 15
      RETURN
      END

      SUBROUTINE ADVANC
COMMON / FIELDS /
      PHI,GAMA,FG,GAMOLD,
      T,A,S,XAL,PHA,PHMEAN,GAMEAN,UMEAN,TEMP,TURBKE,
      U,PHILAM,FF,ETA,GA,X,Y
      1 COMMON / VECTORS /
      IPO,IMO,INV,IAO,IAP,MM(3)
      NM,NM2,NM3,NM4,NH,MP1,MP2,MM1,
      M2M,MH,MHP,ICOUNT,ITTEL,INT,KSTEPI,ISTART,
      1 ISCIP,MScip,ITAP,E,NITER,NITOT,NITMAX,IFIG,NCOMP,
      KINT,DX2,DXSQR,DXSQR8,DY,DY2,DYSQR,R,RSQR,
      RSRP,REYNLD,REY,FRACEL,XLAMDA,TIME,DT,DTI,PI,H,
      EKMEAN,REKTURB,UVBAR,ATERM,BTERM,ALPHA,BETA,XN,F6
      XNM1,UMNFLO,UFL0,TOL,FA,FB,FC,F1,F2,F3,F4,F5,F6
      DOT,BLANK,XX
      DX,DX2,DXSQR,DXSQR4,DXSQR8,DY,DY2,DYSQR,R,RSQR,
      RSRP,REYNLD,REY,FRACEL,XLAMDA,TIME,DT,DTI,PI,H,
      EKMEAN,REKTURB,UFL0,TOL,FA,FB,FC,F1,F2,F3,F4,F5,F6
      XNM1,UMNFLO,UFL0,TOL,FA,FB,FC,F1,F2,F3,F4,F5,F6
      1 2 3 COMMON / SYMBOL /
      DOUBLE PRECISION
      1 2 3 DIMENSION PHI(64,201),GAMA(64,201),FG(64,201),GA(64,201),
      DOUBLE PRECISION UMEAN(201),TEMP(201),TURBKE(201),U(201),
      PHILAM(201),T(201),S(128),XALPHA(64),
      PHMEAN(201),GA(201),IAP(64),IAP(64),
      ETA(201),GA(201),INV(32),IAO(64),IAP(64),
      IPO(64),IMO(64),INV(32),IAO(64),IAP(64),
      1 2 3 DIMENSION DCUBLE PRECISION GJ1,GJ2,GJ3,GJ4
      REAL#8 LAMDA,LAMDAB,LAMDAC,LAMDAE,LAMDAF,LAMDAG
      COMMON MRLLOAD,NCYCLS,LINR

```



```

1      -LAMDA*D(U(J)*(GAMA(IP,J)-GAMA(IM,J))
2      -LAMDAE*(PHI(IP,J)-PHI(IM,J))
C      COMPUTE GAMMA AT WALL FROM TRANSPORT EQN. FOR COMPARISON WITH
C      GAMMA COMPUTED FROM THE POISSON EQN.
DC    11   I=1,M
IM=IMO(I)
IP=IPO(I)
LAMDA=2*DO*CT/(REYNLD*DXSQR)
Q=RENSQR*(GAMA(IN,NM2)-2.*GAMA(I,NM1)+GAMA(I,N))+GAMA(IP,N)
1      -2.*GAMA(IN)+GAMA(IN)+GAMA(IN)
FG(I,N)=GAMOLD(I,N)+LAMDA*Q
11     CONTINUE
DC    21   I=1,M
GAMOLD(I,N)=GAMA(I,N)
21     CONTINUE
DO    20   I=1,M
DC    20   J=2,NM1
GAMOLD(I,J)=GAMA(I,J)
GAMA(I,J)=FG(I,J)
20     CONTINUE
L=ICOUNT+1
IF(ICOUNT .EQ. KSTEP)GO TO 69
IF(ONE .EQ. INT)GO TO 69
C      COMPARE VALUES OF GAMMA COMPUTED FROM TRANSPORT EQN WITH VALUES
C      COMPUTED FROM POISSON EQN
C
WRITE(6,105)ICOUNT
WRITE(6,98)(I,I=1,10)
DO 17 J=NM4,N
WRITE(6,99)J,Y(J),(FG(I,J),I=1,5)
17     CONTINUE
WRITE(6,98)(I,I=11,20)
DO 19 J=NM4,N
WRITE(6,99)J,Y(J),(FG(I,J),I=6,10)
19     CONTINUE
69     CONTINUE
FORMAT(1H,'5X','I=';11X,10(13,8X))
99     FORMAT(1X,'J=';13,1X,Y=';F6.3,2X,5(E14.7,1X))
105    FORMAT(1HO,*GAMA NEAR WALL COMPUTED FROM TRANSPORT EQN CYCLE',I4)
CALL PRESUR
TIME=TIME+DT
NITER=0
GC TO 40
C
30     CALL STEP
KSTEP=KSTEP+KINT
40     RETURN

```

END

00007610

SUBROUTINE PRESUR  
COMMON / FIELDS / PHI,GAMA,FG,GAMOLD  
COMMON / VECTOR / T,A,S,XAL,PHA,PHMEAN,GAMEAN,UMEAN,TEMP,TURBKE,  
1 COMMON / ARRAYS / IPO,IM0,INV,IAO,IAP,MM(3)  
1 COMMON / PARAMS / NM,NP1,NM2,NM3,NM4,NH,MP1,MP2,MP3,MM1,  
1 M2,M,MH,MHP,NPROB,ICOUNT,ITEL,INT,KSTAR,T,IFIG,MCOMP,  
2 ISCIP,MScip,ITAP,E,NITER,NITOT,NITMAX,  
3 KINT  
3 COMMON / FACTOR / DXDX2,DXSQR,DXSQR4,DXSQR8,DY,DY2,DYSQR,R,RSQR,  
1 RSQRP,REYNLD,REY,FRACEL,XLAMDA,TIME,DT,PI,H,  
2 EKMEAN,EKTURB,UVBAR,ATERM,BTERM,ALPHA,BETA,XM,XN,  
3 XNM1,UMNFLO,UFLO,TOL,FA,FB,FC,F1,F2,F3,F4,F5,F6  
DCUBLE PRECISION 1 DXDX2,DXSQR,DXSQR4,DXSQR8,DY,DY2,DYSQR,R,RSQR,  
1 RSQRP,REYNLD,REY,FRACEL,XLAMDA,TIME,DT,PI,H,  
2 EKMEAN,EKTURB,UVBAR,ATERM,BTERM,ALPHA,BETA,XM,XN,  
3 XNM1,UMNFLO,UFLO,TOL,FA,FB,FC,F1,F2,F3,F4,F5,F6  
COMMON MRLOAD,NCYCLES,INR  
DIMENSION PHI(64,201),GAMA(64,201),FG(64,201),GAMOLD(64,201)  
DOUBLE PRECISION UMEAN(201),TEMP(201),TURBKE(201),U(201),  
1 PHILAM(201),T(201),A(128),S(32),XALPHA(64),  
2 PHMEAN(201),GAMEAN(201),X(64),Y(201),FF(32),  
3 ETA(201),GA(201),  
IPO(64),IMO(64),INV(32),IAO(64),IAP(64)  
\*  
THIS ROUTINE SOLVES A POISSON EQUATION FOR THE STREAM FUNCTION  
BY MEANS OF THE DISCRETE FOURIER TRANSFORM.  
OBTAIN THE FOURIER TRANSFORM OF GAMA. STCRE IN ARRAY PHI.  
CC 20 J=1,N  
DO 10 I=1,M  
1A=IAO(I)  
1P=IAP(I)  
A(I,A)=GAMA(I,J)  
A(I,P)=0  
CCNTINUE  
10 CCNTINUE  
C CALL DHARM(A,MM,INV,S,2,IFFRR)  
PHI(1,J)=A(1)  
DO 20 I=2,M  
PHI(I,J)=A(I+1)  
20 CCNTINUE

```

C      CBTAIN THE MEAN VALUE OF GAMMA FROM THE ZERO MODE
C      DO 25 J=1,N
C      GAMMEAN(J)=PHI(1,J)/XM+3.0*D(Y(J))
C      25 CCNTINUE
C      OBTAIN THE SPECTRUM OF SQUARED VORTICITY
C      L=ICOUNT+1
C      IF(L .EQ. INT) CALL SPCTR(-1)
C      C SOLVE FOR THE FOURIER TRANSFORM OF PHI. STORE IN ARRAY PHI.
C
C      DO 40 I=1,M
C      PHI(I,N)=0.
C      PHI(I,1)=0.
C      ALPHA=XALPHA(I)
C      DO 30 J=1,NM4
C      T(J)=PHI(I,J+2)
C      30 CCNTINUE
C      CALL TRISOL
C      DO 41 J=3,NM2
C      PHI(I,J)=T(J-2)
C      41 CCNTINUE
C      PHI(I,2)=PHI(I,3)*.25
C      PHI(I,1,NM1)=PHI(I,1,NM2)*.25
C      PHI(I,1,2)=.5*PHI(I,3)-PHI(I,4)/9.
C      PHI(I,1,NM1)=.5*PHI(I,NM2)-PHI(I,NM3)/9.
C      40 CCNTINUE
C      CBTAIN THE MEAN VALUE OF PHI FROM THE ZERO MODE
C      DO 45 J=2,NM1
C      PHMEAN(J)=PHI(1,J)/XM
C      CCNTINUE
C      PHMEAN(N)=0. DO
C      PHMEAN(1)=0. DO
C      OBTAIN THE ENERGY SPECTRUM
C      IF(L .EQ. INT) CALL SPCTR(1)
C
C      1000 CCNTINUE
C      IF(L .EQ. MRLOAD) CALL MODES(1,2,1)
C      IF(L .EQ. MRLOAD) CALL MODES(3,4,1)
C      IF(ICOUNT .EQ. NCYCLS) CALL MODES(1,4,1)
C      IF(ICOUNT .EQ. NCYCLS) CALL MODES(3,4,1)
C      1004 CCNTINUE
C      C INVERT THE FOURIER TRANSFORM OF PHI
C
C      DO 70 J=2,NM1
C      A(1)=PHI(1,J)

```

```

A(2)=0 I=3 MP1
DO 50 PHI(I-1,J)
50  CONTINUE
      A(MP2)=0.
      IC=5
      DO 60 I=MP3,M2M,2
      A(I)=PHI(I-IC,J)
      I=P+1
      A(IP)=-PHI(IP-IC,J)
      IC=IC+4
      CONTINUE
      CALL DHARM(A,MM,INV,S,-2,IFERR)
      DO 70 I=1,M
      IA=IAO(I)
      PHI(I,J)=A(IA)
      CONTINUE
      70 FORMAT(10X,*** FFT OF GAMMA ***//)
      11 FORMAT(10X,*** SOLUTION FOR FFT OF PHI ***//)
      12 FORMAT(10X,*** SOLUTION FOR PHI ***//)
      13 FORMAT(10X,*** FFT OF EXACT SOLUTION FOR PHI ***//)
      14 FORMAT(10X,*** COMPUTE NEW VALUES OF VORTICITY AT WALLS

      DO 80 I=1,M
      IP=IPO(I)
      IM=IMD(I)
      GAMA(I,2)=(PHI(IP,2)-2.*PHI(IM,2))/DXSQR +(PHI(I,3)
      1 -2.*PHI(I,2))/DYSQR
      1 GAMA(I,NM1)=(PHI(IP,NM1)-2.*PHI(I,NM1)+PHI(IM,NM1))/DXSQR
      1 +(PHI(I,NM2)-2.*PHI(IM,NM1))/DYSQR
      1 GAMA(I,N)=(8.0*D0*PHI(I,NM1)-PHI(I,NM2))*ATERM
      GAMA(I,1)=(8.0*D0*PHI(I,NM2)-PHI(I,3))*ATERM
      GAMA(I,N)=(1.5*PHI(I,NM2)-4.*PHI(I,NM3))/9./DYSQR
      GAMA(I,1)=(1.5*PHI(I,3)-4.*PHI(I,4))/9./DYSQR
      CONTINUE
      80 IF(ICOUNT.EQ.0)KSTEP GO TO 87
      IF(LL.EQ.0)GO TO 87
      WRITE(6,109)ICOUNT
      WRITE(6,98)(I,I=1,10)
      DO 18 J=NM4_N
      WRITE(6,99)J,Y(J),(GAMA(I,J),I=1,5)
      18 CONTINUE
      WRITE(6,98)(I,I=11,20)
      DO 21 J=NM4_N
      WRITE(6,99)J,Y(J),(GAMA(I,J),I=6,10)
      21 CONTINUE
      IFIG=1

```

```

98 FORMAT(1H, 15X, 'I'=11X, '10=(13,8X)
99 FORMAT(1X, 13*X, 'Y='F6.3, 2X, 5(E14.7,1X))
100 FORMAT(1H, '2X, 'GAMA NEAR WALL COMPUTED FROM POISSON EQN CYCLE*, 14)
101 RETURN
102 END

```

000C8810

```

SUBROUTINE SPCTR( INDEX )
COMMON / FIELDS / PHI,GAMA,FG,GAMOLD
COMMON / VECTOR / T,A,S,XALPHA,PMEAN,GMEAN,UMEAN,TEMP,TURKE,
1 COMMON / ARRAYS / IPO,IMO,INV,IAO,IAP,NM(3)
COMMON / PARAMS / NM1,NM2,NM3,NM4,NH,MP1,MP2,MM1,
1 M2,M,MH,MH,BTERM,INTER,TTEL,INT,KSTEP,ISTART
2 ISCTIP,MSCTIP,ITAPE,NITER,NITOT,NITMAX,IFIG,FCOMP,00010050
KINT
DX2DX2,DXSQR,DXSQR4,DY2DY2,DYSQR,R,RSGR,00010060
RSQR,P,REYNLD,REY,FRACEL,XLAMDA,TIME,DT,DTT,PI,H,00010070
EKMEAN,EKTURB,UVEAR,ATERM,BTERM,ALPHA,BETA,XM,XNC0010080
EXNM1,UMNFFLU,BUFFLO,TOL,FA,FB,FC,F1,F2,F3,F4,F5,F600010090
DOT,BLANK,XXX
DX2DX2,DXSQR,DXSQR4,DY2DY2,DYSQR,R,RSGR,00010100
RSQR,P,REYNLD,REY,FRACEL,XLAMDA,TIME,DT,DTT,PI,H,00010110
EKMEAN,EKTURB,UVEAR,ATERM,BTERM,ALPHA,BETA,XM,XNC0010120
EXNM1,UMNFFLU,BUFFLO,TOL,FA,FB,FC,F1,F2,F3,F4,F5,F600010130
00010140
00010150
C0010160
C0010170
00010180
00010190
00010200
00010210
00010220
00010230
00010240
00010250
00010260
00010270
00010280
00010290
00010300
00010310
00010320
00010330
00010340
00010350
00010360
00010370
* * * * *
1 COMMON / SYMBOL /
2 DOUBLE PRECISION /
3
1 2 3
DIMENSION PHI('64',201),GAMA('64',201),FG('64',201),GAMOLD('64',201)
DOUBLE PRECISION UMEAN('201'),TEMP('201'),TURKE('201'),U('201')
1 2 3
PHILAM('201'),T('201'),A('128'),S('32'),XALPHA('64'),
PHIMEAN('201'),GAMMEAN('201'),X('64'),Y('201'),FF('32'),
ETA('201'),IGA('201'),IPO('64'),IMD('64'),IINV('32'),IAO('64'),IAP('64'),
* * * * * * * * * * * * * * * * * * * * * * * * * * * * * * * * * * * * * * *
* * * * * * * * * * * * * * * * * * * * * * * * * * * * * * * * * * * * * * * * * *

```

THIS ROUTINE COMPUTES THE KINETIC ENERGY OF THE DISTURBANCE MOTION AS A FUNCTION OF Y AND WAVE NUMBER IN THE X DIRECTION. WAVE OR MODE NUMBER ONE CORRESPONDS TO THE MEAN VALUE OF THE DISTURBANCE. THE SPECTRUM OF THE TURBULENT ENERGY IS CONTAINED IN MODE NUMBERS TWO THROUGH NH. ARRAY FG IS USED FOR STORAGE OF THE SPECTRAL VALUES

```

1 IF (ICOUNT .EQ. KSTEP) RETURN
2 IF (FIG=1)
3 IF (INDEX .LT. 0) GO TO 40
5 L=MH+1
DO 10 J=2,NM1
      JN=J-1

```

CCCCCCCCCCCC

```

JP=J+1
FG(I,J)=FC*(PHI(L,M,JM)-PHI(M,JP))**2
FG(L,J)=FC*(PHI(M,JM)-PHI(M,JP))**2
DO 10 I=2,MH
LL=IAO(I)
LP=LL+1
LN=LL-1
0001038
0001039
0001040
0001041
0001042
0001043
0001044
0001045
0001046
0001047
0001048
0001049
0001050
0001051
0001052
0001053
0001054
0001055
0001056
0001057
0001058
0001059
0001060
0001061
0001062
0001063
0001064
0001065
0001066
0001067
0001068
0001069
0001070
0001071
0001072
0001073
0001074
0001075
0001076
0001077
0001078
0001079
0001080
0001081
0001082
0001083
0001084

1  FG(I,J)=FA*(FB*((PHI(LM,JM)**2+PHI(LL,JM)**2+PHI(LL,JM)*JP)**2+PHI(LL,JM)*JP)**2+PHI(LL,JM)*JP)**2+DO*(PHI(LL,JM)*JP)**2-2*DO*(PHI(LL,JM)*JP)**2+FF(I)*(PHI(LL,JM)*JP)**2+2*PHI(LL,JM)*JP)**2+FF(I)*(PHI(LL,JM)*JP)**2)
2
3
10 CCNTINUE

C MEAN VALUES
C
T(1)=0.0
DO 20 I=1,MHP
DO 15 J=2,NM1
T(J)=FG(I,J)
15 CCNTINUE
CALL ASUM(T,NM1,SUM)
ETA(I)=SUM/XNM1
GA(I)=FG(I,NH)
20 CCNTINUE

C TITLE
C
L=ICOUNT+1
WRITE(6,22) L
22 FORMAT(10X,'ENERGY SPECTRUM FOR CYCLE NUMBER ',I5)
WRITE(6,21)
21 FORMAT(14X,'MEAN SPECTRUM',36X,'MODE',20X,'MIDSTREAM SPECTRUM')
DO 30 I=1,MHP
ETA(I)=FG(I,16)
GA(I)=FG(I,186)
30 CCNTINUE
WRITE(6,23) Y(16),Y(186)
23 FORMAT(10X,'SPECTRUM FOR Y=',F6.4,32X,'MODE',18X,'SPECTRUM FOR Y='
1 F6.4)
1 CALL PLOTS(ETA,GA,MHP)

C IF(ICOUNT .GT. -1) GO TO 100
C PRINT THE ENERGY IN SEVERAL MODES AS FUNCTIONS OF Y.
ETA(1)=0.0
ETA(N)=0.0
GA(1)=0.0

```

```

GA(N)=C•DO
I1=2
I2=3   KL=1 N1
DO 39   J=2 N1
ETA(J)=FG(I1,J)
GA(J)=FG(I2,J)
CONTINUE
35   WRITE(6,36) I1,I2
      FORMAT(14X,'ENERGY IN MODE ',I2,35X,'J',20X,'ENERGY IN MODE ',I2)
      CALL PLOTSP(ETA,GA,N)
I1=4
I2=5
39   CONTINUE
      GO TO 100
C     SIMILAR OPERATIONS FOR THE SPECTRUM OF SQUARED VORTICITY
C
40   F6=1.0 DO /XM**2
      DO 50 J=1,N
         FG(I,J)=F6*PHI(I,J)**2
         FG(MHP,J)=F6*PHI(M,J)**2
      DO 50 I=2,MH
         LL=IAO(I)
         FG(I,J)=F6*(PHI(LL-1,J)**2+PHI(LL,J)**2)
      CONTINUE
50   DC 60 I=1,MHP
      DO 55 J=1,N
         T(J)=FG(I,J)
      55   CONTINUE
      CALL ASUM(T,N1,SUM)
      ETA(I)=SUM/XNM1
      GA(I)=FG(I,NH)
      CONTINUE
60   CONTINUE
C     TITLE
C
C     L=ICOUNT+1
C     WRITE(6,61) L
      FORMAT(10X,'VORTICITY SPECTRUM FOR CYCLE NUMBER ',I5)
61   WRITE(6,62) L
      CALL PLOTSP(ETA,GA,MHP)
      DO 70 I=1,MHP
         ETA(I)=FG(I,16)
         GA(I)=FG(I,186)
      70   CONTINUE
      WRITE(6,23) Y(16),Y(186)

```

100 CALL PLOTS(ETA,GA,MHP)  
RETURN  
END

00011330  
00011340  
00011350

SUBROUTINE TRISOL  
COMMON / FIELDS /  
 PHI,GAMA,FG,GAMOLD,  
 PHIMEAN,UMEAN,Umean,TEMP,TURKE,  
 T,A,S,XALPHA,PHIMEAN,UMEAN,TEMP,TURKE,  
 U,PC,IM0,INV,IAO,IAP,M(3)  
1 COMMON / ARRAYS /  
 NM,NP1,NP2,NM1,NM2,NM3,NM4,NH,MP1,MP2,MP3,MN1,  
 MM2,MM,MHP,NPROB,ICONTR,ITEL,T,NITOT,NITMAX,IFIG,MCIMP,  
 IFIG1,P,MSCLIP,ITAPE,NITER,NITOT,NITMAX,KINT  
2 COMMON / FACTOR /  
 DX,DX2,DXSQR,DXSQR4,DXSQR8,DY,DY2,DYSQR,R,RSQR,  
 DSSQR,P,REYNLD,REY,FRACT,XLAMDA,TIME,DT,DTT,PI,H  
1 2 EKMEAN,EKTURB,UVBAR,ATERM,BTERM,ALPHA,BETA,XN  
3 DCUBLE PRECISION ,XNM1,UNFNFLD,UFLD,TOL,FA,FB,FC,F1,F2,F3,F4,F5,F6  
1 2 DSSQR,P,REYNLD,REY,FRACT,XLAMDA,TIME,DT,DTT,PI,H  
3 DIMENSION PHI(64,201),GAMA(64,201),FG(64,201),GA,OLD(64,201)  
DOUBLE PRECISION UMEAN(201),TEMP(201),TURKE(201),U(201),A(128)  
1 2 PHILAM(201),T(201),A(128),S(32),Y(32),XALPHA(64),  
3 DIMENSION PHI(201),GAMA(201),X(64),Y(201),FF(32),  
 ET(201),GA(201),INV(32),IAO(64),IAP(64)  
\*  
00008820  
00008830  
00008840  
00008850  
00008860  
00008870  
00008880  
00008890  
00008900  
00008910  
00008920  
00008930  
00008940  
00008950  
00008960  
00008970  
00008980  
00008990  
00009000  
00009010  
00009020  
00009030  
00009040  
00009050  
00009060  
00009070  
00009080  
00009090  
00009100  
00009110  
00009120  
00009130  
00009140  
000C9140  
THIS SUBROUTINE SOLVES THE SYSTEM OF EQUATIONS  $P*X = DYSQR*Y$ .  
X AND Y ARE VECTORS. DYSQR IS A SCALAR. P IS A TRIDIAGONAL MATRIX.  
WITH ALL MAIN DIAGONAL ELEMENTS = ALPHA, UPPER AND LOWER DIAGONAL  
ELEMENTS = UNITY. ON INPUT Y IS STORED IN ARRAY T. ON OUTPUT T  
CONTAINS THE SOLUTION VECTOR X. ALL VECTORS HAVE DIMENSION NM2  
COLORED CARDS DENOTE REVISED TRI SOL TO INCLUDE THE CHANGES  
RESULTING FROM ALTERING BOUNDARY CONDITIONS TO BE CONSISTENT  
WITH ZERO SLOPE FOR PHI AT THE WALLS  
DOUBLE PRECISION XFF  
SOLUTION BASED ON APPROX PSI AT WALL BY  $\text{PSI} = A1*Y + A2*YSQ$   
 $+ A3*Y**3$   
FOR ZERO SLOPE  $\text{PHI}(2) = .5*\text{PHI}(3) - 1/9*\text{PHI}(4)$   
 $NM5 = N - 5$   
 $XFF = 8*D0/9*D0$   
 $GA(1) = -ALPHA + .5*D0$



C

```

IM1=IAP(IMOD1)
IM1P=IM1+1
IM2=IAP(IMOD2)
10 P=IM2+1 EQ 2 GO TO 20
IF(1PHI(IM1,NH)**2+PHI(IM1P,NH)**2
5 A1=PHI(IM1,NH)/A1
A2=-PHI(IM1P,NH)/A1
A3= PHI(IM2,NH)
A4= PHI(IM2P,NH)
WRITE(6,11) IMOD1,IMOD2
DO 10 J=1,N
ETA(1)=A2*PHI(IM1,J)-A1*PHI(IM1P,J)
ETA(2)=A1*PHI(IM1,J)+A2*PHI(IM1P,J)
ETA(3)=PHI(IM2P,J)-A3
ETA(4)=PHI(IM2P,J)-A4
WRITE(6,12) J,ETA(1),ETA(2),Y(J),ETA(3),ETA(4),J
10 CONTINUE
11 FORMAT(1HO,5X,'J',4X,'REAL' MODE '13', 'Y', 9X,
11 ,REAL' MODE '13', 'IMAG', '6X', 'J')
12 FORMAT(4X,I3,2(3X,F10.6),6X,2(F10.6,3X),I3)
GC TO 40
20 WRITE(6,21) IMOD1,IMOD2
DO 30 J=1,N
ETA(1)=PHI(IM1,J)**2+PHI(IM1P,J)**2
ETA(1)=DSQRT(ETA(1))/XM
ETA(2)=ATAN2(PHI(IM1,J),PHI(IM1P,J))
ETA(3)=PHI(IM2,J)**2+PHI(IM2P,J)**2
ETA(3)=DSQRT(ETA(3))/XM
ETA(4)=ATAN2(PHI(IM2,J),PHI(IM2P,J))
WRITE(6,12) J,ETA(1),ETA(2),Y(J),ETA(3),ETA(4),J
30 CONTINUE
21 FORMAT(1HO,5X,'J',4X,'MAG' MODE '13', 'PHAS', '6X', 'J')
11 ,MAG' MODE '13', 'PHAS', '6X', 'J')
40 IF(IGE 1
1 RETURN
END

SUBROUTINE STEP
COMMON / FIELDS / PHI,GAMA,FG,GA,MOLD
COMMON / VECTOR / T,A,S,XAL,PHI,PHMEAN,GAMEAN,Uemean,TURBKE,
1 COMMON / ARRAYS / IFC,PHILAM,FF,ETA,GA,Y
1 COMMON / PARAMS / MM(3),NP1,NP2,NM1,NM2,NM3,NM4,NH,MP1,MP2,MP3,MM1,
12 COMMON / PROB / M2MM,MH,MHP,KSTEPISTART,ITEL,ICONT,ITOL,NITER,NITOL,NITMAX,NITCOMP,00004790

```

```

3 COMMON / FACTOR /
1  KINT DX2 *DXSQR ,DXSQR4 *DXSQR8 ,DY ,DY2 *DYSQR ,R
2   RSQRP *REYNLD ,REY ,FRACEL ,XLAMDA ,TIME ,DT ,PI ,H ,00004810
3   EKMEAN ,REKTURB ,UVBAR ,ATERM ,ALPHA ,BETA ,F3 ,F2 ,F1 ,F6 ,00004820
1  DOT ,BLANK ,XXX ,00004830
2  XNM1 ,UMNFLO ,UFL0 ,TOL ,FA ,FB ,FC ,F1 ,F2 ,F3 ,F4 ,F5 ,F6 ,00004840
3  EKMEAN ,REKTURB ,UVBAR ,ATERM ,ALPHA ,BETA ,XN ,00004850
1  XNM1 ,UMNFLO ,UFL0 ,TOL ,FA ,FB ,FC ,F1 ,F2 ,F3 ,F4 ,F5 ,F6 ,00004860
2  EKMEAN ,REKTURB ,UVBAR ,ATERM ,ALPHA ,BETA ,XN ,00004870
3  XNM1 ,UMNFLO ,UFL0 ,TOL ,FA ,FB ,FC ,F1 ,F2 ,F3 ,F4 ,F5 ,F6 ,00004880
1  R  DXT ,DYSQR ,DXSQR4 *DXSQR8 ,DY ,DY2 *DYSQR ,R ,RSQRP ,
2  REYNLD ,REY ,FRACEL ,XLAMDA ,TIME ,DT ,PI ,H ,00004890
3  EKMEAN ,REKTURB ,UVBAR ,ATERM ,ALPHA ,BETA ,XN ,00004900
1  XNM1 ,UMNFLO ,UFL0 ,TOL ,FA ,FB ,FC ,F1 ,F2 ,F3 ,F4 ,F5 ,F6 ,00004910
2  EKMEAN ,REKTURB ,UVBAR ,ATERM ,ALPHA ,BETA ,XN ,00004920
3  XNM1 ,UMNFLO ,UFL0 ,TOL ,FA ,FB ,FC ,F1 ,F2 ,F3 ,F4 ,F5 ,F6 ,00004930
1  XNM1 ,UMNFLO ,UFL0 ,TOL ,FA ,FB ,FC ,F1 ,F2 ,F3 ,F4 ,F5 ,F6 ,00004940
2  XNM1 ,UMNFLO ,UFL0 ,TOL ,FA ,FB ,FC ,F1 ,F2 ,F3 ,F4 ,F5 ,F6 ,00004950
3  XNM1 ,UMNFLO ,UFL0 ,TOL ,FA ,FB ,FC ,F1 ,F2 ,F3 ,F4 ,F5 ,F6 ,00004960
1  * * * * * * * * * * * * * * * * * * * * * * * * * * *
2  * * * * * * * * * * * * * * * * * * * * * * * * * * *
3  * * * * * * * * * * * * * * * * * * * * * * * * * * *
1  COMMON / SYMBOL /
2  DOUBLE PRECISION ,
3  DIMENSION PHI(64,201) ,GAMA(64,201) ,FG(64,201) ,GA
1  DOUBLE PRECISION TEMP(201) ,TURBKE(201) ,U(201)
2  COMMON PHILAM(201) ,T(201) ,A(128) ,S(32) ,XALPHAF(64),
3  PHILAM(201) ,TURBKE(201) ,U(201) ,X(64) ,Y(201) ,FF(32),
1  ETA(201) ,GA(201) ,GAMEMAN(201) ,X(64) ,Y(201) ,IAP(64),
2  IPO(64) ,IMO(64) ,INV(32) ,IAQ(64) ,IAP(64)
1  DOUBLE PRECISION GJ1 ,GJ2 ,GJ3 ,Q
2  DOUBLE PRECISION CRIT ,TST ,PUNT ,GAMAIJ
3  COMMON MRLOAD ,NCYCLS ,LINR
1  REAL*8 LAMDA ,LAMDAB ,LAMDAC ,LAMDAE ,LAMDAE
2  THIS ROUTINE COMPUTES NEW VALUES OF VORTICITY AT TIME+DT BY
3  MODIFIED EULER IMPLICIT TIME DIFFERENCING.
1  ARRAY FG IS USED TO STORE TERMS EVALUATED AT TIME T.
2
3  IF(KINT .EQ. 1) GO TO 6
1  IF(ICOUNT .EQ. 0) GO TO 6
DO 5 I=1,M
DO 5 J=1,N
GAMA(I,J)=5*(GAMA(I,J)+GAMOLD(I,J))
GAMOLD(I,J)=GAMA(I,J)
5 CONTINUE
CALL PRESUR
TIME=TIME-DT/2.00
6 CALL TIMER
LAMDA=RSQRP*DT/(REYNLD*DQSQR)
LAMDAB=(1.0*DO-LAMDA)/(1.0*DO+LAMDA)
LAMDAC=DT/(2.0*DO*(1.0*DO+LAMDA)*DQSQR)
LAMDAD=DT/(4.0*DO*(1.0*DO+LAMDA)*DX)
LAMDAE=3.0*DO*LAMDA
DO 10 I=1,M
IP=IPO(I)
IM=IMO(I)
DO 10 J=2,NM1
JP=J+1

```

```

JW=J-1
IF(LINR.EQ.1)GO TO 8
GJ1=(PHI(IM,J)-PHI(IP,J))*(GAMA(IP,J)-GAMA(IM,J))
1 GJ2=(PHI(IP,J)*PHI(I,JM))*(GAMA(IP,J)-GAMA(IM,J))
1 GJ2= GAMMA(IP,JM)*PHI(I,JM)-PHI(IP,J)
1 +GAMMA(IP,JM)*PHI(I,JM)-PHI(IP,J)
2 +GAMMA(IP,JM)*PHI(I,JM)-PHI(IP,J)
3 +GAMMA(IP,JM)*PHI(I,JM)-PHI(IP,J)
GJ3= GAMMA(IP,JP)*(PHI(IM,JP)-PHI(IP,JP))
1 +GAMMA(IP,JM)*(PHI(IM,JM)-PHI(IP,JM))
1 +GAMMA(IP,JM)*(PHI(IP,JM)-PHI(IP,JM))
3 +GAMMA(IP,JM)*(PHI(IP,JM)-PHI(IP,JM))
GJ=(GJ1+GJ2+GJ3)/12.D0
GO TO 81
8 GJ=0.D0
81 CONTINUE
Q=RSQR*(GAMA(I,JP)+GAMA(I,JM))+GAMA(IP,J)+GAMA(IM,J)
FG(I,J)=LAMDAB*GAMA(I,J)+LAMDAC*(GJ+Q)
1 1 IP=1PO(1)
1 2 IM=1MO(1)
10 NCNTINUE
NITSUM=0
FIRST SWEEP. START Y PASS AT LOWER WALL
15 PUNT=0
DO 20 I=1,M
1 1 IP=1PO(1)
1 2 IM=1MO(1)
DO 20 J=3,NM2
JP=J+1
JW=J-1
IF(LINR.EQ.1)GO TO 18
GJ1=(PHI(IP,J)-PHI(I,JM))*(GAMA(IP,J)-GAMA(IM,J))
1 GJ2=(PHI(IP,J)*PHI(I,JM))*(GAMA(IP,J)-GAMA(IM,J))
1 +GAMMA(IP,JM)*PHI(I,JM)-PHI(IP,J)
2 +GAMMA(IP,JM)*PHI(I,JM)-PHI(IP,J)
3 +GAMMA(IP,JM)*PHI(IM,J)-PHI(IP,J)
GJ3= GAMMA(IP,J)*(PHI(IM,JP)-PHI(IP,JP))
1 +GAMMA(IP,JM)*(PHI(IM,JM)-PHI(IP,JM))
2 +GAMMA(IP,JM)*(PHI(IP,JM)-PHI(IP,JM))
3 +GAMMA(IP,JM)*(PHI(IP,JM)-PHI(IP,JM))
GJ=(GJ1+GJ2+GJ3)/12.D0
GJ=R*GJ

```

CC

```

GO TO 118
18 GJ=0,DO
      CONTINUE
      Q=RSQR*(GAMA(I,JP)+GAMA(I,JM))+GAMA(IP,J)+GAMA(IM,J)
      Q=Q*REY
      GAMAIJ=LAMDAC*(GJ+Q)-LAMDAD*U(J)*(GAMA(IP,J)-GAMA(IM,J))
      -LAMDAE*(PHI(IP,J)-PHI(IM,J))+FG(I,J)
1   CONTINUE
20 CALL PRESUR
C
C     SECOND SWEEP. START Y PASS AT UPPER WALL
      DO 30 I=1,M
      IP=IP0(I)
      IM=IMO(I)
      J=NM2
      DO 30 JC=3,NM2
      JP=J+1
      JN=J-1
      IF(LINR.EQ.1)GO TO 28
      GJ1=(PHI(IM,JP)-PHI(IP,J))*((GAMA(IP,J)-GAMA(IM,J))
      + (PHI(IP,JP)-PHI(I,JM))*((GAMA(IP,J)-GAMA(IM,J)))
1   GJ2=GAMA(IP,JP)*(PHI(I,JM)-PHI(IP,J))
      1  +GAMA(IM,JM)*(PHI(I,JM)-PHI(IP,J))
      2  +GAMA(IP,JM)*(PHI(IP,J)-PHI(IM,JM))
      3  +GAMA(IM,JP)*(PHI(IM,JP)-PHI(IP,JP))
      GJ3=GAMA(IM,JP)*(PHI(IM,JP)-PHI(IP,JP))
      1  +GAMA(IM,JM)*(PHI(IP,JM)-PHI(IM,JM))
      2  +GAMA(IP,JM)*(PHI(IP,JM)-PHI(IM,JM))
      3  GJ=(GJ1+GJ2+GJ3)/12.D0
      GJ=R*GJ
      GC TO 128
      GJ=0,DO
28   CONTINUE
      Q=RSQR*(GAMA(I,JP)+GAMA(I,JM))+GAMA(IP,J)+GAMA(IM,J)
      Q=Q*REY
      TST=GAMA(I,J)
      GAMAIJ=LAMDAC*(GJ+Q)-LAMDAD*U(J)*(GAMA(IP,J)-GAMA(IM,J))
      -LAMDAE*(PHI(IP,J)-PHI(IM,J))+FG(I,J)
1   TEST FOR CONVERGENCE
      CRIT=DABS(1-GAMA(I,J)/GAMAIJ)
      PUNT=PUNT+CRIT
      GAMAIJ=GAMA(I,J)
      J=J-1
29   CONTINUE
      GO TO 118

```

```

NITER=NITER+2
TST=PUNT/(XM*NM2)
TST=PUNT/(XM*NM4)
IF(TST .LT. TOL) GO TO 31
IF(NITER .GT. NITMAX) GO TO 31
CALL PRESUR
GO TO 15
C          NITOT=NITOT+NITER
C          IF ICOUNT EQUALS KSTEP THEN SUBROUTINE SPCTRM WILL BE BYPASSED
C          SO THAT NO SPECTRA WILL BE CALCULATED DURING THE ITERATIONS
C          IN SUBROUTINE STEP
KSTEP=KSTEP+1
CALL PRESUR
KSTEP=KSTEP-1
RETURN
END

```

31.

40

```

SUBROUTINE TIMER
COMMON / FIELDS / PHI,GAMA,F6,GAMOLD
COMMON / VECTOR / T,A,S,XALPHA,PHMEAN,U MEAN,T TEMP,TURBKE,
1 COMMON / ARRAYS / UPH,ILOM,INV,IAO,IAP,Y MM(3)
COMMON / PARAMS / NM,NP1,NP2,NM1,NM2,NM3,NM4,NH,MPI1,MP2,MM1,
2 M2M,MHH,MHP,NPROB,ICOUNT,ITELL,INTKSTEP,ISTART,000066270
ISCIP,MSCLP,ITAPE,NITER,NITOT,NITMAX,IFIG,MCOMP,000066280
KINT,DX2,DXSQR,DXSQR4,DXSQR8,DY,DY2,DYSQR,R R SQR,000066290
RSQRP,REYNLD,REY,FRACELXLAMDA,TIME,DT,PI,H,000066300
EKMEAN,EKTURB,ATERM,BTERM,ALPHA,BETA,XN,000066310
XNM1,U MNFL,O,UFLO,TOL,FA,FB,FC,F1,F2,F3,F4,F5,F6,000066320
3 COMMON / SYMBOL / DOT,BLANK,XXX,DOT,DX2,DXSQR,DXSQR4,DXSQR8,000066330
DCUBLE,PRECISION,000066340
RSQRP,REYNLD,REY,FRACELXLAMDA,TIME,DT,PI,H,000066350
EKMEAN,EKTURB,UVBAR,ATERM,BTERM,ALPHA,BETA,XN,000066360
XNM1,U MNFL,O,UFLO,TOL,FA,FB,FC,F1,F2,F3,F4,F5,F6,000066370
DIMENSION PHI(64,201),GAMA{64,201},GA MOLD{64,201},F6 000066380
DOUBLE PRECISION U MEAN{201},TEMP{201},U{201},000066390
PHILAM{201},T{201}{128},S{32},X ALPH A{64},000066400
PHMEAN{201},GAMEAN{201},X{64},Y{201},FF{32},000066410
ETA{201},GA{201},000066420
IP0{64},IMO{64},INV{32},IAU{64},IAP{64} 000066430
* * * * * * * * * * * * * * * * * * * * * * * * * * * 000066440
THIS ROUTINE COMPUTES A NEW VALUE OF DT.

```

CC C C C

```

UMAX=0.
DO 10 I=1,M,4
  IP=IPO(I)
  IM=IMO(I)
  DO 10 J=1,NH,2
    FLIP=(PHI(I,J)-PHI(I,J+2))/DY2+U(J+1)
    FLIPR=(PHI(IP,J)-PHI(IM,J))/DX2
    UMAX=AMAX1(UMAX,ABS(FLIP))
    UMAX=AMAX1(UMAX,ABS(FLIPR))
    CONTINUE
    DTT=FRACEL*DX/UMAX
    DT=FRACEL*DY/VMAX
    DT=DMIN1(DT,DTT)
    ITEL=1
    IF(DT .EQ. DTT) ITEL=-1
    DT=FRACEL*DX*DY/(UMAX*DY+VMAX*DX)
    DTT=XLAMDA*DX*DY*REYNLD/4.0
    DT=DMIN1(DT,DTT)
    IF(DT .EQ. DTT) ITEL=0
    RETURN
  END
10

```

```

SUBROUTINE PLOTS(AX,BX,NN)
COMMON /SYMBOL / DOT,BLANK,XXX
COMMON /PICTUR / ALINE(49),BLINE(49),APLOT(201),BPLT(201)
THIS ROUTINE PRINTS ONLINE PLOTS OF THE POSITIVE NN-DIMENSIONAL
VECTORS AX AND BX.
* * * * * * * * * * * * * * * * * * * * * * * * * * *
DOUBLE PRECISION AX(1),BX(1)
PUT AX & BX IN APLOT & BPLT
DO 10 I=1,NN
  APLT(I)=AX(I)
  BPLT(I)=BX(I)
  CONTINUE
10
C FIND LARGEST ELEMENT IN APLOT & BPLT
C
C
C
C
C
C
C
C
C
C
ABIG=0.
BBIG=0.
DO 20 I=1,NN
  ABIG=AMAX1(ABIG,ABS(APLOT(I)))
  BBIG=AMAX1(BBIG,ABS(BPLT(I)))
  CONTINUE
20

```

```

C C SET UP TOP HORIZONTAL AXIS
C DO 30 I=1,49
     BLINE(I)=DOT
     CCNTINUE
     WRITE(6,31) ALINE,BLINE
 31  ALINE(I)=DOT
     FORMAT(14X,49A1,20X,49A1)
C BLANK ALINE & BLINE. PUT PLOTTING SYMBOL IN COMPUTED ELEMENT
C DO 40 I=2,49
     ALINE(I)=BLANK
     BLINE(I)=BLANK
     CCNTINUE
     ALINE(I)=DOT
     BLINE(I)=DOT
C DO 50 I=1,NN
     JA=APOINT(I)/ABIG*48.+1.
     JB=BPOINT(I)/BBIG*48.+1.
     ALINE(JA)=XXX
     BLINE(JB)=XXX
     WRITE(6,51) APOINT(I),ALINE,I,BPOINT(I),BLINE
 51  FORMAT(1X,E10.4,2X,49A1,2X,I3,3X,E10.4,2X,49A1)
     ALINE(JA)=BLANK
     BLINE(JB)=BLANK
     ALINE(I)=DOT
     BLINE(I)=DOT
     CCNTINUE
C SET UP BOTTOM HORIZONTAL AXIS
C DO 60 I=1,49
     ALINE(I)=DOT
     BLINE(I)=DOT
     CCNTINUE
     WRITE(6,61) ALINE,BLINE
 61  FORMAT(14X,49A1,20X,49A1//)
     RETURN
END

```

```
SUBROUTINE ASUM(A,NN,SUM)
DOUBLE PRECISION A(1)
DOUBLE PRECISION SUM
```

```
THIS ROUTINE COMPUTES THE SUM OF THE FIRST NN ELEMENTS OF A,
AND STORES THE RESULT IN SUM
```

```
SUMM=0.DC
DO 10 I=1,NN
SUMM=SUMM+A(I)
COUNT=COUNT+1
SUM=SUMM
RETURN
END
```

C C C

```
10
SUBROUTINE LOAD
COMMON / VECTOR / PHI,GAMA,FG,GAMOLD,T,A,S,XALPHA,PHMEAN,GAMEAN,Umean,TEMP,TURBKE,
COMMON / ARRAYS / U,PHILAM,FF,ETA,GAP,X,Y,IPO,IMO,INV,IAO,IAP,MM(3)
COMMON / PARAMS / NUMBER(31)
COMMON / FACTOR / FACTO
COMMON / SYMBOL / DOT,BLANK,XXX
COMMON / PRECISION / FACTO(42)
DIMENSION PHI(64,201),GAMA(64,201),FG(64,201),GAMOLD(64,201),U(201),U(201)
DIMENSION UMEAN(201),TEMP(201),TURBKE(201),XALPHA(64)
DOUBLE PRECISION PHILAM(201),T(201),A(128),Y(32),XALPHA(64),
PHMEAN(201),GAMEMEAN(201),X(64),Y(201),FF(32),
ETA(201),GA(201),IPO(64),IMO(64),INV(32),IAU(64),IAP(64)
2
3
DIMENSION PHI0(2101)
COMMON/PHICCM/PHI0
COMMON/MRLOAD/ITAPE
ITAPE=NUMBER(25)
REWIND ITAPE
READ (ITAPE) PHI0
READ (ITAPE) MRLOAD
READ (ITAPE) PHI,GAMA,FG,GAMOLD,T,A,S,XALPHA,PHMEAN,GAMEAN,Umean,TEMP
READ (ITAPE) TURBKE,U,PHILAM,FF,ETA,GAP,X,Y,IPO,IMO,INV,IAO,IAP,MM
READ (ITAPE) NUMBER
READ (ITAPE) FACTO
READ (ITAPE) DOT,BLANK,XXX
REWIND ITAPE
CALL DHARM(A,MM,INV,S,O,IFER)
RETURN
```

```
00014580
00014590
00014600
00014610
00014620
00014630
00014640
00014650
00014660
00014670
00014680
00014690
00014700
00014710
00017630
00017640
00017650
00017660
00017670
00017680
00017690
00017700
00017710
00017720
00017730
00017740
00017750
00017760
00017770
00017810
00017820
00017830
00017840
00017850
00017860
00017870
00017880
00017890
```

END

```
      SUBROUTINE RELOAD  
COMMON / FIELDS / PHI,GAMA,FG,GAMOLD,  
COMMON / VECTOR / T,A,S,XALPHA,PHMEAN,GAMEAN,UMEAN,TEMP,TURBKE,  
1 COMMON / ARRAYS / U,PHILAM,FF,ETA,GAP,X,Y  
COMMON / PARAMS / IPO,IQ,IAO,IAP,MM(3)  
COMMON / NUMBER / NUMBER(31)  
COMMON / FACTOR / FACTO  
COMMON / SYMBOL / DOT,BLANK,XXX  
DOUBLE PRECISION FACTO(42)  
DIMENSION PHIGAMA(64,201) FG(64,201) GAMOLD(64,201)  
DOUBLE PRECISION UMEAN(201) TEMP(201) TURBKE(201) U(201)  
DOUBLE PRECISION PHILAM(201),T(201),A(128),S(32),XALPHA(64),  
PHMEAN(201),GAMEAN(201),X(64),Y(201),FF(32),  
12 ETA(201),GA(201)  
3 DIMENSION IPO(64),IMO(64),INV(32),IAO(64),IAP(64)  
COMMON/PHICOM/PHIO  
COMMON/MRLOAD/  
DIMENSION PHIO(2,101)  
ITAPE=NUMBER(25)  
REWIND ITAPE  
WRITE(ITAPE)PHIO  
WRITE(ITAPE)MRLOAD  
WRITE(ITAPE)PHI,GAMA,FG,GAMOLD  
WRITE(ITAPE)T,A,S,XALPHA,PHMEAN,UMEAN,TEMP  
WRITE(ITAPE)TURBKE,U,PHILAM,FF,ETA,GA,X,Y  
WRITE(ITAPE)IPCO,IMO,INV,IAO,IAP,MM  
WRITE(ITAPE)NUMBER  
WRITE(ITAPE)FACTO  
WRITE(ITAPE)DOT,BLANK,XXX  
REWIND ITAPE  
RETURN  
END
```

```
      SUBROUTINE PRMTRS  
COMMON / FIELDS / PHI,GAMA,FG,GAMOLD,  
COMMON / VECTOR / T,A,S,XALPHA,PHMEAN,GAMEAN,UMEAN,TEMP,TURBKE,  
1 COMMON / ARRAYS / U,PHILAM,FF,ETA,GAP,X,Y  
COMMON / PARAMS / NP1,NP2,NM1,NM2,NM3,NM4,NH,MP1,MP2,MP3,MML,  
12 NM2,MH,MHP,NPROB,ICOUNT,ITEL,NITOT,NITMAX,IFIG,MCOMP,  
3 KINT,MSCI,ITAPE,NITER,NITOT,NITMAX,IFIG,MCOMP,  
1 DX,DY2,DXSQR4,DXSQR8,DYSQR,R,RSQR,  
RSCRP,REYNLD,REY,FRACEL,XLAMD,A,TIME,DT,DTT,PI,H,
```

```

2 EKMEAN,EKTURB,UVBAR,ATERM,BTERM,ALPHA,XM,XN
3 'XNM1,UMNFL0,UFL0,TOL,FA,FB,FC,F1,F2,F3,F4,F5,F6
1 2 DX2,DXSQR,DXSQR4,DXSQR8,DY2,DYSQR,DTT,PI,H
2 RSCP,REYNLD,REYFRAC,ELAMBTERM,TIME,DTT,PI,H
3 EKMEAN,EKTURB,UVBAR,ATERM,BTERM,ALPHA,BETA,XM,XN
1 2 'XNM1,UMNFL0,UFL0,TOL,FA,FB,FC,F1,F2,F3,F4,F5,F6
2 RSCP,REYNLD,REYFRAC,ELAMBTERM,TIME,DTT,PI,H
3 EKMEAN,EKTURB,UVBAR,ATERM,BTERM,ALPHA,BETA,XM,XN
1 2 'XNM1,UMNFL0,UFL0,TOL,FA,FB,FC,F1,F2,F3,F4,F5,F6
2 RSCP,REYNLD,REYFRAC,ELAMBTERM,TIME,DTT,PI,H
3 EKMEAN,EKTURB,UVBAR,ATERM,BTERM,ALPHA,BETA,XM,XN
1 2 'XNM1,UMNFL0,UFL0,TOL,FA,FB,FC,F1,F2,F3,F4,F5,F6
2 RSCP,REYNLD,REYFRAC,ELAMBTERM,TIME,DTT,PI,H
3 DIMENSION PHI(64,201),GAMA(64,201),FG(64,201)
1 2 DOUBLE PRECISION UMEAN(201),TEMP(201),TURBK(201),U(201)
2 PHILAM(201),T(201),A(128),S(32),XALPHA(64),
3 PHEAN(201),GMEAN(201),X(64),Y(261),FF(32),
1 2 ETA(201),GA(201)
2 IPO(64),IMO(64),INV(32),IAO(64),IAP(64)
3 DIMENSION PHASE(11,6)
1 2
3 C
1 2 COMPTES PHI PHASE AT VARIOUS Y LOCATIONS
2 3 IF(ICOUNT.EQ.0) GO TO 11
1 2 JJ=1
2 3 WRITE(6,10) (Y(J),J=NH,181,20)
1 2 DO 20 J=NH,181,20
1 2 DO 19 I=2,11
1 2 LL=IAO(I)
1 2 LM=LL-1
1 2 ARG1=PHI(LL,J)
1 2 ARG2=PHI(LL,J)
1 2 PHASE(1,J)=ATAN2(ARG1,ARG2)
1 2 IF(J.NE.181) GO TO 19
1 2 ARG1=PHI(LL,196)
1 2 ARG2=PHI(LL,196)
1 2 PHASE(1,6)=ATAN2(ARG1,ARG2)
1 2 CONTINUE
1 2 JJ=JJ+1
1 2 MMX=1
1 2 DC 30 I=2,11 ICOUNT, TIME,(PHASE(I,J),J=1,6),MMX
1 2 WRITE(6,40) MMX+1
1 2
30 CONTINUE
10 1 FORMAT(1H0,3X,'CYCLE',7X,'TIME',3X,'PHASE AT Y=',F6.3,
1 1 10X,1H5,7X,'MODE')
40 1 FORMAT(1I7,3X,F10.6,3X,F8.3,10X,5(F8.3,5X),13)
1 1 IFIG=1
1 1 RETURN
1 1 END

```

DISTRIBUTION LIST

	No. Copies
1. Defense Documentation Center Cameron Station Alexandria, Virginia 22314	20
2. Library, Code 0212 Naval Postgraduate School Monterey, California 93940	2
3. Chairman, Department of Aeronautics Naval Postgraduate School Monterey, California 93940	1
4. Professor T. H. Gawain, Code 57Gn Department of Aeronautics Naval Postgraduate School Monterey, California 93940	5
5. Assistant Professor W. H. Clark, Code 57Cv Department of Aeronautics Naval Postgraduate School Monterey, California 93940	5
6. Lieutenant Commander George D. O'Brien, USN 4817 Bayard Boulevard Washington, D. C. 20016	3
7. Mr. Ronald Bailey Theoretical Branch NASA Ames Research Center Moffett Field, California 94035	1
8. Information Research Associates 2140 Shattuck Avenue Berkeley, California 94720	2
9. Los Alamos Scientific Laboratory Los Alamos, New Mexico 87544 Attn: Dr. F. Harlow	1
10. Commander Naval Air Systems Command Attn: Dr. E. S. Lamar - 1 Dr. H. J. Mueller - 1 Navy Department Washington, D. C. 20360	2

11. Commanding Officer 2  
Naval Ship Research and Development Center  
Carderoc, Maryland  
Attn: Dr. F. Frenkiel - 1  
Dr. J. Schott - 1
12. Office of Naval Research 2  
Navy Department  
Washington, D. C. 20360  
Attn: Morton Cooper; Code 438 - 1  
Ralph Cooper - 1
13. Dr. W. C. Reynolds 1  
Dept. of Mechanical Engineering  
Stanford University  
Stanford, California 94034
14. Professor C. E. Menneken, Code 023 1  
Dean of Research Administration  
Naval Postgraduate School  
Monterey, California 93940
15. Dr. Jacob Fromm 1  
International Business Machines, Corp.  
Research Laboratories  
San Jose, California 95114

UNCLASSIFIED

Security Classification

DOCUMENT CONTROL DATA - R & D

(Security classification of title, body of abstract and indexing annotation must be entered when the overall report is classified)

1. ORIGINATING ACTIVITY (Corporate author) Naval Postgraduate School Monterey, California 93940	2a. REPORT SECURITY CLASSIFICATION Unclassified	
3. REPORT TITLE A Numerical Investigation of the Non-Linear Mechanics of Wave Disturbances in Plane Poiseuille Flows		
4. DESCRIPTIVE NOTES (Type of report and, inclusive dates) Technical Report		
5. AUTHOR(S) (First name, middle initial, last name) T. H. Gawain and W. H. Clark		
6. REPORT DATE 2 September 1971	7a. TOTAL NO. OF PAGES 121	7b. NO. OF REFS 16
8a. CONTRACT OR GRANT NO.	9a. ORIGINATOR'S REPORT NUMBER(S) NPS-57Gn71091A	
b. PROJECT NO.	9b. OTHER REPORT NO(S) (Any other numbers that may be assigned this report)	
c.	d.	
10. DISTRIBUTION STATEMENT This document has been approved for public release and sale; its distribution is unlimited.		
11. SUPPLEMENTARY NOTES	12. SPONSORING MILITARY ACTIVITY Naval Postgraduate School Monterey, California 93940	

13. ABSTRACT

The response of a plane Poiseuille flow to disturbances of various initial wavenumbers and amplitudes is investigated by numerically integrating the equation of motion. It is shown that for very low amplitude disturbances the numerical integration scheme yields results that are consistent with those predictable from linear theory. It is also shown that because of non-linear interactions a growing unstable disturbance excites higher wavenumber modes which have the same frequency, or phase velocity, as the primary mode. For very low amplitude disturbances these spontaneously generated higher wavenumber modes have a strong resemblance to certain modes computed from the linear Orr-Sommerfeld equation.

In general it is found that the disturbance is dominated for a long time by the primary mode and that there is little alteration of the original parabolic mean velocity profile. There is evidence of the existence of an energy equilibrium state which is common to all finite-amplitude disturbances despite their initial wavenumbers. This equilibrium energy level is roughly 3-5% of the energy in the mean flow which is an order of magnitude higher than the equilibrium value predicted by existing non-linear theories.

DD FORM 1 NOV 1973

(PAGE 1)

S/N 0101-807-6811

120

UNCLASSIFIED

Security Classification

A-31408

**UNCLASSIFIED**

Security Classification

14. KEY WORDS	LINK A		LINK B		LINK C	
	ROLE	WT	ROLE	WT	ROLE	WT
Hydrodynamic stability						
Finite-differences						
Turbulence						
Plane Poiseuille Flow						

**DD FORM 1 NOV 65 1473 (BACK)**

S/N 0101-807-6821

**UNCLASSIFIED**

Security Classification